

## General Disclaimer

### One or more of the Following Statements may affect this Document

- This document has been reproduced from the best copy furnished by the organizational source. It is being released in the interest of making available as much information as possible.
- This document may contain data, which exceeds the sheet parameters. It was furnished in this condition by the organizational source and is the best copy available.
- This document may contain tone-on-tone or color graphs, charts and/or pictures, which have been reproduced in black and white.
- This document is paginated as submitted by the original source.
- Portions of this document are not fully legible due to the historical nature of some of the material. However, it is the best reproduction available from the original submission.

# The Johns Hopkins University

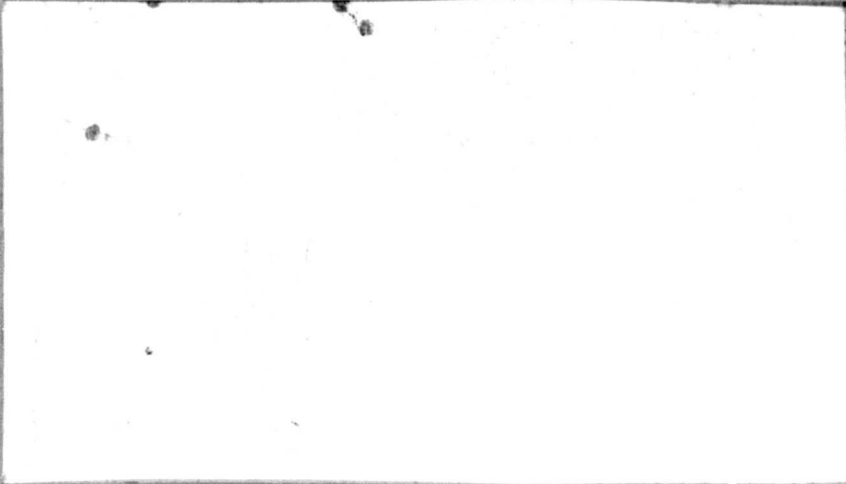
(NASA-CR-175989) DYE LASER TRAVELING WAVE  
AMPLIFIER Final Report, Dec. 1980 - Dec.  
1984 (Johns Hopkins Univ.) 189 p  
HC A09/MF A01

N85-30308

CSCI 20E

G3/36

Unclas  
21657



**ELECTRICAL  
ENGINEERING  
& COMPUTER  
SCIENCE**


Final Report for NASA Cooperative  
Agreement NCC5-24  
"Dye Laser Traveling Wave Amplifier"

F. Davidson and J. Hohman

Electrical Engineering & Computer Science Department  
The Johns Hopkins University  
Baltimore, Maryland 21218

July 1985

Report covers the period Dec. 1980 - Dec. 1984.



**Injection-Locking of Cavity-Dumped  
Flashlamp Pumped Dye Lasers**

*by*

**James L. Hohman**

**A dissertation submitted to The Johns Hopkins  
University in conformity with the requirements  
for the degree of Doctor of Philosophy**

**Baltimore, Maryland**

**1985**



## ABSTRACT

Injection-locking has long been recognized as an effective method of externally controlling the spectral characteristics of a laser. This technique has been employed primarily in applications where high energy yet narrow-linewidth pulsed laser emission is required. In pulsed injection-locked systems, line-narrowing is accomplished by injecting a low energy, narrow-linewidth pulse into a high power laser oscillator. If injection occurs prior to the onset of lasing in the high power oscillator, a "head-start" is given to that radiation which is within the spectral band of the injected signal. If this "head-start" is substantial enough, lasing is initiated at the wavelength and the linewidth of the injected signal. In the work presented here, this technique was applied to a cavity-dumped coaxial flashlamp pumped dye laser in an effort to obtain nanosecond duration pulses which have both high energy and narrow-linewidth. In the absence of an injected laser pulse, the cavity-dumped dye laser was capable of generating high energy ( $\sim 60\text{mJ}$ ) nanosecond duration output pulses. These pulses, however, had a fixed center wavelength and were extremely broadband ( $\sim 6\text{nm}$  FWHM). Experimental investigations were performed to determine if the spectral properties of these outputs could be improved through the use of injection-locking techniques. A parametric study to determine the specific conditions under which the laser could be injection-locked was also carried out. Significant linewidth reduction (to  $> 0.0015\text{nm}$ ) of the outputs was obtained through injection-locking but only at wavelengths near the peak lasing wavelength of the dye. It was found,

however, that, by inserting weakly dispersive tuning elements in the laser cavity, these narrow-linewidth outputs could be obtained over a wide (24nm) tuning range. Since the weakly dispersive elements had low insertion losses, the tunability of the output was obtained without sacrificing output pulse energy.

## ACKNOWLEDGEMENTS

The author would like to express his deep appreciation to Professor Frederic Davidson for the guidance, support and patience he provided during the writing of this dissertation and throughout the author's entire graduate education. I would also like to acknowledge the valuable assistance of Professors Etan Bourkoff and C. Harvey Palmer throughout the course of this work. Much thanks go to Morgan Thoma and Peter Fuhr for their council and friendship during my years here. I am especially indebted to Peter for his loan of the spectrometers used in these investigations. Finally, I would like to acknowledge the Goddard Space Flight Center of the National Aeronautics and Space Administration without whose funding this work would not have been possible. In particular, I would like to thank Dr. John Degnan of NASA for his support of this research. This dissertation is gratefully dedicated to my parents.

## TABLE OF CONTENTS

	Page No.
CHAPTER 1 - GENERAL INTRODUCTION	..... 1
CHAPTER 2 - INTRODUCTION TO DYE LASERS AND INJECTION-LOCKING	..... 8
2.1 Introduction	..... 8
2.2 Properties of Organic Dye Lasers	..... 9
2.3 Basic Principles of Laser Operation	..... 14
2.4 Early Dye Laser Systems	..... 19
2.5 Techniques for Tuning Dye Laser Emission	..... 21
2.6 Historical Introduction to Injection-Locking	..... 22
2.7 General Principles of Injection-Locking	..... 28
2.8 Spectral-Temporal Evolution in Injection-Locked Cavity-Dumped Lasers	..... 30
2.9 Injection Time Considerations	..... 40
2.10 Injected Signal Strength Requirements	..... 47
2.11 Tunability of Injection-Locked Systems	..... 51
2.12 Triplet State Effects	..... 52
CHAPTER 3 - DESIGN AND OPERATION OF THE CAVITY-DUMPED CFP DYE LASER	..... 55
3.1 Introduction	..... 55
3.2 Flashlamp Design and Operation	..... 56

3.3 Dye and Coolant Circulation	.....	59
3.4 Determination of Optimal Dye Concentration	.....	64
3.5 Basic Oscillator Design and Operation	.....	69
3.6 Description of Oscillator Components	.....	73
3.7 Diagnostic Equipment	.....	75
3.8 Alignment of the Cavity-Dumped Oscillator	.....	78
3.9 Initial Temporal and Radiometric Performance of the Laser	.....	80
3.10 Beam Waist Considerations	.....	87
3.11 Effects of the Organic Dye on System Performance	.....	89
3.12 Time Dependent Wavelength Development	.....	91
 <b>CHAPTER 4 - INJECTION-LOCKING OF THE CAVITY-DUMPED CFP LASER</b>	 .....	 95
4.1 Introduction	.....	95
4.2 Master Oscillator	.....	96
4.3 Trigger and Timing Circuitry	.....	99
4.4 Injection-Locked Laser Alignment	.....	104
4.5 Initial Injection-Locking Experiments	.....	108
4.6 MO Linewidth Considerations	.....	112
4.7 Installation of High-Power Polarizing Beamsplitters	.....	114
4.8 Dependency of Injection-Locking Performance on Cavity Dispersion	.....	118
4.9 Injection-Locking Performance Using An		

	Intracavity Prism	..... 126
	4.10 Additional Resonator Design Considerations	..... 131
	4.11 Effects of a Lower Loss Pockels Cell	..... 134
<b>CHAPTER 5</b>	<b>- PARAMETRIC ANALYSIS OF LASER PERFORMANCE</b>	<b>..... 136</b>
	5.1 Introduction	..... 136
	5.2 Direct Measurement of $\rho$ Using An OMA	..... 139
	5.3 Effect of Cavity Dispersion on $\rho$	..... 141
	5.4 Dependency of $\rho$ on $E_i$	..... 146
	5.5 MO Beam Diameter Considerations	..... 150
	5.6 Evaluation of Fluorescence "Noise" Level	..... 152
	5.7 Variation of Laser Pulse Energy with $E_f$	..... 154
	5.8 Spatial Profile of the Output Pulse	..... 158
<b>CHAPTER 6</b>	<b>- CONCLUSIONS AND SUGGESTIONS FOR FUTURE INVESTIGATIONS</b>	<b>..... 161</b>
	6.1 Conclusions	..... 161
	6.2 Possible Use of CW Master Oscillators	..... 163
	6.3 Flashlamp Rise-time Effects	..... 166
	<b>REFERENCES</b>	<b>..... 169</b>
	<b>VITA</b>	<b>..... 176</b>

## LIST OF FIGURES

Figure No.	Title	Page No.
2.1 -	Energy Level Diagram for an Organic Dye Molecule (from [1])	..... 10
2.2 -	Absorption and Emission Processes for Rhodamine 6G (from [1])	..... 13
2.3 -	Relative growth of the photon flux at the natural wavelength of the cavity, $\phi_o$ , and at the wavelength of the injected pulse, $\phi_i$ , with and without ( $\Psi=0$ ) an injected pulse for injection occurring 500ns prior to the peak of the flashlamp pumping pulse.	..... 43
2.4 -	Relative growth of the photon flux at the natural wavelength of the cavity, $\phi_o$ , and at the wavelength of the injected pulse, $\phi_i$ , with and without ( $\Psi=0$ ) an injected pulse for injection occurring 400ns prior to the peak of the flashlamp pumping pulse.	..... 44
2.5 -	Relative growth of the photon flux at the natural wavelength of the cavity, $\phi_o$ , and at the wavelength of the injected pulse, $\phi_i$ , with and without ( $\Psi=0$ ) an injected pulse for injection occurring 300ns prior to the peak of the	

	flashlamp pumping pulse.	..... 45
3.1 -	Flashlamp Trigger Circuitry	..... 57
3.2 -	Dye and Coolant Circulation System	..... 62
3.3a -	Amplified CW Probe Beam	..... 66
3.3b -	Fluorescence Present w/o Probe Beam	..... 66
3.4 -	Small Signal Gain Coefficient Measured as a Function of Flashlamp Discharge Energy and Dye Concentration	..... 67
3.5 -	Small Signal Gain Coefficient Measured as a Function of Flashlamp Discharge Energy and Wavelength	..... 68
3.6 -	Schematic of Basic Cavity-Dumped Ring Oscillator	..... 70
3.7 -	Overall Optical System Schematic	..... 76
3.8 -	Temporal Profile of a Cavity-Dumped Pulse Extracted ~ 200ns Prior to the Peak of the Pumping Pulse	..... 81
3.9 -	Temporal Profile of a Cavity-Dumped Pulse Extracted ~ 400ns After the Peak of the Pumping Pulse	..... 82



3.10 -	Double Exposure Taken of the Fluorescence Emitted from the Dye Cell With and Without Lasing	..... 86
4.1 -	Schematic of the Master Oscillator (MO) and Coupling Optics	..... 98
4.2 -	Block Diagram of the Timing Circuitry	.....101
4.3 -	Passive Decay of the Injected Pulse	.....106
4.4 -	Transmission Profiles of the High Power Polarizing Beamsplitters	.....116
4.5 -	Schematic of the Cavity-Dumped CFP Dye Laser with a Birefringent Tuner	.....119
4.6 -	Injection-Locked Output for $\lambda_i = 590\text{nm}$	.....121
4.7 -	Injection-Locked Output for $\lambda_i = 587\text{nm}$	.....122
4.8 -	Injection-Locked Output for $\lambda_i = 583\text{nm}$	.....123
4.9 -	Schematic of the Cavity-Dumped CFP Dye Laser with a Birefringent Tuner and a Polarizing Prism	.....125
4.10 -	Schematic of the Linearly Configured CFP Dye Laser with a Littrow Prism	.....127
4.11 -	Temporal Profile of the Injection-Locked CFP Dye Laser Output Pulse	.....132
5.1 -	Final Configuration of the CFP Dye Laser Cavity	.....138

5.2 -	OMA Display of the Spectral Profile of the MO Output	.....140
5.3 -	OMA Display of the Tuned Laser Output, (a) without injection-locking and (b) injection-locked with a $3\mu\text{J}$ MO pulse for $578\text{nm} \leq \lambda_i \leq 602\text{nm}$	.....143
5.4 -	OMA Display of the Untuned Laser Output, (a) without injection-locking and (b) injection-locked with a $3\mu\text{J}$ MO pulse for $\lambda_i = 590\text{nm}$	.....144
5.5 -	Variation of $\rho$ with $\lambda$ in an Untuned Cavity	.....145
5.6 -	Variation of $\rho$ with Injected Pulse Energy, $E_i$ ,	.....148
5.7 -	Injection-Locked Output Pulse Energy, $E_a$ , as a Function of the Flashlamp Discharge Energy, $E_f$	.....156
5.8 -	Injection-Locked Output Pulse Energy, $E_a$ , as a Function of Wavelength	.....157
5.9	Comparison of the Spatial Profile of the Output Pulses with the Theoretically Predicted Profiles of a Completely Gain Saturated Pulse and an Unsaturated $TEM_{00}$ Gaussian Pulse	.....160

## CHAPTER 1 - GENERAL INTRODUCTION

The development of laser systems which can produce nanosecond duration laser light pulses that are spectrally pure, continuously tunable in wavelength and that contain high energy (i.e. tens to hundreds of millijoules) has become very important in recent years because of their many applications in both applied and basic research. The continuously tunable organic dye laser is often used in atomic and molecular spectroscopy for the determination of excited state lifetimes and relaxation rates [1,2]. Moderate laser pulse energy is necessary for high resolution UV spectroscopy since the second harmonic conversion efficiency is proportional to the square of the intensity of the fundamental [3]. The narrow laser pulse linewidths are required in order to selectively excite the energy levels of interest. Another common application of such laser systems is found in their use as sources in LIDAR (light detection and ranging) systems [4]. LIDAR techniques use the resonant scattering of high energy laser pulses to make remote measurements of atmospheric constituents and parameters (i.e. species concentration, temperature, pressure, etc.). Here, the ideal laser source consists of nanosecond duration pulses that contain as much energy as possible, yet have optical linewidths that are as narrow as the Fourier transform limit will allow. The maximum probing range of such remote sensing systems is limited by the energy of the transmitted laser signal whereas the accuracy is strongly dependent on the spectral purity of the laser pulse. The use of a continuously tunable source, such as an

organic dye laser, adds much versatility to the system as the laser output can be tuned to cover a number of frequencies.

Narrowband, high peak-power dye laser pulses have been commonly generated for such applications by using either high power pulsed solid-state or excimer lasers as the pump source for the dye laser. These pumping schemes, although effective, possess some inherent disadvantages. For example, the harmonic generation of the infrared solid-state sources, required for organic dye excitation, increases the overall complexity of the system. And although excimer lasers have proven to be nearly ideal dye laser pump sources in many ways (high average power, high repetition rate, direct pumping), their high system cost and size make them inconvenient for many applications.

This work addresses an alternative means of generating dye laser pulses with these characteristics using a standard coaxial flashlamp pumped (CFP) system. High-energy nanosecond duration pulses from CFP dye lasers have been obtained in the past through the use of a variety of cavity-dumping or *Q*-switching techniques [5,6] The output pulses from such systems were typically broadband ( $\Delta\lambda \sim 1-10\text{nm}$ ), however, as conventional line-narrowing techniques require the installation of lossy dispersive elements such as etalons, gratings, etc., into the laser cavity. The use of such lossy elements severely reduces the energy efficiency of the system. As a rule, it is found that attempts to achieve both high output power and narrow output linewidths from a single oscillator force contradictory compromises. Using multistage systems, however, there are two approaches that can be used to resolve this apparent dichotomy. One method involves directing a low energy but spectrally pure pulse through a

series of high power amplifier stages [7]. Without any wavelength discrimination in the amplifiers, however, a significant percentage of the extracted energy is in the form of broadband amplified spontaneous emission which reduces the spectral purity of the output [8]. This technique is also extremely energy inefficient. An alternative technique is to control the spectral properties of a laser externally without the use of intracavity dispersive elements and without loss of energy, by injection-locking the laser to a narrowband pulse. In such a pulsed injection-locked system, the injected signal arrives at the laser just at the onset of lasing. If of sufficient intensity, the pulse will act as a "seed", inducing a preferential buildup of radiation in the laser at the wavelength of the injected pulse.

Since the technique was first demonstrated with dye lasers, there has been a variety of work published specifically on the injection-locking of flashlamp pumped dye lasers [9-15]. Injection-locked dye laser systems have been developed that are capable of producing  $\sim 100$  kilowatt peak-power pulses with linewidths as small as 35MHz [12]. The tuning range of such systems, however, has generally been limited by the homogeneous linewidth of the dye to about 2nm. All of these investigations have been involved with the injection-locking of "long-pulse" ( $\sim 1\mu\text{s}$  duration) flashlamp pumped systems. There have been no published accounts, to date, of attempts to injection-lock  $Q$ -switched or cavity-dumped flashlamp pumped dye lasers.

The principle objective of this work was to extend these previous efforts and experimentally investigate the feasibility of simultaneously generating high energy as well as narrow-linewidth nanosecond duration pulses by injection-locking a cavity-dumped CFP dye laser. Several

methods of extending the tuning range of the laser without sacrificing either the spectral purity or energy of the outputs were also studied. These efforts were accompanied by a parametric study to determine the conditions under which the laser could be injection-locked. The effects on overall laser performance of such parameters as injected pulse energy, wavelength, and linewidth, the pulse injection time (with respect to the flashlamp pumping pulse), and the dispersive properties of the cavity-dumped oscillator were carefully measured. Although results obtained from prior experiments on "long-pulse" non-cavity-dumped systems were useful in yielding some expectation as to the important parametric dependencies [16,17], they cannot be directly applied to explain or predict the behavior of injection-locked cavity-dumped dye lasers. Gain saturation, triplet state and other time dependent effects, which are much more significant in cavity-dumped systems, strongly influence these dependencies. In addition, the behavior of a tuned cavity-dumped oscillator depends on a number of parameters which are not of consequence in the "long-pulse" systems.

A theoretical description of the spectral and temporal evolution of the radiation in an injection-locked dye laser is presented in Chapter 2. A general equation is developed to describe the relative growth of the photon flux in the laser cavity at both the injected pulse wavelength and the natural lasing wavelength of the system. This equation is given in the most general form in order to make explicit the various factors that the injection-locking process is dependent on and the nature of these dependencies. In particular, it highlights many effects peculiar to tuned, cavity-dumped systems (i.e. saturation effects, triplet state effects, etc.,) that are

neglected in the analyses of "long-pulse" systems. Because of the number of independent parameters in the general equation, many of which can only be based on additional models, exact numerical predictions of the various performance features of the system were not attempted. By making some simplifying assumptions, however, the development of the photon fluxes was computed for a brief period of time following the arrival of the injected signal. During this brief time ( $\sim 100$ ns), saturation and triplet state effects can be neglected. These computations, performed for different injection times, graphically illustrate many of the factors involved in injection-locking the system.

The actual development and performance of the cavity-dumped oscillator is discussed in Chapter 3. An inherent difficulty in generating high energy dye laser pulses with flashlamp pumps is caused by the short excited state relaxation times of the organic dye molecules. Energy delivered by the excitation source is only stored by the dye molecules for a period of  $\sim 5$ ns which corresponds to the fluorescence decay time of the upper laser state. Because of this, the energy efficiency of the system is generally related to how rapidly emission can be stimulated. Any spontaneous decay, whether radiative or not, represents a loss. The effectiveness of the excimer and solid-state pumped systems is attributable primarily to the fact that the excitation is in the form of a short, but extremely intense, pumping pulse. The intensity of the laser radiation grows extremely rapidly and saturates the gain of the dye within only a few spontaneous decay times. In cavity-dumped CFP systems the net excitation occurs at a slower rate, so that the intensity of laser radiation increases more gradually toward the saturation regime. Because of this

more gradual growth, the energy efficiency of flashlamp pumped systems is typically very low. The performance of the CFP system is primarily limited by the optical cavity losses which determine, in part, the extent to which the system can be driven into saturation. These losses can be attributed to either passive losses (reflection/transmission losses, scattering, etc.,) or to more complicated time and/or wavelength dependent losses (triplet state losses, thermally induced losses, etc.,). The preliminary phase of the research was devoted to studying the effect that intracavity losses due to resonator optics, dye concentration, flashlamp discharge energy, and cavity-dumping time (with respect to the flashlamp pumping pulse) had on the energy and temporal profile of the output laser pulses.

The spectral characteristics of the laser output are given in Chapter 4 where the preliminary investigations into the injection-locking of the oscillator are described. The theoretical analysis of pulsed injection-locking, presented in Chapter 2, indicated some of the factors which should have influenced the performance (i.e. the energies, linewidths, tunability and temporal cleanliness of the output pulses) of the system. During this second stage of the work, the primary objective was to experimentally verify these predictions and to, at least qualitatively, determine the exact nature of the dependency on these factors. The effect that various cavity configurations had on system performance was also analyzed. In particular, the effects of incorporating weakly dispersive, low insertion loss tuning elements into the cavity were observed to see if broad tunability could be achieved without sacrificing output pulse energy. It was expected that as long as the cavity losses were not increased substantially, that the added dispersion would not only allow for wide tunability but, also enable the



laser to be injection-locked with weaker injected pulses.

Once the design of the amplifier was optimized, more precise and quantitative measurements of the spectral characteristics of the outputs were conducted using an Optical Multichannel Analyzer (OMA). A full characterization of the system performance is presented in Chapter 5. These results indicate a good qualitative agreement with the behavior predicted by the spectro-temporal evolution equation presented in Chapter 2. More significantly, they indicate that injection-locking of a single stage cavity-dumped amplifier is a useful technique for generating high energy, narrow-linewidth, widely tunable, nanosecond duration pulses.

It should be noted that, while these investigations were performed using a CFP dye laser system, the techniques used in this work should be directly adaptable to other types of laser systems as well. Some specific examples of where these results can be applied as well as some suggestions for improving the CFP system performance are discussed in the concluding chapter.

## CHAPTER 2 - INTRODUCTION TO DYE LASERS AND INJECTION-LOCKING

### 2.1 - Introduction

The overall objective of this work was to develop a laser system capable of generating pulses with the characteristics specified in Chapter 1. These characteristics dictated much of the system development. The generation of continuously tunable visible outputs, for example, dictated the use of organic dyes as the laser medium. Similarly, a cavity-dumped system was chosen because it provided the best method of producing high-energy, nanosecond duration pulses from a CFP system. The additional requirement that these pulses be narrowband led to the investigation of injection-locking the cavity-dumped CFP laser.

In this chapter, the theoretical foundations for this work are presented. The basic properties of organic dyes are detailed along with a historical accounting of the development of dye laser systems. Emphasis will be placed on the development of previous injection-locked flashlamp pumped systems. Various methods of tuning these systems are also discussed. Prominent among these is that of injection-locking, a technique which, by using external spectral control, achieves both of the generally contradictory requirements of high-power and narrow linewidths. A detailed analysis of injection-locking is presented as well as a discussion of the factors which affect the injection-locking process.

## 2.2 - Properties of Organic Laser Dyes

The term "organic dye" is a generic one which refers to any organic substance containing a series of conjugated bonds (i.e. alternating single and double bonds). Organic laser dyes constitute a particular subclass of dyes that possess both strong absorption and emission bands in the visible region of the spectrum. Whereas the actual absorption profile of the dyes cannot be derived rigorously because of the complexities introduced by their large molecular size (a typical dye molecule may contain more than 50 atoms), simple models have been found that are capable of explaining many experimental observations [1].

The most often used model for describing the properties of organic dyes is the energy level diagram shown in Figure 2.1. The states shown are electronic energy states with  $S_0$  representing the ground state and  $S_1$ ,  $S_2$ ,  $T_1$ ,  $T_2$  representing bands of excited states. The number of active electrons (i.e. those electrons in the molecule which contribute to the molecules characteristic absorption and emission spectra) is always even. In the ground state, the magnetic spins are always aligned for a total electron spin of zero, as required by the Pauli exclusion principle. When one electron of the pair is excited (by the absorption of a visible or ultraviolet photon), however, there is no such restriction on its spin-state. In a singlet state, (i.e.  $S_0$ ,  $S_1$ , ...,  $S_n$ , ...) the spins of the electron pair are antiparallel, whereas in a triplet state, (i.e.  $T_1$ ,  $T_2$ , ...,  $T_n$ , ...) the spins are parallel. As detailed by Drexhage [1], for every singlet state, except for the ground state,  $S_0$ , there exists an associated triplet state of slightly lower energy. Absorption excites an electron from the ground state,  $S_0$ , into another singlet state ( $S_1$ ,  $S_2$ , ...) as this transition is spin allowed.

ORIGINAL PAGE IS  
OF POOR QUALITY

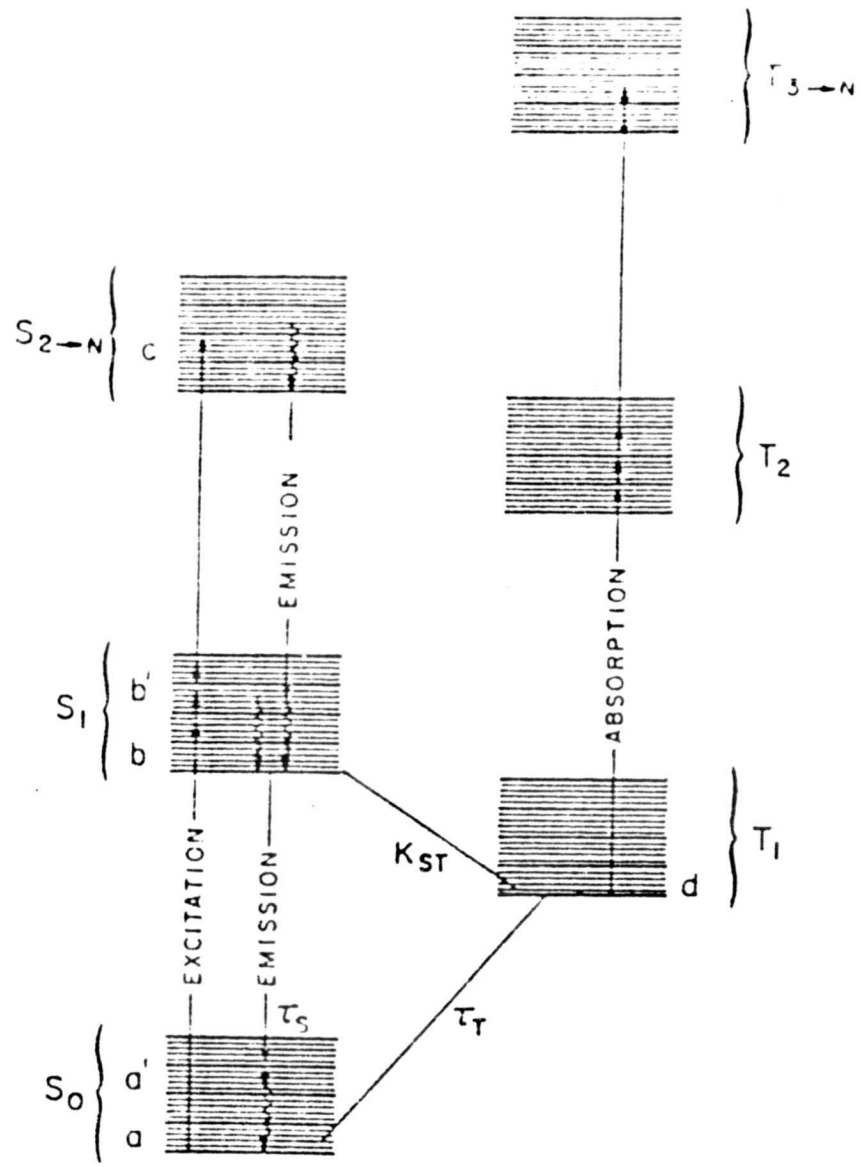


Figure 2.1: Energy Level Diagram for an Organic Dye Molecule (from [1])

However, while in an excited state the electron may undergo a spin-flip and hence eventually reside in the associated triplet state.

Each electronic spin state ( $S_0$ ,  $S_1$ ,  $T_1$ , etc.) possesses many substates which correspond to the quantized vibrational states of the dye molecule (indicated by the heavy lines in Figure 2.1). The typical separation between adjacent vibrational states is  $1500\text{cm}^{-1}$  as compared with a  $20,000\text{cm}^{-1}$  separation between adjacent spin states [18]. The complexity of the system is further compounded by a series of molecular rotational states, with separations as small as  $15\text{cm}^{-1}$ , that are superimposed on each vibrational state [18]. The frequent collisions between the relatively large dye molecule and the surrounding solvent molecules broadens each of these states which results in a quasi-continuum of states around each electronic spin-state.

An electron in the ground state,  $a$  (Figure 2.1), as mentioned before, is excited by the absorption of a visible or ultraviolet photon to one of the states in the continuum around  $S_1$ , ( $a \rightarrow b'$ ), or  $S_2$ , ( $a \rightarrow c$ ), respectively. Due to the large collisional rate of the dye molecule with the solvent molecules ( $\sim 10^{12}\text{sec}^{-1}$ ) thermalization by the nonradiative decay from  $b'$  to the lowest vibrational state in  $S_1$ ,  $b$ , occurs within about one picosecond ( $10^{-12}\text{sec}$ ). The energy associated with this transition is dissipated as heat which generates thermal gradients in the solvent that deteriorate the optical quality of the dye solution. For this reason, ultraviolet excitation, corresponding to the  $a \rightarrow c$  transition, is avoided whenever possible.

To achieve optimal lasing efficiency, it would be desirable for the dye

molecules to remain in  $b$ , the upper laser level, until they were stimulated to return to the lower laser level,  $a$ , a thermally unpopulated state in the  $S_0$  continuum. However, there are a variety of competing decay mechanisms including spontaneous emission which occurs rapidly ( $\tau_s = 5 * 10^{-9}$  sec). Nonradiative decay mechanisms,  $b \rightarrow S_0$ , (generically termed internal conversion) are generally negligible for efficient laser dyes, such as Rhodamine 6G, the dye that will be used throughout this work. The most significant competing process, especially for long-pulse lasers, is the  $b \rightarrow d$  transition in which the excited electron undergoes a spin-flip and "crosses over" to populate the triplet state,  $T_1$ . Although the probability for this process (called intersystem crossing) is generally small due to the requisite spin-flip as evidenced by a decay time,  $k_{ST} \sim 100\text{-}300\text{ns}$  [19,20] several percent of the excited molecules in  $S_1$  may make this transition. Molecules which populate  $d$  remain there for a time that is long compared to the characteristic times involved in the laser transition as the transition  $T_1 \rightarrow S_0$  is spin-forbidden. Its relatively long relaxation time,  $\tau_T$ , ranges from  $10^{-7}$  to  $10^{-3}$ sec depending on the environment of the dye molecule [19]. The triplet state,  $T_1$ , thus acts as a trap, and for high excitation rates, a nonnegligible fraction of the total number of dye molecules may accumulate in  $T_1$ . An increasing  $T_1$  population has the effect of decreasing the number of active dye molecules that are available for the lasing process. If  $N_T$ , the population of  $T_1$ , gets too large it will stop laser action altogether. Lasing may also be quenched when  $N_T \ll N$ , for just as the transitions  $S_0 \rightarrow S_1$ ,  $S_1 \rightarrow S_2$  are spin-allowed, so are the transitions  $T_1 \rightarrow T_2$ . In fact, the  $T_1$  molecules have a large absorption cross-section for the  $T_1 \rightarrow T_n$  transitions. Unfortunately, however, this

ORIGINAL PAGE IS  
OF POOR QUALITY

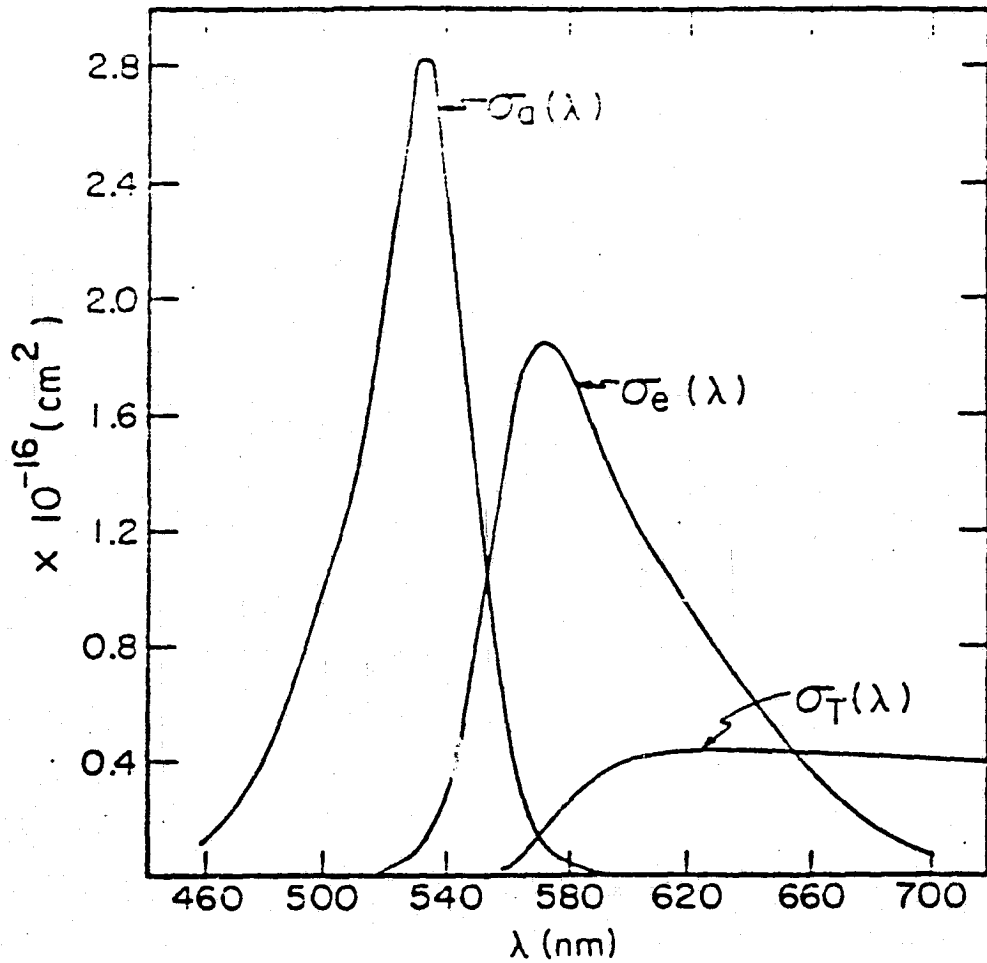


Figure 2.2: Absorption and Emission Processes for Rhodamine 6G (from [1])

absorption spectrum overlaps the  $S_1 \rightarrow S_0$  fluorescence of the dye. Thus, the  $T_1 \rightarrow T_2$  absorption process produces an optical loss at the lasing wavelengths. As this loss is dependent on the triplet state population, the greater  $N_T$  becomes, the greater the loss becomes. Efforts to reduce these losses, made during the development of the dye laser, will be discussed later.

The absorption and emission profiles that correspond to these transitions for Rhodamine 6G are shown in Figure 2.2. The strength of the various absorption, fluorescence or phosphorescent processes is indicated by the value of the molecular cross-section,  $\sigma$ , as a function of wavelength. The most significant feature of the profiles is the displacement of the absorption,  $\sigma_a$ , and emission (fluorescence),  $\sigma_e$ , peaks (termed a Stokes shift). This displacement results from the nonradiative  $c \rightarrow b$ ,  $b' \rightarrow b$  transitions. It is, of course, these nonoverlapping profiles that enable laser action. The broad absorption profile with decided peaks in the visible ( $\sim 5300\text{\AA}$  for R6G/ETOH) and the ultraviolet ( $\sim 2400\text{\AA}$ ) allow the dyes to be pumped with a variety of excitation sources including broadband flashlamp radiation.

### 2.3 - Basic Principles of Laser Operation

A population inversion,  $\Delta N = N(b) - N(a')$  (c.f. Figure 2.1), can be induced in the dye solution, through the use of a sufficiently intense excitation source such as a flashlamp. Since the decay from the lower laser state ( $a'$ ) is extremely rapid with respect to that of the upper laser state ( $b$ ), dye lasers are good examples of "four-level" systems where  $\Delta N \sim N(b)$ . The population inversion allows radiation resonant with one



of the  $b \rightarrow a'$  transitions to be coherently enhanced as it passes through the dye solution. The amplification resulting from a passage of distance  $l$  through the dye solution is given by the basic gain equation

$$\frac{I_\lambda(l)}{I_\lambda(0)} = e^{\delta(\lambda)l} \quad [\text{II.1}]$$

where the exponential gain coefficient,  $\delta(\lambda)$  is defined by

$$\delta(\lambda) = \Delta N \frac{\lambda^2}{8\pi t_s} g(\nu) \quad [\text{II.2}]$$

where  $t_s$  is the decay time for spontaneous emission from  $b \rightarrow a'$ , and  $g(\nu)$  is the lineshape function, which describes the distribution of the emitted frequencies. The spontaneous emission time for Rhodamine 6G is  $\sim 5$  ns although this figure varies slightly depending on the solvent [20,21]. Dye lasers are homogeneously broadened systems which have lineshape functions that closely follow a Lorentzian distribution,  $g(\nu)$ , where

$$g(\nu) = \frac{\Delta\nu}{2\pi[(\nu-\nu_0)^2 + (\frac{\Delta\nu}{2})^2]} \quad [\text{II.3}]$$

for a transition of center frequency  $\nu_0$ . The FWHM width of the homogeneous broadening,  $\Delta\nu$ , is proportional to the interaction (or dephasing) time of the dye molecules. As mentioned in Section 2.2, due to the large size of the dye molecules with respect to those of the solvent, the interaction time is very small (typically  $< 10^{-12}$  sec). For Rhodamine 6G, the homogeneous linewidth,  $\Delta\nu \sim 5 \times 10^{12}$  Hz [18] (corresponding to a  $\Delta\lambda$  of  $\sim 6$  nm).

The basic gain equation given in equation [II.1] is, however, only applicable in those cases in which small signal intensities are involved. As the intensity of the radiation increases, the presence of stimulated emission, which also depopulates  $b$ , effectively decreases the  $b \rightarrow a'$  transition time. Thus, for a constant excitation rate, the population inversion is saturated to a lower value than that encountered in the small signal case,  $\Delta N^0$ . The dependency of  $\Delta N$  on the signal intensity is given below

$$\Delta N = \frac{\Delta N^0}{1 + (I_\nu / I_s)} \quad [\text{II.4}]$$

In this relation,  $I_\nu$  is the intensity of the radiation and  $I_s$ , defined as the saturation intensity, is the intensity at which the net inversion is reduced by a factor of 2. Implicit in this equation is the assumption that the laser is operated in a quasi-CW manner. In other words, it is assumed that the laser pulse duration is at least comparable to the spontaneous emission time of the upper laser level. The saturation intensity, which is solely a function of the laser medium, is given by

$$I_s = \frac{8\pi n^2 h \nu \Delta \nu}{(t_b / t_s) \lambda^2} \quad [\text{II.5}]$$

where  $t_b$  is the net decay time out of  $b$  through all relaxation mechanisms, and  $n$  is the refractive index of the medium. Assuming that  $t_b / t_s \sim 1$ , which is a realistic assumption for most dyes, the saturation intensity of an ethanolic solution of Rhodamine 6G is  $\sim 22 \text{ kW/cm}^2$ .

The basic laser gain equation [II.1] must also be modified to account for distributed loss mechanisms in the gain medium such as the scattering

of radiation from impurities in the dye solution or excited state absorption ( $S_1 \rightarrow S_2$ ,  $T_1 \rightarrow T_2$ ). These effects are accounted for in an inclusive loss coefficient,  $\alpha(\lambda)$ , in equation [II.6] below. Additional losses contributed by the optical resonator components are accounted for by the coefficient,  $R$ , which is the percentage of radiation that is returned to the laser medium on each round trip. Thus, the resulting threshold condition for oscillation is that

$$Re^{(\delta(\lambda) - \alpha(\lambda))l} = 1 \quad [\text{II.6}]$$

As the pumping rate is increased, the intensity of the radiation inside the resonator will increase exponentially until the net round trip gains equal unity, where laser oscillation begins. Any further increase in the pumping rate will momentarily increase  $\Delta N$  but, as the intensity of the radiation increases, the inversion will be saturated to its previous level. The energy that was added to the system by increasing the pump rate is stored in the oscillating field. The inversion,  $\Delta N$ , and the net gain  $\delta$  are thus "clamped" to their threshold values which are determined by the net losses.

By varying the quality factor (i.e.  $Q$ ) of the cavity, thereby circumventing many of the restrictions imposed by steady state operation, very intense short duration pulses can be obtained. The cavity  $Q$  is commonly defined by

$$Q = \omega \left[ \frac{\text{field energy stored by the resonator}}{\text{power dissipated by the resonator}} \right] \quad [\text{II.7}]$$

In typical "Q-switching" arrangements, the cavity  $Q$  is degraded (i.e.

losses are increased) to the point that laser oscillation ceases. In the absence of an oscillating field,  $\Delta N$  is free to be pumped to a large, unsaturated value. When the inversion has been maximized, the  $Q$  is once again switched to its originally high value. At this point, since the net gain is well above that required to achieve threshold, the intensity of the radiation builds up very quickly and, for a period of time determined by the cavity losses, is much greater than that obtained under steady state operation. A percentage of this high intensity radiation is then coupled out of the cavity on each transit.

A special form of  $Q$ -switching, known as cavity-dumping, was used in this work for the extraction of the high peak-power pulses. It is a special case in that it functions in a manner opposite to that of most  $Q$ -switching techniques. In cavity-dumped systems, the cavity  $Q$  is initially kept extremely high. Typically, no output coupling is allowed and the only losses that are permitted are those which are unavoidable in the resonator design. Since the losses are kept to a minimum, the intracavity fields can grow to large intensities before saturating the population inversion to the point determined by the threshold condition. Thus, as the pumping rate increases, energy is continuously added to the recirculating field as it tries to fully saturate the inversion. When the radiation that is trapped inside the resonator reaches its peak value, the cavity  $Q$  is spoiled and the radiation is "dumped" from the resonator at one time. The resulting output pulse then has a duration equal to the resonator transit time and an intensity corresponding to the degree of saturation.

## 2.4 - Early Dye Laser Systems

The first success in achieving laser action with an organic dye was reported by Sorokin and Lankard in 1966 [22]. They used a Q-switched ruby laser to pump a solution containing chloroaluminum phthalocyanine and observed stimulated emission near  $7560\text{\AA}$ . The emission was broad-band with  $\Delta\lambda \sim 40\text{\AA}$ . This observation was followed shortly by the work of Schaefer et al. [23] and Spaeth and Bortfield who used a polymethine dye [24]. All of these early efforts used ruby lasers as the pump sources. McFarland in 1967 [25], noting that dyes in the fluorescein family exhibited near unity fluorescent efficiencies, suspected that they would make ideal candidates for laser mediums. Using frequency-doubled, Q-switched ruby or Nd:YAG lasers as the pumping source, he observed lasing action in fluorescein ( $\lambda = 535\text{nm}$ ) and a variety of rhodamine dyes over the wavelength region ( $565 \leq \lambda \leq 585\text{nm}$ ). Further investigations, by a variety of authors, was then undertaken to extend the range of lasing wavelengths and to develop improved dyes [1].

During this time, only Q-switched solid-state lasers were employed as pump sources. This not only restricted laser emission to those dyes that absorbed the harmonics of these sources, but also restricted the duration of the dye laser pulse to the nanosecond regime ( $\sim 10\text{-}50\text{ns}$ ). In 1967, Sorokin and Lankard realized that the coherence of the pump source was nonessential and discussed the feasibility of using flashlamps as pump sources [26]. The only requirements were a pump with high peak intensity and a short risetime. Later, Sorokin et. al. observed laser emission with a number of dyes, including R6G, using a coaxial air-argon flashlamp as a pumping source [27]. However, it was noted that the laser pulse

terminated well before the flashlamp pumping reached its peak emission ( $t \sim 300\text{ns}$ ). This observation was attributed to triplet state losses as observed intersystem crossing rates were ( $\sim 100\text{-}300\text{ns}$ ). At that time, it was thought that the accumulation of molecules in the triplet states was an inherent problem which precluded the development of longer pulse systems.

Snavely and Schaefer, in 1969, demonstrated that  $O_2$ , dissolved in the dye solution, could be used to depopulate the triplet state [28]. Through collisions with the dye molecule, the  $O_2$  stimulated a spin-flip, thus, allowing the desired  $T_1 \rightarrow S_0$  transition. They were then able to observe dye laser pulses with durations as long as  $140\mu\text{s}$ . They believed that the generation of longer duration pulses was limited by thermally induced refractive index variations in the dye solution. It was later shown by Marling et al. [29], that for most dyes, there exists an optimum concentration of  $O_2$  since  $O_2$ , by collisionally inducing spin-flips, also increases the intersystem crossing rate,  $k_{ST}$  ( $S_1 \rightarrow T_1$ ).

Pappalardo et al. demonstrated the effectiveness of cyclooctatetraene (COT) as a triplet quencher, in obtaining dye laser pulses of  $\sim 800\mu\text{s}$  duration [30]. Again, termination was attributed to thermally induced distortions in the dye solution which were due, primarily, to the ultraviolet excitation of the flashlamp. The search for a CW dye laser finally reached fruition in 1970 when Peterson, Tuccio and Snavely reported the first continuous operation of an organic dye laser by focusing a CW argon-ion laser beam to a small spot within a water solution of rhodamine 6G to generate laser emission near  $597\text{nm}$  [31].

## 2.5 - Techniques for Tuning Dye Laser Emission

Most of the applications for dye lasers were dependent on their unique capability of being continuously tunable over a broad visible range and on their ability to have the laser energy coupled, without substantial loss, into a narrow spectral line. Thus, simultaneous with the attempts to overcome the triplet state losses, so as to generate longer pulses, were investigations into various tuning and line-narrowing techniques.

In some of the first papers on dye lasers, tuning was achieved over a range of  $\sim 200\text{\AA}$  by varying many of the parameters associated with the dye solution including concentration [23], solvent [32] and temperature [33]. Schaefer et al. demonstrated that wide tunability could be achieved by varying the dye concentration and the  $Q$  of the laser resonator [23]. Weber et al. also investigated the effects of cavity  $Q$  and dimensions on the laser wavelength [34]. Almost all of these results were explained by alterations in the long wavelength end of the ground state absorption profile. As either the concentration, cell length, or cavity  $Q$  increased, the singlet state absorption forced the laser emission to longer wavelengths.

The first significant narrowing of the output of dye lasers by the use of a wavelength selective resonator (as opposed to just depending on the absorption properties of the dye itself) was reported by Soffer and McFarland [35]. By using a diffraction grating in the Littrow configuration in place of one of the dye cavity mirrors, in a Q-switched laser pumped dye laser, they observed bandwidths of  $\sim 0.6\text{\AA}$ . The most significant feature, however, was that the spectral narrowing occurred with only a slight loss in energy. A similar grating arrangement was also used by Sorokin et al. [27] in a flashlamp pumped dye laser.

The use of one or more intracavity prisms provided a very convenient method of tuning the dye laser emission. Prisms, although not as dispersive as gratings (unless used in a chain), are also not as lossy. This property made them ideal for CW dye laser applications and high-energy systems where cavity losses, not output linewidth, was the primary concern. Lyot and other forms of birefringent crystal tuners have also been commonly used as low insertion loss tuning elements. In cases where narrow linewidth was the prime concern, the use of tilted intracavity etalons together with prisms have been effective in the production of single longitudinal mode outputs with output linewidths corresponding to bandwidths as low as  $\sim 35\text{MHz}$  that were tunable throughout the full lasing spectrum of the dye [36].

The vast number of other techniques (i.e. acousto-optic tuning, electro-optic tuning, etc.) that have been used for tuning both CW and pulsed dye laser systems precludes the presentation of a very detailed historical account here. However, the tuning elements mentioned above are among the most commonly used.

## **2.6 - Historical Introduction to Injection-Locking**

As mentioned above, linewidth reduction has been conventionally achieved by incorporating various dispersive elements into the laser cavity. One fact that is consistent among all types of tuning elements is that the highly dispersive elements (i.e. gratings, etalons) generally possess large insertion losses. Thus, as a rule, it is found that attempts to achieve both high output power and narrow output linewidths force contradictory compromises. High-power systems are generally dependent on the



maintenance of minimal cavity losses whereas the generation of narrow linewidths requires the installation of lossy intracavity elements.

It was originally thought that with the use of a standard oscillator-amplifier scheme, narrow linewidths and high-powers could be simultaneously achieved [7]. However, with no wavelength discrimination in the amplifier, the effects of broadband fluorescence and amplified spontaneous emission proved substantial enough so as to significantly reduce the spectral purity of the outputs [8]. It was discovered, though, that if the narrowband pulse was of sufficient intensity and injected into the amplifier under the right conditions, that the build-up and oscillation of radiation in the amplifier could be controlled. In this manner, the narrowband pulse, instead of making single passes through a series of amplifiers, could be regeneratively amplified in a multi-pass amplifier. This form of external spectral control has been termed injection-locking and has become a widely used technique for the simultaneous generation of high output powers and narrowband outputs.

The classical problem of locking a pair of oscillators was analyzed as long ago as 1946 by Adler [37]. This work was later extended to specifically concern the locking of laser oscillators. Experimentally, injection-locking was first observed in 1966 by Stover and Steier who achieved phase locking between two single mode He-Ne lasers [38]. Buczek and Freiberg described frequency stabilization of a high-power CW  $CO_2$  ring laser by locking it to a stable low-power reference laser [39]. These investigations concentrated on the behavior of the system under CW injection-locking. In this case, the injected signal had to be large enough to extinguish the natural free-running frequency. The wavelength

difference between the injected signal and the natural free-running frequency had to be small.

In a pulsed oscillator, this constraint can be relaxed considerably. Much smaller injected signals are required since the mode competition during the initial stage in lasing action is very sensitive. Pulsed injection-locking was reported by Bjorkholm and Danielmeyer for a pulsed parametric oscillator, which was locked to an injected signal from a single mode CW  $ND^{3+}:YAG$  laser [40]. Numerous experiments applying the same principle to dye lasers have been performed in recent years. Erickson and Szabo first demonstrated injection-locking of a pulsed dye laser in 1971 in which they locked a  $N_2$ -pumped dye laser oscillator to a pulsed Argon laser [9]. Vrethen and Breimer also demonstrated this principle in short pulse (10-20ns), low energy (10-20 $\mu$ J) dye laser systems [41]. In both of these cases, although there was a significant reduction in the dye laser pulse linewidth, the "master oscillator" (MO) was a fixed frequency laser, so the tunability of the dye was not exploited.

There have been numerous efforts made to injection-lock flashlamp pumped (FLP) dye laser oscillators due to the potential of obtaining high pulse energies with narrow linewidth and tunability. Magyar and Schneider-Muntau demonstrated the narrowband operation of a high-energy FLP dye laser which was injection-locked by another, smaller FLP dye laser of 0.01nm linewidth [10]. These authors found it necessary to include an absorbing dye cell in the high-power cavity in order to obtain a clean spectrum and suppress unwanted modes of oscillation. Maeda et al. used a similar configuration to obtain an amplifier output of 4J at a linewidth of 0.005nm [14].

When a FLP laser or other pulsed source is used as the MO it is difficult to obtain ultra-narrow bandwidths and the problem of synchronization between the two lasers is very critical. The use of CW dye lasers as the injection source can eliminate both of these problems. Turner et al. used a CW dye laser to injection-lock a high-gain FLP dye laser to reduce the linewidth of the amplifier output to 0.1nm. This work was also the first to capitalize on the tunability of the dye. By installing an electro-optic tuning element in the FLP laser, narrowband injection-locked outputs were obtainable over a broad frequency band [11]. Also using a CW injection source, Blit et al. obtained extremely narrowband (30MHz), 50 mJ pulses from a FLP dye laser [12]. The spectral brightness of these pulses was  $\sim 10^{10}$ W/nm.

All of the pulsed injection-locking studies reported on to date, however, have been performed with "long" ( $\sim 1\mu$ sec) pulse flashlamp pumped systems. Microsecond duration outputs have been generated which, although of only moderate peak-power ( $\sim 100$ kW), have large spectral brightness. By injection-locking a cavity-dumped amplifier, much larger peak-power pulses should be obtainable and, if complete locking is possible, these pulses should possess at least the spectral brightness achieved with longer pulsed systems. The installation of a low loss tuning element into the amplifier should also allow such outputs to be produced over a wide range of frequencies. Thus, by combining these techniques with a cavity-dumping scheme, it should be possible to generate extremely high-power, nanosecond duration pulses from a flashlamp pumped system. Through injection-locking, these pulses should also be made widely tunable and narrowband.

It should be noted, at this time, that the term "injection-locking" has been suggested by several authors to be a misnomer when used to describe the control of pulsed laser systems. There are, indeed, fundamental differences in the CW locking techniques employed by Adler [37], Stover and Steier [38], etc., and the pulsed injection-locking of Erickson and Szabo [9]. In the rigorous definition of the term, the master oscillator must control the phase of the forced oscillator [42]. This is accomplished as the injected field adds to the recirculating field, compensating for any net phase shift caused by a difference between the recirculating field and the cavity frequency. This is possible, of course, only under CW or quasi-steady-state conditions in which the master oscillator injected power is significant with respect to the circulating field in the power amplifier [42].

In the pulsed case, the injected beam merely provides the initial conditions from which oscillations can build-up preferentially (at the frequency of the injected pulse) as opposed to building up from spontaneous emission (noise). In this case, the recirculating field in the power amplifier "forgets" the phase information of the injected master oscillator pulse very early in the development of the amplified pulse.

Theoretical analyses have also distinguished the cases of CW and pulsed injection-locking. Ganiel, Hardy and Treves [17] detailed the injection-locking process in pulsed dye lasers by describing the amplifier through a set of coupled rate equations for the population densities and photon fluxes at all wavelengths. By imposing the appropriate initial and boundary conditions, the numerical solutions then yielded information on the spectro-temporal evolution of the pulse, parameterized by the characteristics of the injected pulse. Flamant and Megie [15] derived an

analytical relation, for both the CW and pulsed cases, for the locking efficiency of the forced oscillator by using a spectro-temporal equation that describes the behavior of the multimode pulsed dye laser.

In both of these studies, the modal fine structure caused by the Fabry-Perot resonances of the cavity was disregarded. The results described only the spectral envelope of the laser radiation as they believed that in order to phase-lock the amplifier (i.e. single mode operation) the injected pulse must be intense enough to extinguish all other free-running modes thus limiting the tunability of the system. Analyses of injection-locking in dye lasers where the injected radiation is resonant within the forced oscillator has been performed more recently by Chow [43] and Coulaird, et.al. [44]. Although some authors have tried to distinguish between these two cases by referring to the pulsed case as "injection-seeding" or "pulsed injection-locking" [42], the term injection-locking has been commonly used in the literature when referring to either case.

In this work, where we are only concerned with the pulsed case, the term injection-locking will be used as well. The analysis that we will be concerned with here deals with the behavior of a pulsed dye laser system with the injection of a pulsed narrowband signal. Specifically we are interested in the temporal evolution of all of the spectral components of the pulse, the tunability of the laser output as the injected wavelength is tuned across the gain curve of the dye laser and its dependence on the injected pulse intensity. Both the theoretical and operational analysis of the injection-locked system are complicated by the interrelation of these features.

One factor that need not be considered in this analysis, however, is that of cavity resonance effects. In prior injection-locking studies, cavity resonance became a concern when injected pulse bandwidths were on the order of magnitude of the longitudinal mode spacing of the amplifier. All previous injection-locking studies, however, have been performed using long pulse ( $\geq 300\text{ns}$ ) or CW systems. In short pulse systems, such as the one described here, intermodal frequency spacings are considerably less than the Fourier transform limited bandwidths. For example, bandwidths obtainable from a 3m, cavity-dumped oscillator are transform limited to  $\geq 100\text{MHz}$ , a figure significantly larger than the 50MHz longitudinal mode spacing. Thus, analysis and operation of the system may be performed without regard for cavity resonance effects.

## 2.7 - General Principles of Injection-Locking

After the initiation of the flashlamp pumping pulse, radiation at all wavelengths begins to build up from spontaneous emission. When a threshold inversion is achieved, the growth of the radiation occurs very rapidly. In the absence of an injected signal, radiation at  $\lambda_0$ , where the gain is the greatest, would quickly reach the dye saturation regime and determine the population inversion. Radiation at other wavelengths, having intrinsically smaller gains, would experience net round trip gains,  $G$ , of less than unity at the inversion level set by radiation at  $\lambda_0$ . If an injected signal at some  $\lambda = \lambda_i$  is present in the cavity just prior to threshold, it accelerates the buildup processes at  $\lambda_i$  and gives the photon flux at that wavelength a "head start" over all other wavelengths. If the head start is substantial enough, radiation contained within the bandwidth of the injected signal,

$\Delta\lambda_i$ , will dominate during the first few round trips where the gain is still exponential. After several round trips, however, the intensity of the pulse reaches the saturation regime where net round trip gains approach unity. At this point, the population inversion is clamped so that  $G(\lambda_i) \approx 1$ . If  $\lambda_i$  was not identical with  $\lambda_o$ , the wavelength with the intrinsically highest gain, radiation at  $\lambda_o$ , for the inversion set by the oscillation at  $\lambda_i$ ,  $\Delta N(\lambda_i)$ , will still have gains such that  $G(\lambda_o) > 1$  and will continue to grow at an exponential rate. Eventually, the photon flux at  $\lambda_o$  will approach that of  $\lambda_i$  and will start to saturate  $\Delta N$  towards a value less than  $\Delta N(\lambda_i)$ . Since the round-trip gains for  $\lambda_i$  will now be less than unity, lasing will be terminated at this wavelength and radiation at  $\lambda_o$  will take its place.

This temporal laser wavelength shift is of prime importance in the analysis and performance of injection-locked systems. In injection-locked, cavity-dumped systems, where the trapped radiation is regeneratively amplified throughout much of the pumping pulse, this effect is of particular importance. In this case, the injection-locked period (i.e. time before any spectral shift occurs) must be comparable to the pumping pulse duration to avoid sacrificing either output pulse energy or spectral purity. The amount of head start given the radiation at  $\lambda_i$  is clearly a function of  $|\lambda_o - \lambda_i|$  as well as of the injected pulse intensity.

Analyses performed by Ganiel et al. [17], and Flamant and Meyer [16] among others, have carefully considered the spectral evolution in a pulsed injection-locked system. These analyses yielded indications as to how the injection-locking performance of the system depends on such parameters

as the injected signal strength,  $E_i$ ; injected signal wavelength,  $\lambda_i$ ; injection-time (in cases where a pulsed MO is used), duration of the pumping pulse, and amplifier dispersion among others. The basic analysis technique involves numerically solving a set of coupled rate equations for the population and photon densities as a function of wavelength. Steady-state assumptions are usually made which, while generally applicable in most pulsed cases, are not appropriate for cavity-dumped systems where the intracavity fields are constantly increasing. The cavity-dumped oscillator will not reach a steady-state condition until the field intensities are well within the saturation regime.

In some cases the fine structure imposed by the Fabry-Perot resonances of the cavity is considered and in others it is ignored. Modal considerations are important in injection-locked CW lasers, where longitudinal mode matching is imperative in order to minimize injected signal strengths and in narrowband pulsed systems where minimal linewidths are desired [12]. In most pulsed applications, however, the desired linewidth reduction is not that great and only the spectral envelope of the radiation needed to be considered. For the cavity-dumped case, where output pulse durations are 10-100 times smaller than the oscillator outputs, they can be ignored for the reasons stated previously.

## **2.8 - Spectro-Temporal Evolution of Cavity-Dumped Amplifiers**

As indicated above, there are some fundamental distinctions between standard pulsed and cavity-dumped injection-locked systems. Because of this, analyses that have been previously performed on injection-locking of pulsed oscillators generally are not applicable for cavity-dumped systems.



**ORIGINAL PAGE IS  
OF POOR QUALITY**

These analyses have, nonetheless, yielded useful insights into the parameters which effect the ability to injection-lock a given amplifier. The basic concept employed in these analyses is that of detailing the temporal evolution of the photon flux densities emitted at various wavelengths by the dye in the amplifier. With particular regard to analyzing injection-locked systems, the interest is in describing the evolution of the photon density at a given wavelength,  $\lambda_i$ , versus that of the natural oscillation wavelength of the system,  $\lambda_o$ , when an external signal is injected into the system at  $\lambda_i$ . It will be assumed throughout these discussions that  $\lambda_i$  will be at least outside of the homogeneous linewidth of the dye so that the evolution of the photon fluxes at  $\lambda_o$  and  $\lambda_i$  may be treated independently. Although this assumption has little effect on the generality of the analysis, especially when a broadly tunable system is under consideration, cases when  $|\lambda_i - \lambda_o| < \Delta\nu$  will be discussed later.

One analysis that is particularly useful in describing the spectral shifts in injection-locked systems was presented by Meyer and Flamant [16]. Although their analysis, like others, makes several assumptions that are invalid for flashlamp-pumped, cavity-dumped systems (i.e. steady-state assumptions, neglect of time dependent loss mechanisms, etc.), it is general enough so that it can be adapted to highlight many of the factors which are peculiar to the system of interest. For this reason, it will be used as the basis for the theoretical analysis presented here.

Before considering a specific analysis of injection-locking, a more general analysis, describing the relative growth of radiation at two wavelengths, is presented. In this general case, the temporal evolution of the photon flux density,  $\phi(\lambda_o, t)$  at wavelength,  $\lambda_o$ , and time,  $t$ , after the

onset of lasing (at  $t = t_0$ ) is given by:

$$\frac{d\phi_o}{dt} = \frac{\phi_o}{T} [l\sigma_o \Delta N(\lambda_o, t) - l\sigma_o^T N_T(t) - \alpha_o] \quad [\text{II.8}]$$

where  $T$  is the cavity round trip time,  $l$  is the length of the dye cell,  $\sigma_o^T$  is the triplet state absorption cross section,  $\alpha$  is the fractional flux loss per round trip, and  $\Delta N$  and  $N_T$  are the time dependent population densities for the inversion ( $N(b) - N(a')$ ), and triplet state respectively. Here,  $\sigma_o \Delta N$ , with  $\sigma_o$  representing the net gain cross section ( $(\sigma_o^e - \sigma_o^a)$  in Figure 2.2), can be used to represent the system gain so long as the photon cavity lifetime,  $t_c = l/(c\alpha)$ , is long with respect to  $\tau_s$ . This assumption, although required for reasons detailed in Section 3.12, is not restrictive for most cavity-dumped dye laser systems. Because of the rapid thermalization of the dye molecules out of the lower lasing states,  $\Delta N(\lambda_o, t) \sim N_1(t)$ , where  $N_1(t)$ , the population density of the upper lasing state, is strictly a function of time. As this is true for all wavelengths, a combination of equation [II.8] with an identical equation at a second wavelength,  $\lambda_i$ , yields

$$\left(\frac{d\phi_o}{dt} \frac{1}{\phi_o}\right) - \left(\frac{d\phi_i}{dt} \frac{1}{\phi_i}\right) = \frac{1}{T} [l(\Delta N(t)(\sigma_o - \sigma_i) - N_T(t)(\sigma_o^T - \sigma_i^T)) - (\alpha_o - \alpha_i)] \quad [\text{II.9}]$$

If the population inversion density is assumed to be time invariant and the triplet state population small, then an integration of [II.9] from the onset of lasing, at  $t = t_0$ , to some later time,  $t$ , gives the basic spectro-temporal evolution equation

$$\frac{\phi_o(t)}{\phi_o(0)} = \frac{\phi_i(t)}{\phi_i(0)} e^{\frac{t}{T} [l \Delta N (\sigma_o - \sigma_i) - (\alpha_o - \alpha_i)]} \quad [\text{II.10}]$$

Although these assumptions are generally very poor, and will be removed later for a more general treatment, use of them yields a simple, but insightful, relation. For, by defining a spectral evolution time constant,  $\tau_{io}$ , as

$$\tau_{io} = T [l \Delta N (\sigma_o - \sigma_i) - (\alpha_o - \alpha_i)]^{-1} \quad [\text{II.11}]$$

the evolution equation can be written as in terms of a simple exponential decay

$$\frac{\phi_o(t)}{\phi_o(0)} = \frac{\phi_i(t)}{\phi_i(0)} e^{-\frac{t}{\tau_{io}}} \quad [\text{II.12}]$$

This basic expression has been used to describe a multitude of phenomena. Examples of applicable cases include, among others, describing broadband shifts in untuned oscillators, progressive narrowing in tuned cavities, and enhancement of intracavity absorption [16].

The particular interest here is in the application of this equation to the case of injection-locking. As such, the injected photon flux, coming from either a CW or pulsed laser, is introduced into the evolution equation by setting  $\phi_i(t) = [\phi_i'(t) + \Psi_i(t)]$  where  $\Psi_i(t)$  is the injected photon flux at  $\lambda_i$  and  $\phi_i'(t)$  is the emission naturally present in the oscillator at  $\lambda_i$  at any time  $t$  up to the time that injection occurs. For the case of a continuous injected signal, this substitution is valid for all  $t$ . In a pulsed case, however, the arrival time of the injected signal at the oscillator must

be taken into account. To maintain generality it will be assumed that the injected pulse arrives at the oscillator at some point,  $t=t_1$ , such that  $t_1 \geq t_0$ . (If the pulse arrives prior to the threshold point, it will be attenuated until threshold occurs by the dye and resonator losses. In this case, the fraction of the pulse that still exists at  $t=t_0$ , can be considered as the effective injected signal,  $\Psi_i$  at  $t=t_0$ ). From the onset of lasing at  $t_0$  to time  $t_1$  there is no injected signal and the basic evolution equation for  $\phi_i(t)$  can be used just as it had been for  $\phi_o(t)$  in equation [II.8]

$$\frac{d\phi_i}{dt} = \frac{\phi_i}{T} [l\sigma_i \Delta N(\lambda_i, t) - l\sigma_i N_T(t) - \alpha_i] \quad [\text{II.13}]$$

The solution to this differential equation for any  $t$  such that  $t < t_1$  is given below, in equation [II.14], where, again, the population inversion,  $\Delta N$ , is assumed to be time invariant and the triplet state population,  $N_T$ , small.

$$\phi_i(t) = \phi_i'(t_0) e^{\frac{t}{T} [l\sigma_i \Delta N - \alpha_i]} \quad [\text{II.14}]$$

Starting from  $t=t_1$ , however, the presence of the injected flux,  $\Psi_i$ , must be accounted for. The evolution equation, akin to that presented in equation [II.13], from  $t_1$  to an arbitrary time  $t_2$  such that  $t_2 \geq t_1$ , is then given by

$$\frac{d\phi_i(t)}{dt} \frac{1}{\phi_i'(t) + \Psi} = T^{-1} [l\sigma_i \Delta N - \alpha_i] \quad [\text{II.15}]$$

An integration of this expression from  $t_1$  to  $t_2$  then yields

ORIGINAL PAGES  
OF POOR QUALITY

$$\ln\left\{\frac{\phi_i(t_2)}{\phi_i(t_1)+\Psi}\right\} = \frac{t_2-t_1}{T} [l\sigma_i \Delta N - \alpha_i] \quad [\text{II.16}]$$

Exponentiating this expression and combining it with equation [II.14], which explicitly evaluates  $\phi_i'(t_1)$ , gives the evolution equation for  $\phi_i$  at  $t_2$ .

$$\phi_i(t_2) = (\phi_i(t_0) + \Psi) e^{\frac{-t_1}{T} [l\sigma_i \Delta N - \alpha_i]} \left[ e^{\frac{t_2}{T} [l\sigma_i \Delta N - \alpha_i]} \right] \quad [\text{II.17}]$$

The evolution equation for  $\phi_o(t_2)$  is simply obtained by solving equation [II.13] for  $\phi_o$ . Since no signal is injected at  $\lambda_o$ , the solution is given by equation [II.18] below and is valid for all  $t$  such that  $t \geq t_0$ .

$$\phi_o(t_2) = \phi_o(t_0) e^{\frac{t}{T} [l\sigma_o \Delta N - \alpha_o]} \quad [\text{II.18}]$$

Now, in order for the injection-locking to be effective, the ratio  $\phi_i/\phi_o$ , must be large at the time the radiation exits the cavity. An explicit expression for this ratio is obtained by combining equations [II.17] and [II.18].

$$\frac{\phi_i(t_2)}{\phi_o(t_2)} = \left( \frac{\phi_i'(t_0) + \Psi e^{\frac{-t_1}{T} [l\Delta N\sigma_i - \alpha_i]}}{\phi_o(t_0)} \right) \left[ e^{\frac{-t_2}{T} [l\Delta N(\sigma_o - \sigma_i) - (\alpha_o - \alpha_i)]} \right] \quad [\text{II.19}]$$

It is clear from this relation that, in the absence of an injected flux, laser oscillation develops at that wavelength where the net gains are the largest. After the onset of oscillation, the flux density at  $\lambda_o$ , grows at an exponential rate with respect to the growth at all other independent wavelengths (represented by  $\lambda_i$  in [II.19]). The flux density at dependent

wavelengths (i.e. those within the homogeneously broadened linewidth of  $\lambda_0$ ) remains a constant fraction of that at  $\lambda_0$ . This value of this fraction is determined by the lineshape function. For independent wavelengths, however, the greater  $|\lambda_0 - \lambda_i|$  becomes, the larger the exponential term becomes, and the faster the relative growth at  $\lambda_0$  occurs. The only means, then, by which to induce lasing at any  $\lambda_i \neq \lambda_0$  is to introduce a sufficiently intense flux,  $\Psi_i$  into the cavity during the onset of oscillation. Although a more detailed discussion as to what constitutes a "sufficient" intensity will be presented in later sections, equation [II.19] can be solved for  $\Psi$  to determine the relative level of the injected flux required to maintain  $\phi_i/\phi_0$  at a desired value at a given point in time. Here, the required injected flux density would be given with respect to the intrinsic noise level in the cavity.

Equation [II.19] clearly indicates that even if lasing can be induced at  $\lambda_i$ , by the injection of an external flux, it will only be for a period of time determined by the relative growth rate. For this work, where regenerative amplification, is to occur throughout the  $\sim 1\mu\text{s}$  duration flashlamp pulse, maintenance of large evolution times places many constraints on the system design. The function of this theoretical analysis is to extract as many of these constraints as possible.

Although equation [II.19] provides a useful determination of how some factors affect the injection-locking process, it was based on some assumptions that are generally invalid for flashlamp pumped, cavity-dumped systems. Because of the approximately Gaussian profile of the flashlamp pumping pulse and saturation effects,  $\Delta N$ , contrary to the assumption previously made, is a strong function of time. It was also improper to

assume a negligible triplet state population as the intersystem crossing time,  $k_{ST} \sim 100-300$ ns, is comparable to the duration of the flashlamp pulse. If these assumptions are not made in the derivation of equation [II.14] then a more general form of the spectral evolution equation becomes

$$\frac{\phi_i(t_2)}{\phi_o(t_2)} = \left( \frac{\phi_i(t_0) + \Psi \left[ e^{-\frac{t_1}{T} \left( l\sigma_s \int_0^{t_1} \Delta N(t) dt - l\sigma_s \tau \int_0^{t_1} N_T(t) dt - \alpha_s t \right)} \right]}{\phi_o(t_0)} \right) \quad \text{[II.20]}$$

$$* \left[ e^{-\frac{t_2}{T} \left( l(\sigma_s - \sigma_s) \int_0^{t_2} \Delta N(t) dt - l(\sigma_s \tau - \sigma_s \tau) \int_0^{t_2} N_T(t) dt - (\alpha_s - \alpha_s) t \right)} \right]$$

One primary distinction between the cavity-dumped case, considered here, and standard pulsed systems is the fact that saturation effects assume great importance. The dependence of the evolution time on saturation effects can be made explicit by setting

$$\Delta N(t) = \frac{\Delta N^o(t)}{1 + I(t)/I_s} \quad \text{[II.21]}$$

where  $I(t)$  is the intensity of the laser oscillation,  $\Delta N^o(t)$  is the nonsaturated population inversion and  $I_s$  is the saturation intensity of the dye as defined in [II.5]. As  $I_s$  varies only slightly over the wavelength range of interest, it will be assumed to be constant. Substituting equation [II.21] into equation [II.20] yields a general form of the spectral evolution equation that is more appropriate for cavity-dumped systems

ORIGINAL PAGE IS  
OF POOR QUALITY

$$\frac{\phi_i(t_2)}{\phi_o(t_2)} = \frac{\phi_i(t_0) + \Psi \left[ e^{-\frac{t_1}{T} \left( l \sigma_i \int_0^t \frac{\Delta N^2(t)}{1+I(t)/I_s} dt - l \sigma_i \tau \int_0^t N_T(t) dt - \alpha_i \right)} \right]}{\phi_o(t_0)} \quad [\text{II.22}]$$

$$* \left[ e^{-\frac{t_2}{T} \left( l (\sigma_o - \sigma_i) \int_0^t \frac{\Delta N^2(t)}{1+I(t)/I_s} dt - l (\sigma_i \tau - \sigma_i \tau) \int_0^t N_T(t) dt - (\alpha_o - \alpha_i) t \right)} \right]$$

By making explicit the dependence of the evolution time on the intensity of the laser oscillation, one non-obvious result is revealed. The stronger the intensity of the intracavity fields become the greater the spectral evolution time from  $\lambda_i$  to  $\lambda_o$  becomes. The net result is that cavity-dumped systems, which quickly enter the saturation regime of the dye, should require weaker injected signal strengths to induce the same degree of injection-locking and tunability than standard flashlamp pumped systems.

Although numerically intractable, the spectro-temporal evolution equation [II.22] does indicate the effect that various parameters have on the injection-locking performance of the system. This performance is generally gauged by a factor,  $\rho$ , called the injection-locking efficiency, which is a ratio of the output flux within the bandwidth of the injected signal to the total output flux

$$\rho = \frac{\phi_i}{\phi_i + \phi_o} \quad [\text{II.23}]$$

Since  $\rho$ , which is related to  $\phi_i/\phi_o$  in equation [II.22], is a directly measurable quantity, it is used to relate empirical observations to the spectro-



temporal evolution equation and to determine which factors the injection-locking is most dependent on. The following sections will be devoted to analyzing these dependencies both from a theoretical and operational level. Specific interest will be given to those topics, such as system tunability and injected pulse energy requirements, which directly impact the objectives of this work and introduce constraints on the design of the system. Other topics sometimes considered in injection-locking studies, such as spatial mode control, will not be considered in great detail but will be mentioned later.

The observed variations of  $\rho$  as a function of parameter changes will only be qualitatively related to the evolution equation [II.22] presented in the last section. Actual predictions or fitting of experimental results are complicated by the sheer number of independent variables present in the equation. Many of these variables, themselves, such as  $I(t)$ ,  $\Delta N^o(t)$  and  $N_T(t)$  can only be described through complicated models which require numerous other relations and parameters. The only method of extracting reliable predictions of experimental results is through computer generated numerical solutions to [II.22]. Even then, however, the simulations that are performed will only be as valid as the models and estimates of these parameters. For the sake of this work, the important dependencies of the injection-locking performance will be determined experimentally. Estimates as to their accuracy can be obtained by using the less general (and less accurate) relations of equations [II.17] and [II.18]

## 2.9 - Injection Time Considerations

One factor that can be immediately deduced from equation [II.22] is the importance of the injection time,  $t_1$ , with respect to the point at which the amplifier achieves threshold,  $t_0$ . Clearly, because the ratio,  $\frac{\phi_0}{\phi_i}$ , increases exponentially as a function of time, the initial conditions encountered for injection at  $t_1$  are different than those at  $t_0$ . As  $t_1$  is increased the impact that a given injected flux density will have on the development of laser oscillation in the amplifier decreases. This effect is explicitly accounted for in equation [II.22] by the exponential coefficient to  $\Psi$ , the injected flux density. As expected, the optimal injection time occurs at  $t_0$ . For systems with a CW master oscillator this is not a concern as the injected signal is certain to be present when the amplifier achieves threshold. This is, however, not the case with pulsed MO systems. In these cases the injected signal must be timed so that it arrives at the amplifier as close to the threshold point as possible. If it arrives after threshold, the exponential "damping" of the injected signal strength reduces the probability of sustaining the injection-locked period for a sufficiently long time. On the other hand, if it arrives prior to threshold, its effectiveness will also be exponentially damped by the absorbing dye solution and the optical cavity losses. Careful synchronization of the two laser systems is, thus, imperative.

In order to examine how this dependency will effect the system of interest in this work, a rough model of the growth of the photon fluxes at both  $\lambda_i$  and  $\lambda_o$  will be given for cases where  $t_1$  is varied with respect to the peak of the flashlamp pumping pulse. Generalized version of equations

[II.17] and [II.18] will be used for calculating the various flux densities as a function of time. In this model,  $\Psi$  is assumed to provide an instantaneous addition of photons at  $\lambda_i$  to the radiation naturally present in the amplifier cavity. Because of the inherent difficulty of accounting for saturation, triplet state and other time dependent effects, this model will only account for the flux growths within 100ns of threshold where these effects are still relatively insignificant. Neglecting saturation effects, the population inversion,  $\Delta N_o$ , is assumed to follow a standard normal Gaussian profile with a FWHM of 300ns where

$$\Delta N(t) = \Delta N_p e^{-(t-t_0)^2/2\sigma^2} \quad \text{[II.24]}$$

The peak inversion,  $\Delta N_p$ , used of  $7.5 * 10^{14} \text{ cm}^{-3}$  was derived from measurements of the small signal gain described in Section 3.4. The evaluation of  $\int_{t_0}^{t_2} \Delta N(t) dt$  is given by the error function,  $\text{erf}(t_2 - t_0)$  where the commonly tabulated  $\text{erf}(t)$  is defined as

$$\text{erf}(t) = \frac{2}{\sqrt{\pi}} \int_0^t e^{-y^2} dy \quad \text{[II.25]}$$

The development of the photon fluxes as a function of time for the case where  $t_1$  precedes the peak of the pumping pulse by 500ns is given in Figure 2.3. For this, and the cases that follow, the parameters substituted into equations [II.17] [II.18] were  $\lambda_o = 590\text{nm}$ ,  $\lambda_i = 600\text{nm}$ ,  $l = 40\text{cm}$ ,  $\alpha_o = \alpha_i = 0.07$  and the cavity transit time,  $T = 10\text{ns}$ . The values of the gain cross-sections,  $\sigma_o$  and  $\sigma_i$ ,  $1.5 * 10^{-16} \text{ cm}^2$  and  $1.3 * 10^{-16} \text{ cm}^2$  respectively, as well as the ratio of  $\phi_o(t_0)$  to  $\phi_i(t_0)$  were obtained from

Figure 2.2.

For the cavity-dumped case considered here, substantial laser oscillation will not develop in the amplifier until the cavity  $Q$  is switched to a high value. Although this point might occur after a threshold inversion has been achieved, any laser radiation present prior to  $Q$  switching is limited by the polarization-sensitive optics to only two passes through the dye cell. After the second pass the radiation exited the cavity. This "two-pass lasing" will be discussed in more detail in Chapter 3. Thus, because of the low level of radiation present inside the amplifier cavity prior to the initial  $Q$ -switching,  $t_0$  will be identified as the point at which the cavity  $Q$  is switched high. The initial conditions for injection-locking are then essentially independent of the cavity  $Q$ -switching time.

Although, as will be described later, the arrival of the injected pulse was carefully synchronized to the  $Q$ -switching time, Figures 2.3 - 2.5 indicate the consequences of making  $t_1 - t_0$  too large. From Figure 2.3 it is clear that, in the absence of an injected signal ( $\Psi=0$ ),  $\phi_o$  will grow exponentially with respect to  $\phi_i$ . In fact, in this relatively low gain region well before the peak of the pumping pulse, radiation at  $\lambda_o$  dominates that at  $\lambda_i$  by an order of magnitude after only  $\sim 120$ ns. If however, a pulse, where  $\Psi=10\phi_o(t_1)$ , is injected into the cavity at  $t_1 = t_0$  a dramatically different result is obtained. Radiation at  $\lambda_i$ , with the "head start" provided by  $\Psi$  dominates that at  $\lambda_o$ . This domination, however, is only for a finite period of time for, as Figure 2.3 indicates,  $\phi_i/\phi_o$  steadily decreases as a function of time. For  $t_2 \sim t_1$ , in Figure 2.3, the ratio,  $\phi_i/\phi_o$  was  $\sim 10$ , but after 120ns this value had been reduced to a factor of 2. If

ORIGINAL PAGE  
OF POOR QUALITY

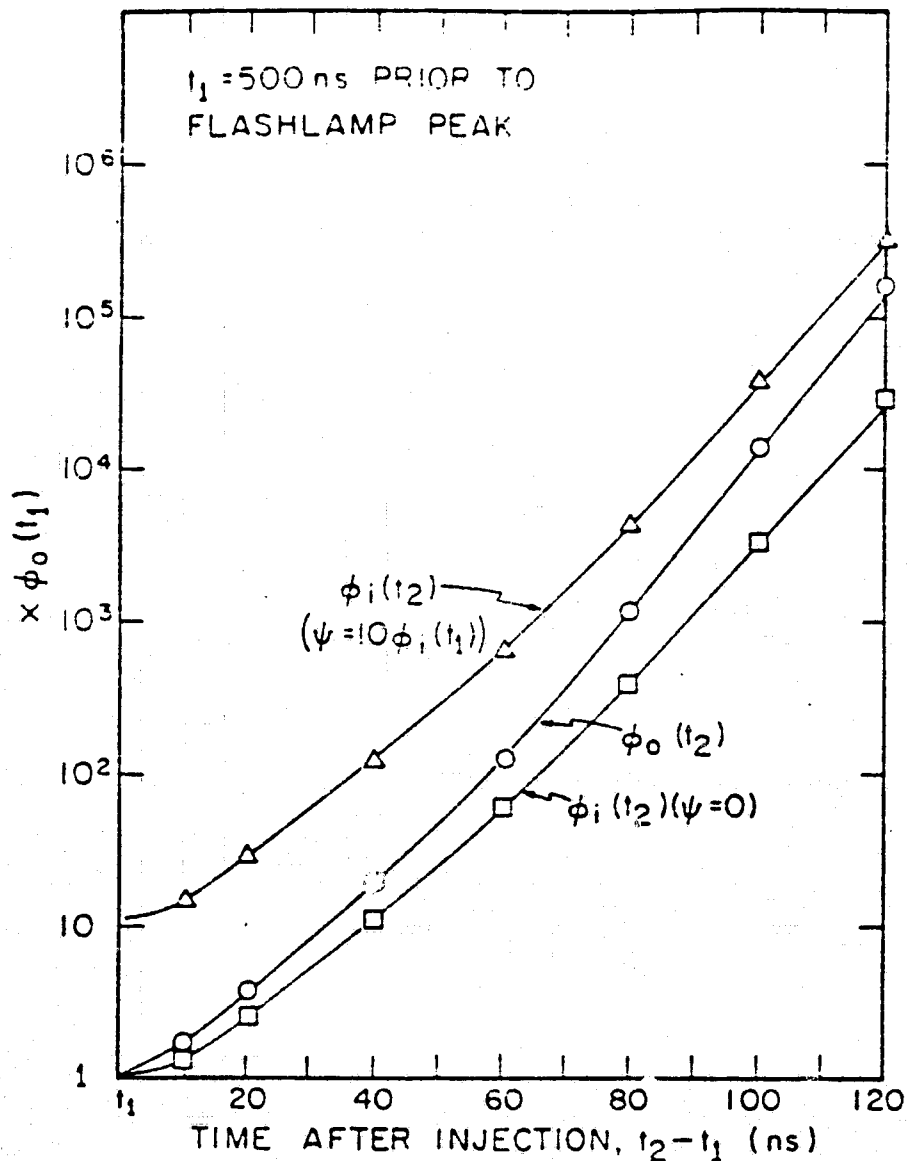


Figure 2.3: Relative growth of the photon flux at the natural wavelength of the cavity,  $\phi_0$ , and at the wavelength of the injected pulse,  $\phi_i$ , with and without ( $\psi=0$ ) an injected pulse for injection occurring 500ns prior to the peak of the flashlamp pumping pulse.

ORIGINAL PAGE IS  
OF POOR QUALITY

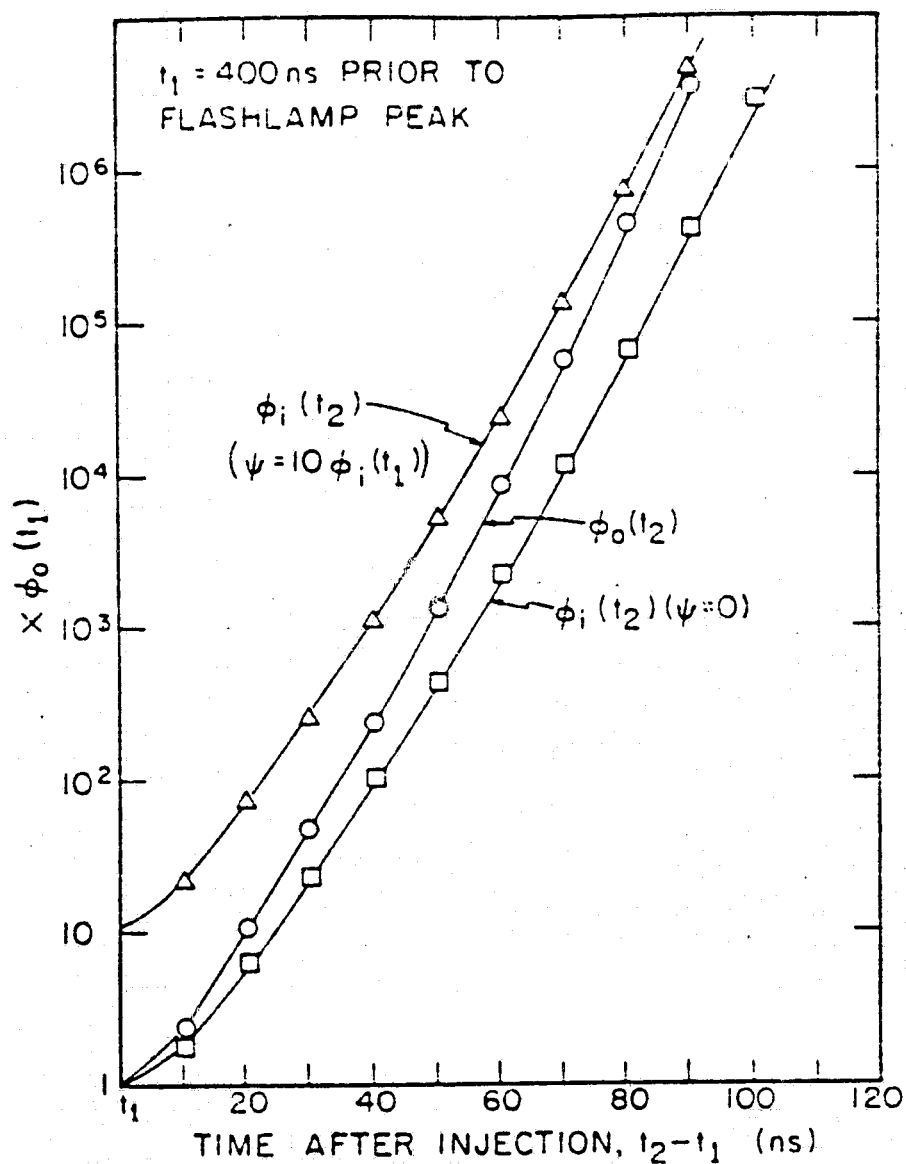


Figure 2.4: Relative growth of the photon flux at the natural wavelength of the cavity,  $\phi_0$ , and at the wavelength of the injected pulse,  $\phi_i$ , with and without ( $\psi=0$ ) an injected pulse for injection occurring 400ns prior to the peak of the flashlamp pumping pulse.

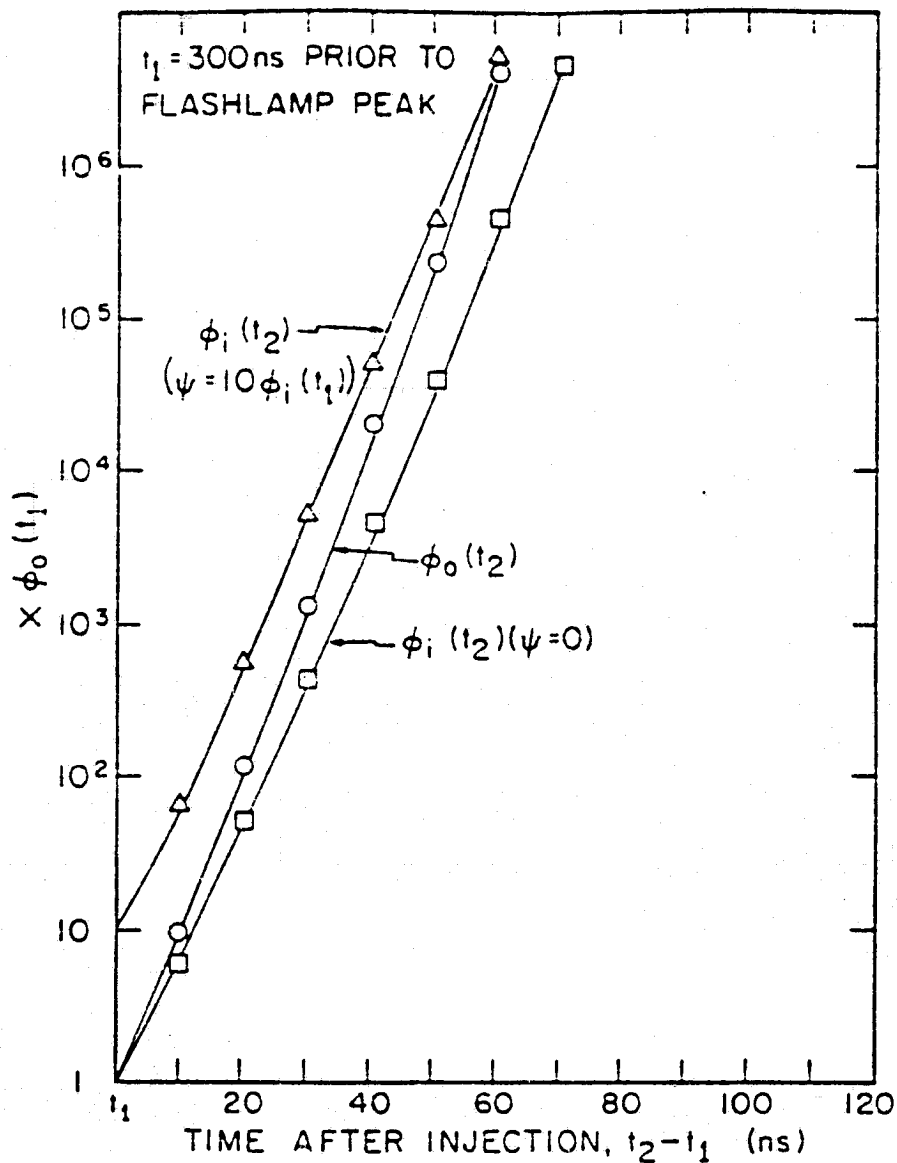


Figure 2.5: Relative growth of the photon flux at the natural wavelength of the cavity,  $\phi_0$ , and at the wavelength of the injected pulse,  $\phi_i$ , with and without ( $\psi=0$ ) an injected pulse for injection occurring 300ns prior to the peak of the flashlamp pumping pulse.

injection occurs 100ns later, at a point 100ns prior to the peak of the flashlamp pulse, the injected signal arrives during a higher gain period where the intrinsic noise level is greater. The development of laser radiation, because of these higher gains, occurs more rapidly at both  $\lambda_i$  and  $\lambda_o$ . The first 100ns of this development is traced in Figure 2.4. In this case, the more rapidly growing  $\phi_o$  requires only 90nsec to overcome the effects of the injected flux and dominate the flux present at  $\lambda_i$ . It should be noted that the injected flux level has been scaled by the intrinsic noise level in the cavity at the point of injection. Thus, the actual injected flux, in this case, is even larger than that considered in the case depicted by Figure 2.3. In Figure 2.5, which depicts the development of the radiation for injection occurring only 300ns prior to the peak of the flashlamp pulse, the situation is worse. Radiation at  $\lambda_o$  dominates that at  $\lambda_i$  at a point only 60ns after injection.

As Figures 2.3 - 2.5 indicate, the period of time for which the radiation at  $\lambda_i$  dominates that at  $\lambda_o$  is a function of a number of parameters. As expected, these parameters include the injected signal strength,  $\Psi$ , the injection time, the gain of the system, the duration of the pumping pulse and the difference  $|\lambda_o - \lambda_i|$ . These figures also illustrate that, for a given system and a given choice of  $\lambda_i$ , the injected signal strength is the only variable that can be altered to increase the evolution time. The effect of doing this, however, can be substantial. For example, by setting  $\Psi = 10^6 \phi_o(t_1)$  in the cases considered in Figures 2.3 - 2.5, the evolution times in each of these cases would have been pushed well beyond 100ns. As will be shown in the following section, injected flux densities of this magnitude are not unreasonable.



## 2.10 - Injected Signal Strength Requirements

Although not explicitly mentioned in the analysis presented in Section 2.8, the injected power requirement is a key parameter in the analysis of injection-locked systems. The power requirement refers, in this case, to the minimal intensity of the injected signal required to completely (i.e.  $\rho=1$ ) injection-lock the amplifier and maintain it for the period of regenerative amplification. The specific intensity required depends greatly on both the characteristics of the injected signal and on those of the amplifier (e.g. its dispersive properties and the duration of the amplification period.) For example, Turner et al. found that they required 30mW from a CW MO to injection-lock their flashlamp pumped dye laser amplifier [11]. By locking onto a single longitudinal mode Blit et al. only required a  $\sim 1$ -10mW CW injected signal [12]. Using a pulsed MO, on the other hand, Megie and Flamant found that they required  $\sim 10\text{W}/\text{cm}^2$  to completely injection-lock their flashlamp pumped amplifier [15].

It would be extremely difficult to predict in advance the requirements that a MO would have to meet in order to injection-lock a given amplifier without a more general means of estimating the the required injected signal strength. Equation [II.22] could be used if a knowledge of all of the parameters was available. One parameter that is generally unpredictable, however, is  $\phi(0)$ . A consequence of [II.22] though is that the basic requirement for injection-locking is that the power level of the injected radiation exceed that of the spontaneous emission (noise) in the forced oscillator. The injected signal then acts as a seed, providing an additional photon flux at the injected wavelength so that radiation at  $\lambda_i$  will have a head-start in "winning" the mode competition at the onset of lasing. It is

conceivable, however, that in order to provide for a sufficient "head start" (i.e. so that the system could be locked for the duration of the pumping pulse) that the injected flux be significantly larger than the fluorescence noise it competes with. In fact, Megie and Flamant found that they required about 1000 times the intrinsic noise level in order to completely injection-lock the amplifier [15]. The nature of the dependency of  $\rho$  on the injected signal strength will be discussed later. However, a lower bound on the required MO signal strength to, at least, initiate injection-locking can be obtained by estimating the strength of the fluorescence noise with which it has to compete to establish laser oscillation.

One model of this process was presented by Ganiel et al. in [8] and [17] where the injected radiation was treated as an equivalent noise input signal,  $\Psi(\lambda)$ . As such,  $\Psi(\lambda)$  is defined as the input photon flux per unit wavelength for which the rate of stimulated emission equals the rate of spontaneous emission into the same spatial mode:

$$\sigma_e(\lambda) \Psi(\lambda) N_1 = E(\lambda) \tau_s^{-1} g N_1 \quad [\text{II.26}]$$

In this relation,  $E(\lambda)$  is defined as the  $S_1 \rightarrow S_0$  fluorescence spectrum normalized so that:  $\int E(\lambda) d\lambda = \Phi$  where  $\Phi$  is the quantum efficiency;  $\sigma_e(\lambda)$ , the stimulated emission cross section, is given by:

$$\sigma_e(\lambda) = \frac{[\lambda^4 E(\lambda)]}{8\pi c \eta^2 \tau} \quad [\text{II.27}]$$

and  $g$  is that fraction of the spontaneous emission which is emitted into the solid angle which has the potential of being coupled back into the medium and developing into laser oscillation. Solving for  $\Psi(\lambda)$  yields:

$$\Psi(\lambda) = \frac{8\pi\eta^2 g c}{\lambda^4} \quad [\text{II.28}]$$

which was identified as the equivalent noise input signal at a given wavelength,  $\lambda$ . The "noise" in direct competition with the injected signal can be at any wavelength,  $\lambda_o$ , such that  $G(\lambda_o) \geq G(\lambda_i)$ . A homogeneously broadened laser medium (such as organic dyes) is assumed. Their analysis then concluded that the minimal injected signal intensity,  $\Psi_i$  (photons  $\text{sec}^{-1} \text{cm}^{-2}$ ), is determined from:

$$\sigma_e(\lambda_i)\Psi_{\min} = \int_{\delta\lambda} \sigma_e(\lambda)\Psi(\lambda)d\lambda \quad [\text{II.29}]$$

where the range of integration,  $\delta\lambda$ , includes all competitive wavelengths. Using the defining expression for  $\Psi(\lambda)$  given above, the final expression for the required injected signal strength, in photons/sec is

$$\Psi_{\min} = 2c\eta^2 g \int [\sigma_e(\lambda)/\sigma_e(\lambda_i)]d\lambda \quad [\text{II.30}]$$

All that is needed to obtain a numerical evaluation of  $\Psi_{\min}$  is an evaluation of  $g$ . In their work, Ganiel et al. calculated  $\Psi_{\min}$  for two specific cases one a single fundamental Gaussian mode ( $TEM_{00}$ ) and the other a highly multimode case. For high-energy applications, where generally large active mediums are to be injection-locked, the multimode case is of particular interest. In this case,  $g$  can be estimated as  $\Delta\Omega/4\pi$ , where  $\Delta\Omega$  is the solid angle subtended by the opening of one side of the dye cell at a distance of  $l$ , the cavity length, from the other end of the dye cell.  $\Psi_{\min}$  then becomes:

$$\Psi_{\min}(\text{multimode}) = 2c \eta^2 \int [\sigma_e(\lambda') / \sigma_e(\lambda)] (\pi r^2 / \lambda L)^2 d\lambda / \lambda^2 \quad [\text{II.31}]$$

In order to provide a numerical example, the specific flashlamp pumped system that was used in this work will be considered. The relevant parameters are  $L = 3\text{m}$ ,  $\lambda = 590\text{nm}$ , and  $r = 0.45\text{cm}$ . We will assume, for the moment that  $\lambda_i \sim \lambda_o$  so that  $\sigma_e(\lambda') \sim \sigma_e(\lambda_i)$  for all relevant  $\lambda$ . A competitive "noise" bandwidth of  $5\text{nm}$  will also be assumed. Using this information  $P_{\min}$  can be approximated to be  $60\text{W}$ . As will be shown later, this figure is within an order of magnitude of the actual amount of power required to injection-lock the system. It should also be noted that in this multimode case the relation for  $P_{\min}$  is dependent on the geometry of the forced oscillator. Specifically,  $P_{\min}$  is proportional to the square of the effective Fresnel number of the amplifier. This dependency was also experimentally confirmed.

An injected signal strength of  $P_{\min}$ , however, only equals the intrinsic fluorescence noise level in the amplifier. Although this should provide the initial buildup of radiation at  $\lambda_i$  required to injection-lock the amplifier, it is doubtful if this "head start" would be sufficient enough to stave off the development of  $\phi_o$  (which grows exponentially with respect to  $\phi_i$ ) for the entire duration of the pumping pulse. In such a case,  $\phi_o$  will equal  $\phi_i$  at some point prior to cavity-dumping. From this point until the amplified pulse is extracted  $\phi_i$  will decrease at an exponential rate. Only a percentage of the cavity-dumped pulse energy would then be at  $\lambda_i$ , as desired, and  $\rho$  would be less than unity. Thus,  $\rho$  is dependent on both  $\Psi_i$ , which provides the "head start", and  $\tau_{i0}$  which determines the growth rate of  $\phi_o$  with respect to  $\phi_i$ ; thereby determining how long the "head start" has to

last. By performing a numerical analysis based on a set of coupled rate equations for the population and photon flux densities, Ganiel et al. were able to show the a spectral shift as a function of time and wavelength [17]. Their results graphically illustrate the effect discussed above. The spectro-temporal evolution equation can also be used to roughly determine the required signal intensity once the "noise" level has been determined. With the proper parameters, it will yield the ratio that the injected signal strength has to maintain over the noise level in order to attain a given value of  $\rho$  at a given wavelength,  $\lambda_i$  for a given period of time,  $t$ .

### 2.11 - Tunability of Injection-Locked Systems

The tunability of injection-locked systems is a feature that is of prime concern for many applications where high-energy but narrowband pulses are required. The limitations on the tuning range arise as a consequence of the spectro-temporal evolution equation discussed in Section 2.8. As equation [II.22] indicated, complete ( $\rho=1$ ) injection-locking is only attainable when the evolution time is at least equal to the duration of the pumping pulse. Generally, however, this is not the case in untuned amplifiers unless  $\lambda_i \sim \lambda_o$ . Even for small values of  $|\lambda_o - \lambda_i|$  (i.e.  $\sim 2\text{nm}$ ), laser emission at  $\lambda_o$  has had enough time, by the termination of the pumping pulse, to develop into a significant fraction of the total pulse energy. As  $|\lambda_o - \lambda_i|$  increases further, the evolution time decreases until it is much less than the flashlamp pulse duration. At this point, in order to keep high injection-locking efficiencies, cavity-dumping must occur before the net gains have been fully saturated (at a sacrifice in pulse energy). This reduction in  $\rho$  as an increasing function of  $|\lambda_o - \lambda_i|$  has been observed in

many investigations of pulsed injection-locked dye lasers.

The inclusion of an intracavity tuning element can, however, simultaneously extend the tuning range and eliminate any broad-band background radiation. Ideally, even with a wide-band tuner,  $\lambda_o$  could be made very close to  $\lambda_i$ . The function of the element would be to eliminate wavelengths for which the spectral evolution time is small and thus suppress the possibility of spectral evolution during the regenerative amplification period. This technique was proven successful by Turner et al. who, by including an *ADP* electro-optic birefringent filter into the amplifier cavity, obtained narrowband injection-locking over the entire dye emission profile [11].

Clearly, the narrower the pass-band of the tuner, the longer that the evolution time can be made. The inherent problem with the use of narrowband tuners in cavity-dumped systems is that they generally have large insertion losses. Since cavity-dumped system efficiencies are limited by optical cavity losses [6], the inclusion of most narrowband tuners would reduce obtainable pulse energies. Wide-band tuners such as that used by Turner et al. are acceptable as long as they can be tuned so that  $\lambda_o$  roughly equals  $\lambda_i$ . As will be demonstrated later, the use of low-loss, wide-band tuners such as birefringent (Lyot) filters and prisms provide sufficient selectivity so that even high-power cavity-dumped amplifiers can be injection-locked over a wide range of wavelengths.

### **2.12 - Triplet State Effects**

In the analysis presented above, no mention was made of the effects

of the triplet states. Because the intersystem crossing time,  $k_{ST}$ , is only  $\sim 100$ - $300$ ns, these effects can only be neglected in short pumping pulse systems. For most flashlamp pumped systems, however, with pumping pulses in the microsecond regime, the triplet states have a significant impact on the performance of the system. With injection-locked systems in particular, there are two primary effects. First, a non-zero triplet state population provides a loss mechanism to the laser radiation and to the conversion efficiency of pump to laser photons due to  $T_1 \rightarrow T_n$  absorption. Thus as  $N_T$  increases with time net gains decrease. This, of course, affects the performance of all long-pulse or CW dye laser systems.

Of specific importance to injection-locked systems, however, is the wavelength dependency of this loss mechanism as it directly impacts on the spectral evolution time. As illustrated in Figure 2.2,  $\sigma_T$  is a strong function of wavelength in R6G as it decreases rapidly for  $\lambda < 600$ nm. The evolution time is a function of the difference between the total round-trip losses at  $\lambda_i$  and  $\lambda_o$ . Being wavelength dependent, the triplet state losses should thus, alter the evolution time. For example, if the triplet state losses become increasingly greater at  $\lambda_o$  than at  $\lambda_i$ , injection-locking should be maintainable for a longer period of time due to the resulting increase in the evolution time. This increase reflects the gradual shift in  $\lambda_o$ , away from its original value, towards  $\lambda_i$ . Of course, the opposite situation, where the evolution time decreases, is also possible.

An illustration of this effect was presented by Ganiel et al. [17] in which a specific example was considered. The cavity photon flux was computed as a function of time at two wavelengths  $\lambda = 590$ nm and  $585$ nm. Initially, injection into the R6G dye laser amplifier was assumed to be at

590nm ( $=\lambda_0$  for short pulsed systems). Neglecting triplet state effects, injection-locking was sustained throughout the duration of the pumping pulse as  $\lambda_o(t)=\lambda_i$  for all  $t$ . When the time-dependent triplet state losses were considered, however, with  $\lambda_0$  gradually shifting toward the lower wavelengths, the increased gain experienced at these wavelengths, specifically at the 585nm line which was considered, caused a shift in the lasing wavelength from 590nm to 585nm. The locking period was, in this case, less than the duration of the flashlamp pumping pulse. When the injected signal was at 585nm, however, and the "head start" provided the photon flux at 585nm was great enough so that the injection-locked period was greater than the evolution time, injection-locking could be maintained throughout the duration of the pumping pulse. standard flashlamp pumped systems.



## CHAPTER 3 - DESIGN AND OPERATION OF THE CAVITY-DUMPED CFP DYE LASER

### 3.1 - Introduction

Cavity-dumping is commonly noted as being the most efficient technique for extracting high-energy, nanosecond duration pulses from flashlamp pumped dye laser systems. The high efficiency can be attributed to the fact that the laser radiation, being totally trapped inside the resonator, will grow in intensity until the net gains have been fully saturated. At this point, where no further increase in pulse energy is possible, the radiation is "dumped" from the system resulting in a high-energy pulse whose duration is equivalent to the cavity round-trip time,  $t = l/c$  (for ring lasers) where  $l$  is the cavity length. In order to optimize system performance, the radiation must be allowed to saturate the gain of the dye as much as possible. The primary limitation on its ability to do this (assuming a sufficiently intense pumping source) is imposed by the optical resonator losses. A minimization of these losses is, thus, imperative for good system performance. In an effort to keep resonator losses low, a polarization-sensitive cavity-dumping scheme was chosen as it required few intracavity optical elements.

This chapter will concentrate on the development of a basic cavity-dumped, flashlamp pumped dye laser oscillator. Included will be detailed descriptions of the required resonator components, detection equipment,

and system operation. The objective here was simply to demonstrate the generation of temporally "clean", high-energy pulses and to study the characteristics of the system so as to optimize its performance in this respect. As such, the variation in system performance as a function of such parameters as dye concentration, dye solution and resonator optics was investigated. The point in time at which cavity-dumping occurred (i.e. the "extraction" time) was also found to be a critical parameter that effected both the temporal profile and energy of the output pulses.

### 3.2 - Flashlamp Design and Operation

The efficient generation of high-energy pulses from dye lasers requires an intense excitation source. The flashlamp pumping system used in this work, to provide this excitation, was commercially manufactured by ILC Technology Inc. and was indicative of typical high-energy commercial units available at the time. It consisted of an ILC Model DYB charging and triggering network together with an ILC Model DYH-15 flashlamp housing. The flashlamp housing coupled the 40cm x 1.1cm dia. inner region of a 350J coaxial, xenon gas flashlamp to the dye circulation system.

The charging/triggering circuitry found in the DYB assembly is shown in Figure 3.1. A positive ground 0-30kV supply was used to charge a low-inductance,  $0.7 \mu\text{F}$  capacitor,  $C_1$ , through a network of charging resistors,  $R_1$ . In addition to limiting the charging current,  $R_1$  also served as a high-voltage fuse. During normal operation, at charging currents of roughly 100mA,  $R_1$  would dissipate  $\sim 20\text{W}$ , well below its maximum rating of 350W. If, however, the lamp was to break down, and form a short

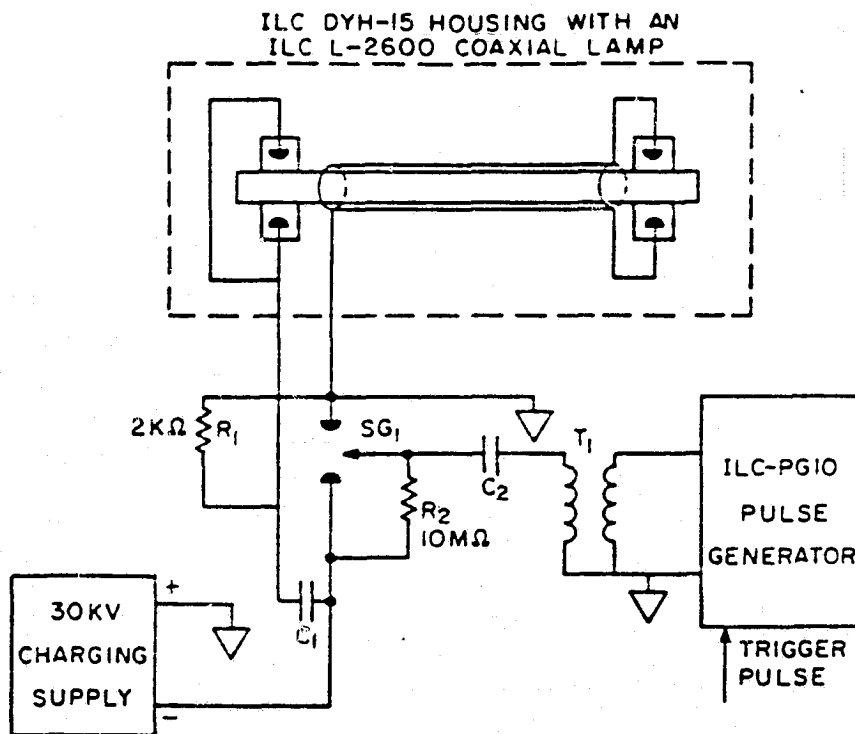


Figure 3.1: Flashlamp Trigger Circuitry

circuit, the current surge through  $R_1$  would be  $\sim 20A$  and the instantaneous power dissipation of  $\sim 300kW$  would destroy the resistors. This action would prevent more than one pulse from being discharged through a broken lamp. The  $C_1$ /anode and cathode-ground/ spark-gap connections were made by copper strip lines to minimize circuit inductance.

The flashlamp discharge was initiated by a triggered spark-gap switch,  $SG_1$ . An external trigger signal, amplified by the high-voltage trigger transformer and pulse forming network shown in Figure 3.1, induced conduction across the pressurized spark-gap. This caused the high-voltage stored across  $C_1$  to be applied directly across the flashlamp. The high-voltage across the lamp connections rapidly ionized the xenon gas forming a conduction path through which the energy stored on  $C_1$  could be discharged. The duration of the flashlamp discharge is directly dependent on the the value of  $C_1$ . ILC studies have shown that use of a  $1.0\mu F$  capacitor at 25kV yielded a discharge pulse width of  $\sim 0.8\mu sec$  (FWHM) while use of a  $0.2\mu F$  capacitor at a similar voltage produced output pulse widths of  $\sim 0.4\mu sec$ . In general, the discharge duration was found to be roughly proportional to  $\sqrt{C_1}$  [45].

The spectrum of a coaxial flashlamp discharge approximates that of a blackbody radiator whose temperature is typically between  $15,000-30,000^\circ K$  [46]. The exact temperature is dependent on a variety of factors which include lamp area, operating voltage and discharge duration. A crude estimate of the effective blackbody temperature of the lamp can be obtained through use of the Stefan-Boltzman relation by equating the power generated per unit area by the lamp,  $P_l = KCV^2/2tA$ , to that generated by a blackbody,  $P_{bb} = \sigma T^4$ . In these relations,  $K$  is the percentage

of energy stored by  $C_1$  that is actually dissipated in the discharge.  $t$  is the duration of the discharge,  $A$  the radiating area,  $\sigma$  is Boltzman's Constant and  $T$  is the blackbody temperature. Using values appropriate for the ILC system, where  $C = 0.7 \mu F$ ,  $V = 30,000 V$ ,  $t = 1.2 \mu sec$  (10% max.),  $A = \pi(24.9cm * (1.1cm + 1.3cm))$ , and  $K = 1$ , the effective lamp temperature was calculated to be  $26,000^{\circ} K$ . Wien's Displacement Law indicates that the peak emission wavelength of the lamp will then occur at  $\lambda = 110nm$ . The UV absorption properties ( $S_0 \rightarrow S_2$ ) of the dye will, thus, account for much of the excitation provided by this system.

### 3.3 - Dye and Coolant Circulation

In a coaxial configuration, the relatively cool dye solution is in direct contact with the hot inner wall of the flashlamp. The resulting thermal diffusion creates strong temperature gradients which generate turbulence in the dye stream and degrade the optical quality of the solution by increasing diffraction losses. If the thermally induced refractive index variation is large and the thermal diffusion rate rapid with respect to the duration of the flashlamp pumping pulse the losses can be significant enough to prematurely terminate laser action [47]. Minimization of this rate is especially critical in highly gain-saturated systems where a significant fraction of the laser pulse passes near the outer wall of the dye cell.

The thermal diffusion rate depends primarily on the thermal capacity of the dye solution and to a lesser extent on the dye flow rate and the pulse repetition rate. A high flow rate ( $\sim 10$  dye changes/sec) and a low repetition rate ( $< 1Hz$ ) help to maintain thermal equilibrium at the beginning of each pulse but have negligible effects during the  $\mu sec$  duration

pumping pulse. Alcohols, especially ethanol and methanol, the most commonly used solvents for flashlamp pumped dyes, typically have a large  $\frac{dn}{dT}$  ( $\sim 5.5 \times 10^{-4}$  per  $^{\circ}\text{C}$  at  $25^{\circ}\text{C}$ ). Water is a much more suitable solvent from a thermal perspective, as it has a much greater thermal capacity and a  $\frac{dn}{dT}$  one third as large as that of most alcohols. Although many dyes do not readily dissolve in water, water-alcohol mixtures have been commonly used.

The absorption/emission process, as described earlier, also contributes a significant amount of heat to the system. About 65% of the energy of each absorbed ultraviolet ( $\lambda \sim 240\text{nm}$ ) photon will be dissipated by the dye molecule as heat. For absorption in the visible,  $\sim 10\%$  of the absorbed energy will be released as heat. Dye cells made with UV absorbing glass or filters have been used to prevent the heating due to UV absorption in systems where high repetition rates or dye lifetimes are major concerns. However, since much of the excitation provided by the coaxial flashlamp is ultraviolet, UV filtering would substantially reduce the excitation rate. Such a reduction in the pumping rate would severely diminish the high-energy capacity of the system.

The use of a triaxial configuration is one technique which has been used to isolate the dye solution from directly contacting the flashlamp. In these experiments, a triaxial configuration was simply attained by the insertion of a 0.9cm I.D. x 1.1cm O.D. UV-grade quartz tube through the dye cell. This created an annular chamber which separated the dye solution, that was circulated through the quartz tube, from the inner wall of the flashlamp. A coolant, typically deionized water which has a large

thermal capacity and is transparent to the pumping radiation, was then circulated through this chamber for added thermal isolation. Occasionally, however, a UV absorbing fluid (for reasons described above) or a spectral transfer dye is circulated in place of or together with the coolant. There is an inherent disadvantage with the use of a triaxial configuration, however. The volume occupied by the triaxial adapter (i.e. the quartz tube) and the coolant would otherwise be occupied by dye solution. In highly gain-saturated systems, even dye molecules near the edge of the dye cell contribute energy to the pulse. Thus, the trade-off for reducing thermal diffraction losses with this technique is that of a smaller active dye volume. It was, nonetheless, felt that the added thermal stability, even at the expense of a slight reduction in pulse energies, would ease the characterization of system performance. Once fully characterized, the triaxial adapter could be removed.

A dual circulation system (Candela DCC-30L), shown in Figure 3.2, was used to circulate both the dye and coolant solutions. This system minimized thermal gradients by maintaining the dye solution (which was also filtered to remove any impurities or bubbles) and the coolant at nearly equal temperatures through use of a heat exchanger. The heat exchanger itself was immersed in a tap-water reservoir to cool both solutions to near room temperatures.

As mentioned above, a spectral transfer dye could be circulated in place of the deionized water in the coolant jacket. These dyes would absorb the UV flashlamp radiation and emit visible radiation that would be absorbed by the Rhodamine 6G laser dye. In addition to being effective in reducing the thermal effects caused by UV absorption, the transfer dye

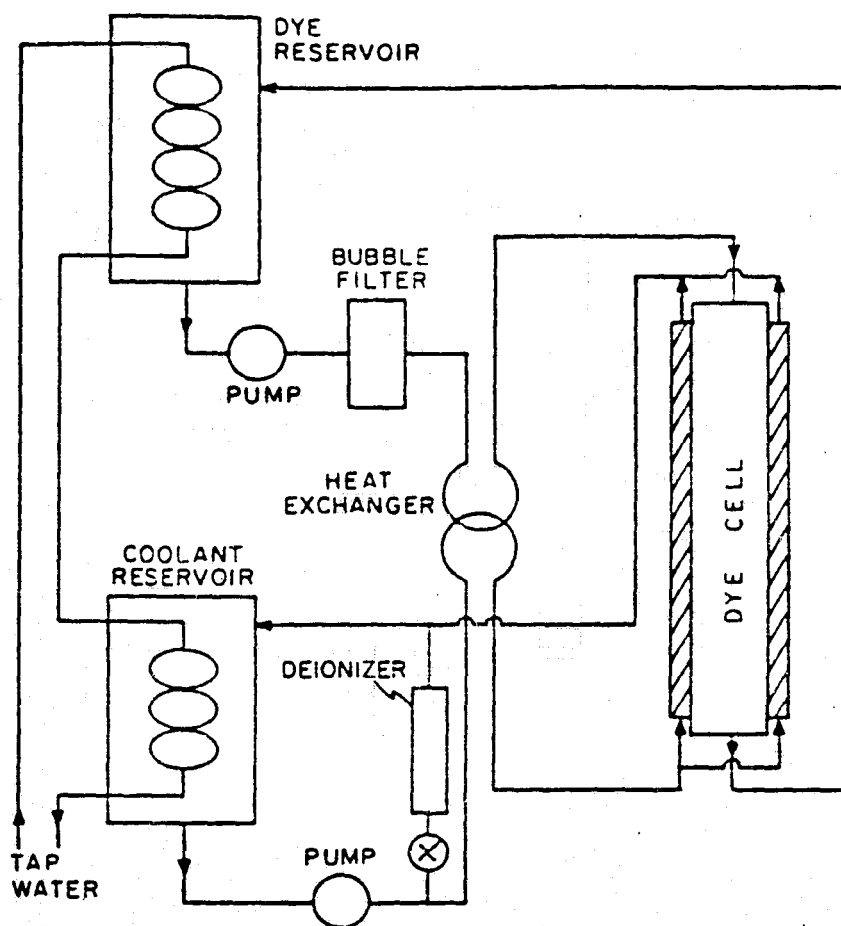


**Figure 3.2: Dye and Coolant Circulation System**



could also be used to convert flashlamp radiation at wavelengths that are not strongly absorbed by the R6G to visible ones that are. Because of the number of requirements that an effective transfer dye would have to meet it is extremely difficult to find one that actually increases system efficiency. For example, the quantum efficiency of the transfer dye must be near unity to avoid attenuating the pumping radiation. The absorption and emission profiles must also be carefully matched to that of the laser dye [48,49].

An investigation into the use of spectral transfer agents was made using a solution of 7-hydroxycoumarin dissolved in a 1:1 mixture of water and methanol. This substance appeared most promising as it possessed a high quantum efficiency ( $\Phi=0.98$ ) and its spectral profiles were suitable for a transfer agent for R6G. Despite this, output pulse energies decreased as an increasing function of the transfer dye concentration. The most likely explanation, which would be applicable for any spectral transfer attempt in a triaxial flashlamp pumped system, is that the transfer dye redirects some of the pumping radiation out of the system. When the absorbed UV flashlamp radiation is reemitted by the transfer dye, it is emitted in a random direction. Thus, flashlamp radiation, initially directed into the dye, could be reradiated out of the system, thereby again effectively decreasing the pumping rate. Although not attempted, one investigation that might have proved successful in this respect was that of dissolving the transfer dye into the laser dye solution.

### 3.4 - Determination of Optimal Dye Concentration

In order to maximize system efficiency the number of pump photons absorbed by the dye molecules must be maximized. Models of the absorption process are complicated by the broad spectral content of the flashlamp discharge and the variation of the discharge spectrum with varying lamp parameters and operating conditions [50,51]. An additional complication arises because those wavelengths which are absorbed by the dye will be absorbed with varying distributions throughout the dye cell depending on  $\sigma_a(\lambda)$  and the dye concentration. It is clear, however, that the radial distribution of absorbed pump photons is a strong function of the dye concentration. If, for example, the dye concentration is too small, many of the pump photons will pass through the dye cell unabsorbed. On the other hand, if the dye concentration is too large the pump photons will be absorbed rapidly near the outer wall of the dye cell. Although the net absorption, and hence gain, is maximized using these larger concentrations the output laser pulse assumes a somewhat annular spatial profile [45]. It is, thus, generally preferable, at some expense in output pulse energies, to maximize the pump photon absorption (i.e. gain) at the center of the dye cell.

The dye concentration which maximized the gain at the center of the dye cell was determined experimentally as follows. A 2mm dia. CW dye laser "probe" beam was passed through the center of the dye cell and focused onto a photodiode. With only pure ethanol in the dye cell, the CW probe beam simply generated a constant voltage level at the output of the photodiode. However, when dye was added and the system excited by the flashlamp pulse, the probe beam was amplified. The photodiode

output of the amplified probe beam is shown in Figure 3.3a. Although there was insufficient gain for lasing action to be initiated on only one pass through the dye cell, amplified spontaneous emission, whose intensity mirrors the intensity of the flashlamp pumping pulse, was detected by the photodiode in addition to the amplified probe beam. The detected spontaneous emission can be treated essentially as background noise, the level of which was determined simply by firing the flashlamp in the absence of the probe beam (Figure 3.3b). A point-by-point subtraction of the output shown in Figure 3.3b (i.e. noise) from the output shown in Figure 3.3a then yielded the output generated by the amplified probe beam alone. Given this signal, together with knowledge of the signal when no amplification occurred (i.e. the constant voltage level), the small-signal gain at each point in the flashlamp pulse can be determined for the wavelength of the probe beam. The small-signal gain can also be measured as a function of wavelength simply by varying the wavelength of the probe beam. Similarly, the small-signal gain can be determined as a function of a variety of parameters including flashlamp discharge energy, dye concentration and solvent.

The small-signal gains,  $\delta_o = \Delta N_{\max} \sigma$ , measured using this technique, are shown in Figures 3.4 and 3.5 as a function of wavelength, flashlamp discharge energy and R6G concentration in ethanol. The gains shown are maximum gains (i.e. those observed at the peak of the pumping pulse). Estimations of the gains at other points in the pumping pulse can be made by an appropriate fitting of the flashlamp pulse to a Gaussian profile. It should be noted that due to the shot-to-shot variations in the intensity of the flashlamp pulse, the gains recorded were actually a statistical average

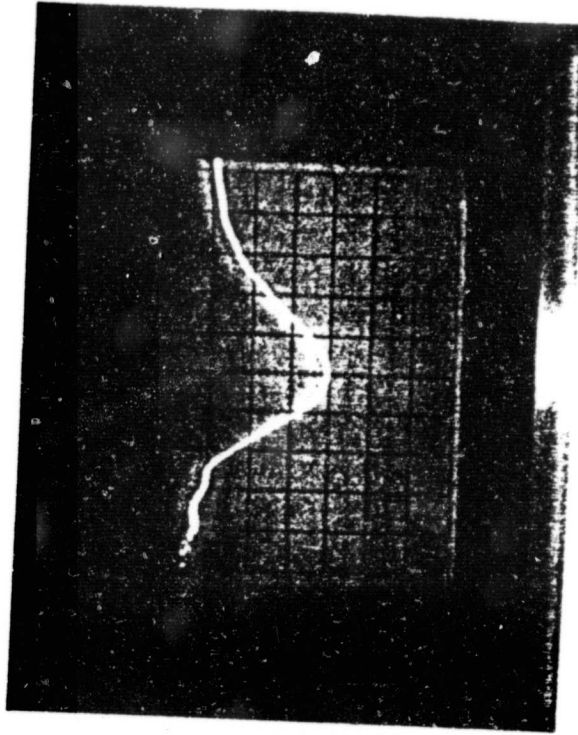


Figure 3.3b: Fluorescence Present w/o  
Probe Beam.

Horiz: 200ns/cm; Vert: 200mV/cm;  
 $E_f$ : 140J,  $\lambda$ : 590nm.

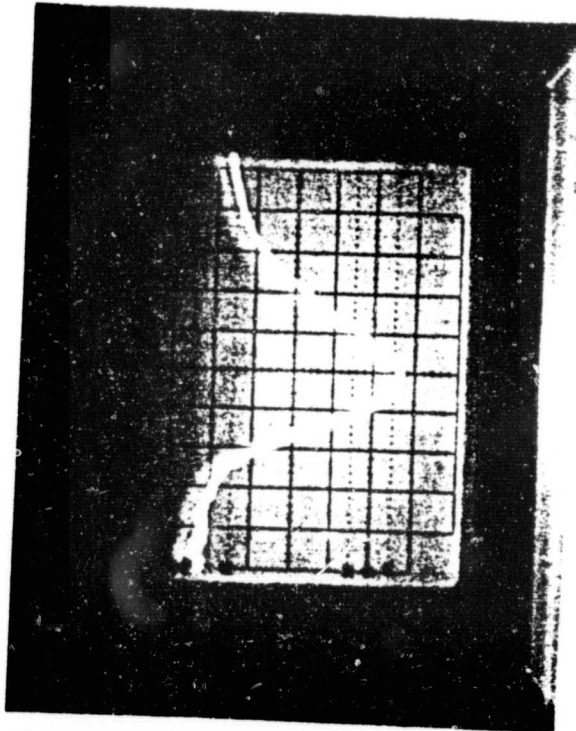
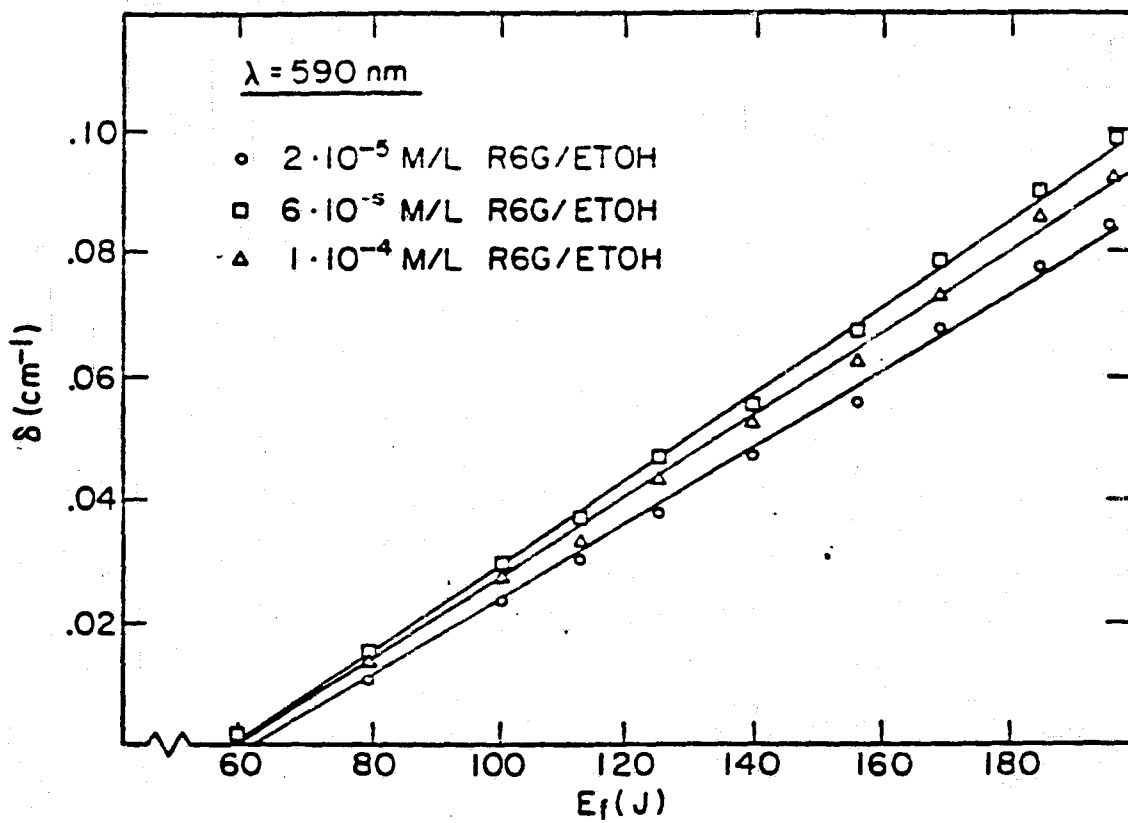


Figure 3.3a: Amplified CW Probe Beam.

Horiz: 200ns/cm; Vert: 200mV/cm;  
 $E_f$ : 140J;  $\lambda$ : 590nm.



**Figure 3.4: Small Signal Gain Coefficient Measured as a Function of Flashlamp Discharge Energy and Dye Concentration**

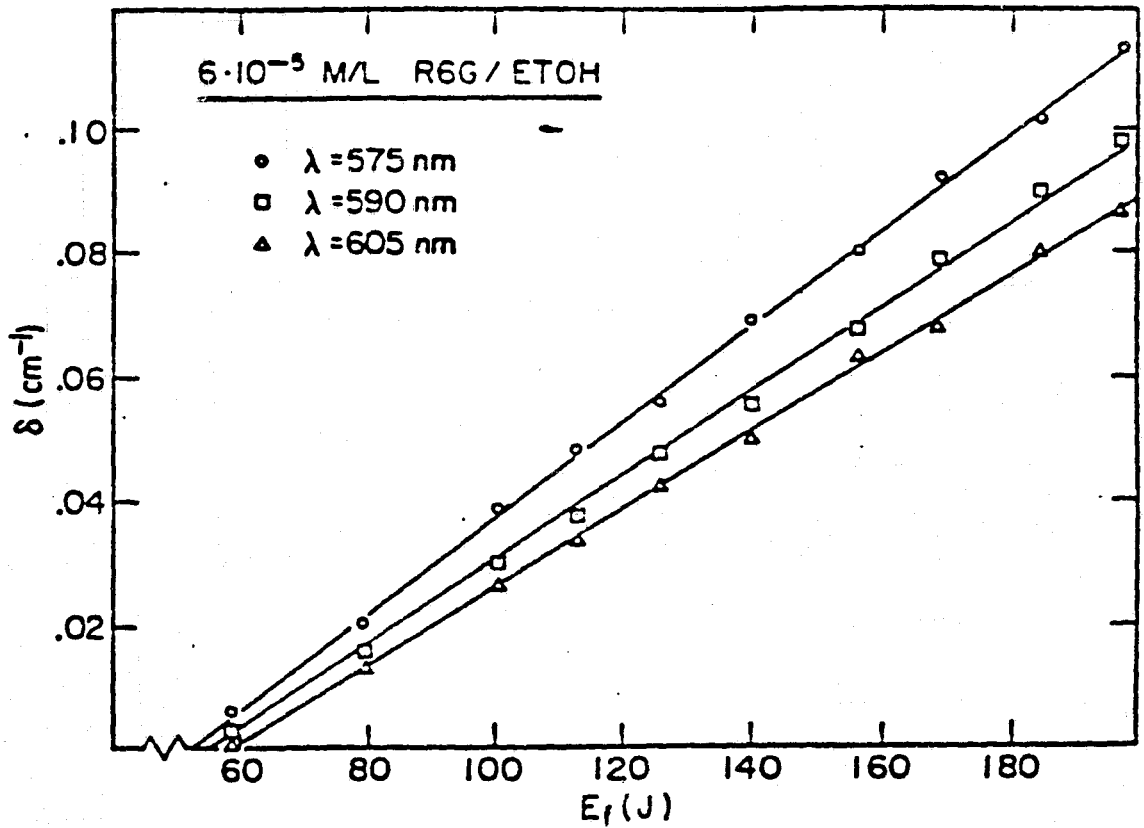


Figure 3.5: Small Signal Gain Coefficient Measured as a Function of Flashlamp Discharge Energy and Wavelength

of the gains recorded during several firings of the flashlamp.

The data presented in Figure 3.4 displays the expected variation of  $\delta_0$  with concentration as the net gains varied only slightly over the range of  $10^{-5}$  -  $1.2 \times 10^{-4}$  M/L. A slight maximum was observed, however, with a  $5 \times 10^{-5}$  M/L ethanolic concentration. These findings were consistent with those obtained by many commercial manufacturers of organic dyes and coaxial flashlamp pumped dye lasers [45,46,52,53].

The variation of  $\delta_0$  with wavelength, shown in Figure 3.5, was somewhat unexpected, however. The manufacturer of the dye (Exciton) claimed, as had other commercial dye manufacturers, that the peak lasing wavelength of an ethanolic solution of R6G was at 590nm. Instead, substantially higher small signal gains were observed at 575nm. The reason for this discrepancy, self-absorption effects, will be discussed in more detail later, in Section 3.12. This data, nonetheless, still provides reasonable numerical estimates, for the purpose of system analysis, of the small signal gain,  $\delta_0$ . From this it can be seen that, for large pumping rates (i.e. flashlamp discharge energies  $> 200\text{J}$ ), the single pass gains can be as large as 50 or more. With single pass gains of this magnitude, the intensity of the radiation trapped inside the resonator should approach the saturation regime after only a few transits through the dye cell.

### **3.5 - Basic Oscillator Design and Operation**

The basic resonator used for cavity-dumping the flashlamp pumped system is shown in Figure 3.6. It was designed using a minimal number of optical components (for a ring laser) in order to keep the optical cavity

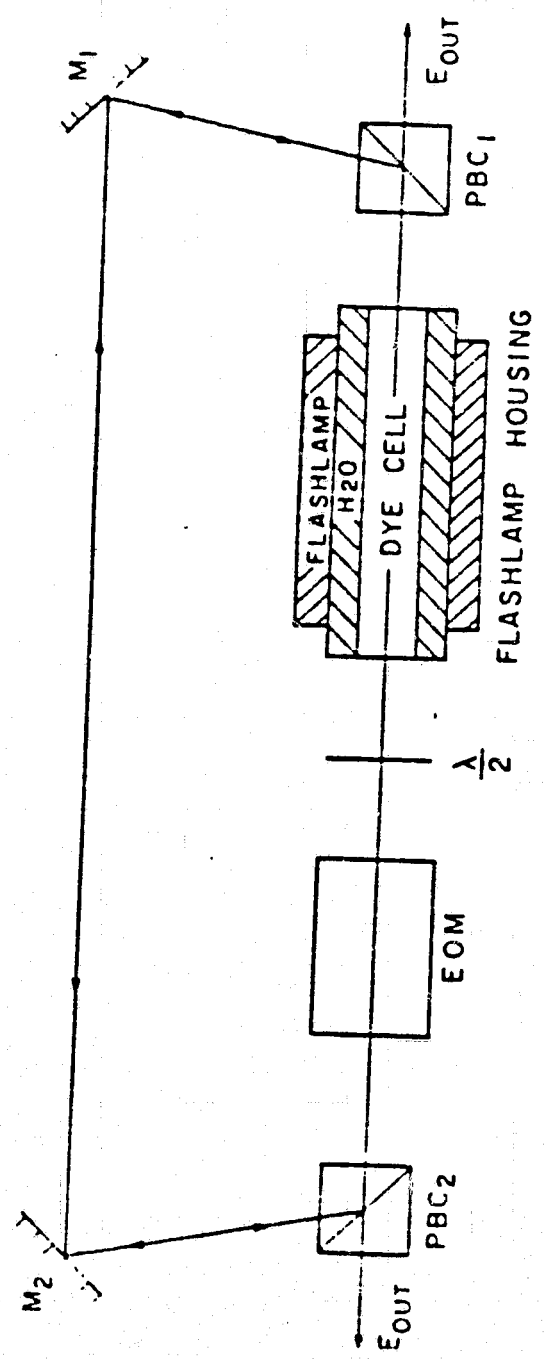


Figure 3.0: Schematic of Basic Cavity-Dumped Ring Oscillator



losses as small as possible. To further reduce cavity losses, all of the components used were treated with either high-power anti-reflection (AR) or high-reflection broadband dielectric coatings. The advantages of a ring configuration will become apparent later when attempts to injection-lock the system are discussed.

Radiation emanating from the dye cell was polarized by either of a pair of broadband polarizing beamsplitter cubes ( $PBC_1, PBC_2$ ). The  $PBC$ 's reflected more than 99% of the incident  $s$ -polarized light and transmitted about 95% of the incident  $p$ -polarized light (the remaining ~ 5% of the  $p$ -polarized light was reflected). Counter-clockwise propagating  $s$ -polarized light was reflected by  $PBC_1$  and directed via turning mirrors  $M_1$  and  $M_2$  to  $PBC_2$  where it was again reflected back through the dye cell. When the proper  $\lambda/2$  voltage was applied to the Pockels cell, it, together with an achromatic  $\lambda/2$  plate, induced a net  $180^\circ$  rotation in the plane of polarization of the incident radiation. The light was then, once again,  $s$ -polarized when it arrived at  $PBC_1$ . In this way, if the laser radiation was completely  $s$ -polarized, it could be totally ( $>99\%$ ) trapped inside the resonator for regenerative amplification. If, however, the radiation possessed a significant " $p$ " component, due either to polarizers with low extinction ratios or to a misalignment of the birefringent elements, the  $PBC$ 's would function like output couplers. A "shoulder" comprised of the  $p$ -polarized radiation exiting the cavity through the  $PBC$ 's would precede the main cavity-dumped output pulse. The failure to maintain a high degree of linear polarization within the resonator, which allows this "leakage" to occur, also has the net effect of increasing cavity losses. This, in turn, restricts the extent to which the gain of the system can be

saturated and, hence, the energy of the cavity-dumped output.

It should be noted that to minimize cavity losses, the trapped radiation was chosen to be reflected by the *PBC*'s where the loss for *s*-polarized light was less than 1%. The 5% "*p*" transmission loss was, thus, a loss that was only encountered when the pulse exited the cavity during cavity-dumping. An additional advantage of using such a configuration is that the *PBC*'s were cascaded. Before returning to the dye cell, the trapped radiation was reflected off both of the *PBC*'s, thereby making the effective extinction ratio of the cavity the square of that provided by only a single *PBC*.

Due to the large single pass gains, the totally confined, regeneratively amplified radiation quickly begins to saturate the gain of the dye. When the intensity of this radiation reached the point where the gain of the dye had been fully saturated, and no additional amplification occurred, the  $\lambda/2$  voltage on the Pockels cell was switched off. After a final pass through the dye cell, the polarization of the light was now only rotated  $90^\circ$  (by the  $\lambda/2$  plate). Left in the *p*-polarized state, it exited the cavity through *PBC*<sub>1</sub>. The clockwise propagating beam, that coexisted in the ring laser, similarly exited the cavity through *PBC*<sub>2</sub>.

Using the cavity-dumping procedure outlined above, the  $\lambda/2$  voltage could be applied to the Pockels cell at any point prior to the initiation of the flashlamp pulse. The time at which the Pockels cell was switched off, however, had a substantial impact on the output pulse energies. If the Pockels cell was switched off early in the flashlamp pumping pulse, the trapped laser radiation did not have sufficient time to fully saturate the gain of the dye resulting in less than optimal output pulse energies. In

fact, when cavity-dumping occurred too early in the flashlamp pulse, sufficient gain remained for the system to begin lasing again. This time, however, it functioned as a two-pass oscillator. If the  $\lambda/2$  voltage was switched off too late, when  $\Delta N_0$  was decreasing, the triplet state population and thermal effects induced losses which decreased output energies. The  $\lambda/2$  voltage "turn-off time" was thus set to optimize extracted pulse energies. As will be shown later, the optimal turn-off time was generally at the peak of the flashlamp pulse.

### 3.6 - Description of Oscillator Components

The Pockels cell initially used was a 95% deuterated  $KD^*P$  crystal manufactured by Lasermetrics. It was surrounded by an index matching fluid and housed in a chamber with broadband AR coated windows in order to minimize losses. Despite this, the transmission losses were,  $\sim 8\%$ . (This large loss figure later prompted the replacement of this cell with one with substantially lower losses.) In the absence of an electric field, the  $KD^*P$  crystal is uniaxial. Thus, there is normally only one refractive index for light propagating in a direction parallel to the optic axis. Although some natural birefringence was observed, it was generally small enough to be considered insignificant for these applications. When an electric field was applied parallel to its optic axis the  $KD^*P$  crystal became birefringent. The orthogonal ordinary and extraordinary waves would then travel through the crystal at different velocities, generating a phase shift between them. This net phase shift can be determined by the following equation:

$$\gamma = \frac{n_o^3 \Gamma_{63} V}{\lambda} \quad \text{[III.1]}$$

where:

$\gamma$  = number of wavelengths retarded

$n_o$  = ordinary index of refraction; (1.52 for  $KD^*P$ )

$\Gamma_{63}$  = electro-optic constant; ( $26.4 * 10^{-6} \mu/V$  for  $KD^*P$ )

$V$  = longitudinally applied voltage

$\lambda$  = wavelength of light ( $\mu$ )

A special consequence of this equation is that if the ordinary and extraordinary waves of a linearly polarized beam were phase shifted by  $180^\circ$  (i.e.  $\gamma = \lambda/2$ ), the beam would again exit the crystal linearly polarized, but with the plane of polarization rotated by  $90^\circ$ . This particular case is the one employed in the cavity-dumping scheme discussed here. As such, the voltage,  $V$ , was set to induce a  $\gamma = \lambda/2$  phase shift for  $\lambda = 590\text{nm}$ . Although slight, there was some variation in the  $\lambda/2$  voltage for the various wavelengths within the emission range of the dye. This necessitated a fine adjustment of  $V$  whenever the lasing wavelength was altered.

A fast photodiode, detecting the flashlamp discharge, was used to trigger the Pockels cell electro-optic modulator (*EOM*) driver. The triggering occurred well before the flashlamp intensity had induced a threshold inversion in the dye solution. After a built-in 30nsec delay, the *EOM* driver applied the high-voltage  $\lambda/2$  pulse to the Pockels cell. The rise-time of the high voltage pulse across the cell was 1-2ns. Triggering the *EOM* in this way eliminated the problem of trying to synchronize the

flashlamp pulse with the Pockels cell turn-on time. Due to the substantial jitter ( $\sim 100\text{nsec}$ ) in the spark-gap switch, this synchronization problem became a major concern when more sophisticated triggering circuitry became necessary. The  $\lambda/2$  pulse duration was adjustable from  $100\text{nsec}$  -  $1.2\mu\text{sec}$  so that the Pockels cell could be switched off at any point during the flashlamp pulse.

As mentioned, an achromatic  $\lambda/2$  plate provided the fixed  $90^\circ$  rotation. The turning mirrors,  $M_1$  and  $M_2$ , both had broadband, high-power reflective coatings. Reflectivities throughout the dye emission band were measured to be greater than 99%.  $M_1$  had an infinite radius of curvature while  $M_2$  was made slightly concave ( $RC=20\text{m}$ ) in order to form a stable resonator. The effects of varying the Gaussian beam characteristics of the resonator, by replacing  $M_1$  and  $M_2$  with mirrors of different curvatures, will be presented later.

### 3.7 - Diagnostic Equipment

After exiting the cavity, the laser pulse had to be attenuated in order to avoid damaging the detection equipment. As shown in the overall schematic presented in Figure 3.7, this was accomplished by reflecting the beam off of a series of glass plates until its intensity was such that more conventional attenuators, such as neutral density filters and diffusers, could be used. The exact value of the attenuation, required for radiometric measurements, was determined by passing an identically polarized 2.2W 514.5nm argon-ion beam through the network of glass plates.

Attenuated output pulse energies were measured using a UDT Model

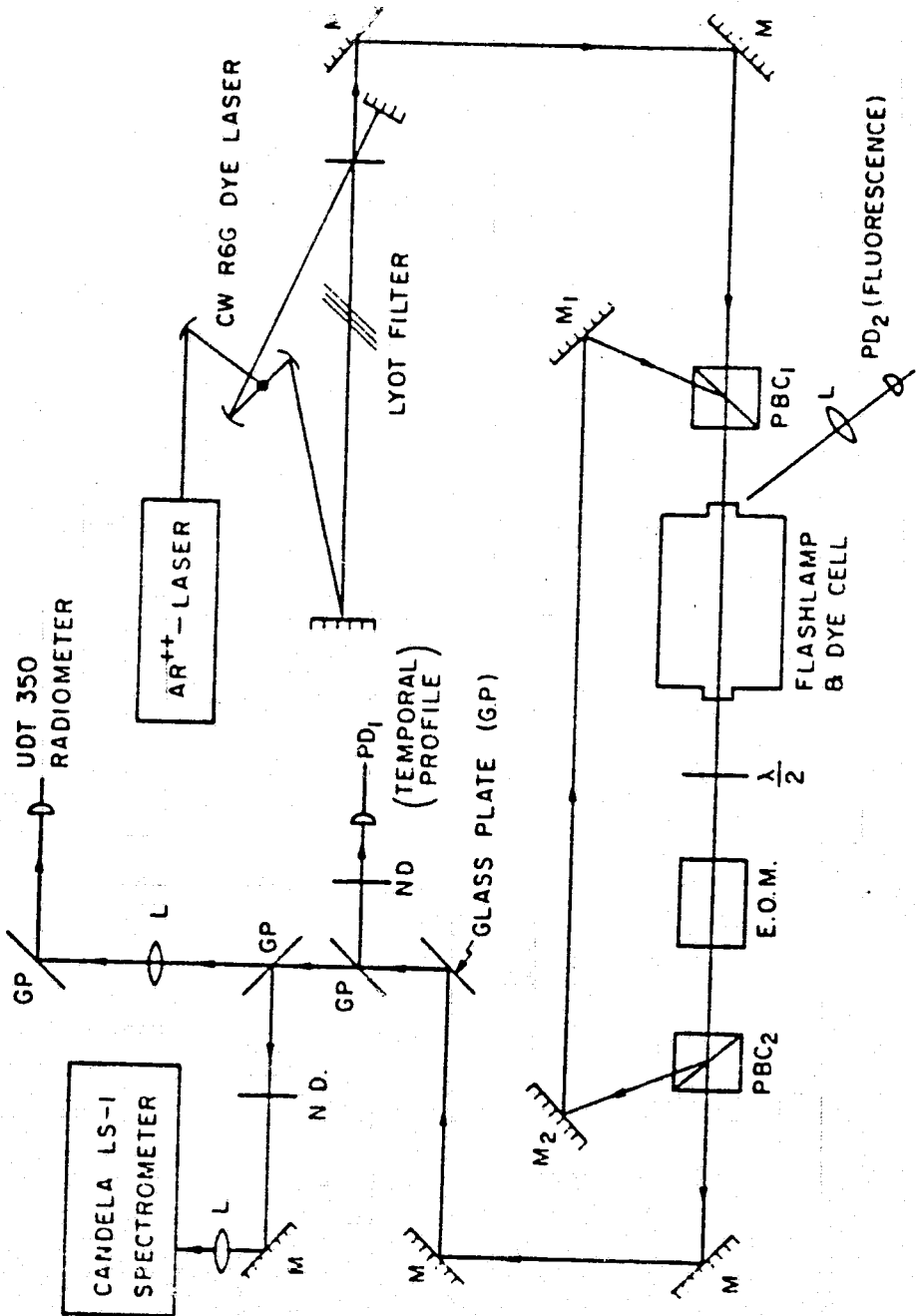


Figure 3.7: Overall Optical System Schematic

350 optometer. The detector head consisted of a silicon PIN photodiode mounted in a UDT Model 2500 integrating sphere. Use of a radiometric filter with the detector assured that a flat response was obtained from 400-700nm.

The temporal profile of the oscillator output was monitored with a fast ( $t_r < 1ns$ ) PIN photodiode ( $PD_1$ ) and a 275MHz storage oscilloscope. Noise induced by the electromagnetic interference, caused by the high-voltage switching, was minimized by mounting the diode in a well shielded box. The batteries used to reverse bias the diode were also mounted inside the shielded box in order to minimize external connections. Because of the high noise level all electrical connections were made using shielded cables.

A Candela LS-1 grating spectrometer was used to spectrally analyze the attenuated oscillator output. In the LS-1, the spectral components of the beam were dispersed by the grating onto a linear photodiode array. The array output was scanned and read into an integrate, sample-and-hold amplifier whose output was fed directly to the vertical input of the oscilloscope. The oscilloscope then displayed relative light intensity vs. wavelength, since time was correlated to position on the diode array (i.e. wavelength). The spectrometer resolution was limited by the diode resolution to a minimum of 0.01nm and by the length of the array to a maximum of 10nm. Linewidth resolution was increased to 1pm when an internally mounted Fabry-Perot etalon was used in place of the grating. The resulting fringe pattern was then recorded by the photodiode array for analysis. During the later phases of the work, when information about the relative energy in a given spectral band was required, this spectrometer was replaced with an optical multichannel analyzer (OMA).

Another fast photodiode,  $PD_2$ , was used to monitor the growth of the laser pulse during amplification. It detected the spontaneous emission which was focused onto the photodiode after being scattered from an edge of the dye cell. With lasing inhibited, by blocking the path of the beam, the spontaneous emission from the dye was directly proportional to the intensity of the flashlamp pumping pulse. The presence of any stimulated emission, however, reduced the spontaneous emission to a level less than that when lasing action was forbidden. Thus, as the intensity of the amplified pulse increased, increasing the stimulated emission rate, it was accompanied by a commensurate drop in the spontaneous emission level. During amplification, the spontaneous emission steadily decreased until it reached a constant value. At this point the intensity of the amplified pulse was assumed to be well within the saturation regime. The display of the  $PD_2$  output was thus useful in optimizing the Pockels cell turn-off time.

### **3.8 - Alignment of the Cavity-Dumped Oscillator**

As with most pulsed laser systems, cavity alignment had to be performed using an external laser. Although a simple He-Ne laser would have sufficed, the CW argon-pumped dye laser that was used for the small signal gain measurements, was used instead, primarily due to the larger power available ( $\sim 50\text{mW}$ ). It was also preferred because the wavelength of the alignment beam could be made closer to the free oscillation wavelength of the cavity-dumped oscillator. This was a concern because of the dispersive properties of the EOM and the  $\lambda/2$  plate. The initial alignment was performed with only pure ethanol circulating through the dye cell in order to avoid the attenuation of the beam by the dye. Once



the alignment was completed the dye solution was then added to the ethanol. Subsequent alignment "checks" were performed using wavelengths where absorption losses in the dye were small (i.e.  $\lambda \sim 600\text{nm}$ ).

Since the resonator would be aligned so as to sustain laser oscillation that propagated in the same direction as the alignment beam, it was imperative that the alignment beam pass directly through the center of the dye cell where the gains were maximized. Once this was set, the resonator optics were adjusted to return the alignment beam back through the center of the dye cell along the same path that it had made on its initial transit. With the  $\lambda/2$  plate set so as to induce a  $90^\circ$  polarization rotation, the alignment beam would remain inside the cavity for at most only two passes. Deliberately "misadjusting" the  $\lambda/2$  plate, however, resulted in the generation of an elliptically polarized beam, a fraction of which, on each transit, was reflected back into the cavity, by  $PBC_2$ . In this way, the cavity was aligned so that the second, third, fourth, fifth, ..., passes of the alignment beam spatially overlapped each other, thus insuring a stably aligned resonator. The fraction of the incident elliptically polarized beam transmitted by  $PBC_2$  was used for the alignment of the attenuation stack and the diagnostic equipment.

Before the  $\lambda/2$  plate was "misadjusted", however, the optic axis of the Pockels cell had to be made parallel with the alignment beam in order to minimize the premature leakage of light out of the cavity. This procedure had to be performed prior to the resonator alignment because a reorientation of the Pockels cell substantially altered the direction of the alignment beam. With the  $\lambda/2$  plate set to induce a  $90^\circ$  rotation, the

linearly (s) polarized alignment beam was passed through the static ( $V=0$ ) Pockels cell. Using  $PBC_2$  as an analyzer, the orientation of the cell was then adjusted to minimize transmission through  $PBC_2$ . After aligning the Pockels cell, the rest of the resonator optics were then aligned using the "spatial overlapping" technique described above.

### 3.9 - Initial Temporal and Radiometric Oscillator Performance

The initial operation of the system was performed with the oscillator and detection equipment aligned and configured as shown in Figure 3.7. Preliminary investigations were devoted to determining the factors that influenced the capacity of the system to deliver high-power pulses and to insure that these pulses possessed "clean", nanosecond duration temporal profiles.

Spectrally, the output pulses had a fixed center wavelength of 590nm with a linewidth of  $\sim 6$ nm FWHM. More detailed spectral characterizations of the outputs are considered in Chapter 4. Output pulse energies and temporal profiles were first monitored as a function of the point in the flashlamp pulse when cavity-dumping occurred (hencewise known as the "extraction time"). Regardless of the extraction time, however, the observed temporal profiles were extremely poor. A significant fraction of the output pulse energy was contained in "shoulders" that preceded and followed the cavity-dumped pulse. Figures 3.8 and 3.9 are traces of the temporal profiles of the output for early and late extraction times respectively. The existence of the trailing "shoulder" in Figure 3.8 was attributable to the fact that, when cavity-dumping occurred early in the pumping pulse, before net gains had decreased to unity, the system, with the

ORIGINAL PAGE IS  
OF POOR QUALITY

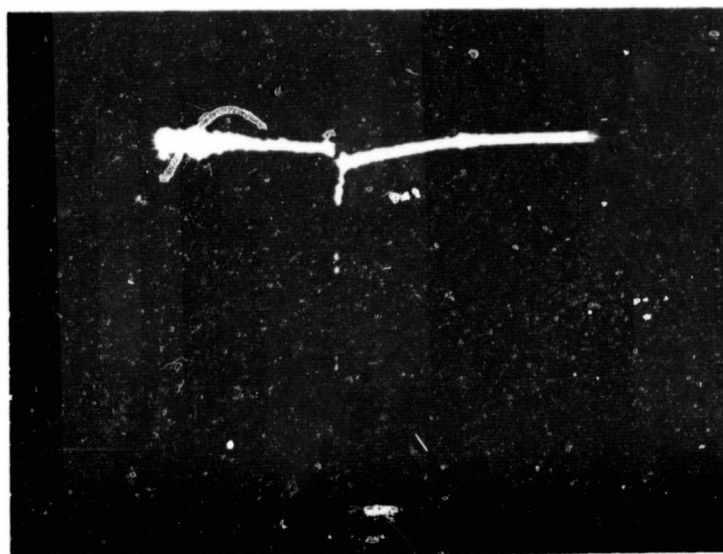


Figure 3.8: Temporal Profile of a Cavity-Dumped Pulse  
Extracted  $\sim 200$ ns Prior to the Peak of the Pumping Pulse.

Horiz: 200ns/cm

ORIGINAL PAGE IS  
OF POOR QUALITY

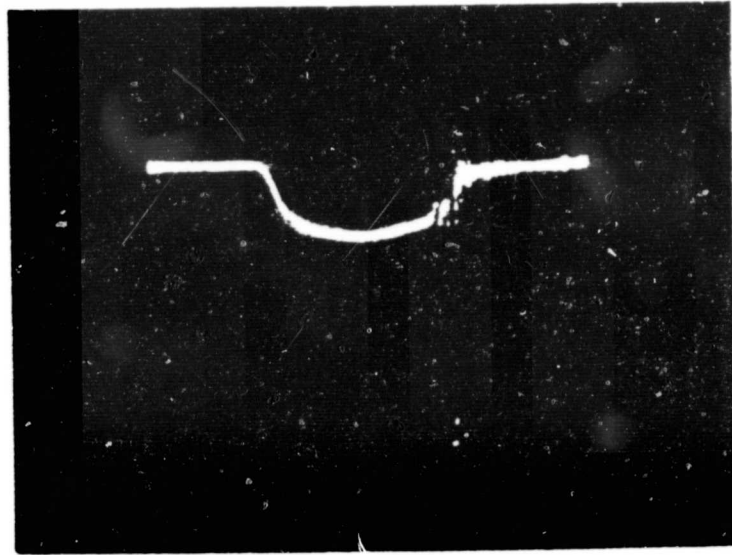


Figure 3.9: Temporal Profile of a Cavity-Dumped Pulse  
Extracted 400ns After the Peak of the Pumping Pulse.

Horiz: 200ns/cm

Pockels cell "off", continued to lase as a two-pass oscillator. More will be said about this later. The existence of a leading "shoulder" when cavity-dumping occurred late in the pumping pulse (Figure 3.9), however, indicated that radiation was leaking out of the cavity prior to the switching of the Pockels cell. Apparently, despite the careful alignment procedure used, the actual lasing axis differed slightly from the axis defined by the alignment beam. The laser radiation then traveled through the Pockels cell along an axis that was not parallel to the optic axis of the crystal. Because of this, it did not undergo an exact  $90^\circ$  rotation and, when incident on  $PBC_2$ , a fraction of the radiation exited the cavity. After an iterative realignment of the Pockels cell, during operation, the intensity of the leakage became negligible and outputs resembled that shown in Figure 3.8.

The trailing "shoulder", attributable to a different phenomenon, still existed. It was thought that if the extraction time was moved to a point, late enough in the flashlamp pulse, where net gains equaled unity, that the two-pass oscillation would be inhibited. This, in fact, proved to be the case. However, as the extraction time was pushed from the peak of the flashlamp pulse to a later point in time, the intensity of the cavity-dumped pulses decreased. This indicated that, due either to gain saturation, triplet-state absorption or other time-dependent loss mechanisms, the net gain had been reduced to unity by the time when the flashlamp intensity was the greatest. It was then questionable as to what sustained the two-pass oscillation. Through placement of a monochromator, set to pass 590nm light, in front of  $PD_1$ , it was discovered that the cavity-dumped pulse alone was centered at 590nm. The trailing "shoulder" was

comprised of broadband radiation centered at 575nm. As the triplet state absorption cross section,  $\sigma_T$ , was considerably less at this wavelength than at 590nm, it was conceivable that net gains at 575nm persisted until a later point in the flashlamp pulse. Although this accounted for the existence of the trailing "shoulder" it was uncertain as how to suppress it without sacrificing the energy of the cavity-dumped pulse. The most likely solution was that of spectrally filtering out the 575nm radiation. More will be said about this in Chapter 4 when the spectral characteristics of the outputs will be carefully considered.

The output of  $PD_2$ , shown in Figure 3.10, detailing the growth of the laser radiation during amplification, graphically demonstrates these observations. The display is a double exposure of two consecutive flashlamp firings, one taken with lasing inhibited and the other with the oscillator lasing. These traces were overlaid to accentuate the differences in the two spontaneous emission profiles. With lasing inhibited, the  $PD_2$  display mimicked the Gaussian shaped profile of the flashlamp pumping pulse as expected. The second trace, taken while the oscillator was lasing, illustrated how rapidly the system was driven into saturation. The two traces appeared identical until about 200ns after the initiation of the flashlamp discharge. At this point, when the laser reached threshold, the intensity of the laser radiation increased rapidly and the spontaneous emission level was driven well below that of the first trace. The saturation regime evidenced by the "leveling off" of the spontaneous emission intensity was reached quickly. As a further indication of saturation, note that the minimum level the spontaneous emission was driven to coincided identically with the level at which threshold was reached. At both of these

points the net gain should be near unity. The gain saturated system was then cavity-dumped near the peak of the flashlamp pumping pulse. This sudden absence of laser radiation in the cavity allowed the spontaneous emission level to increase, to the value attained at the same time in the first trace. Once recovered, the system began to lase again as a two pass oscillator. This was indicated by the return of the spontaneous emission level to that of the first trace.

Output pulse energies were monitored as a function of  $E_f$ , the flashlamp discharge energy, using late extraction times to minimize the amplitude of the trailing "shoulder". However, the recorded pulse energies were less than optimal due to the late extraction times used. Lasing threshold occurred at  $E_f = 90\text{J}$  and cavity-dumped pulse energies of  $\sim 10\text{mJ}$  were observed with  $E_f = 150\text{J}$ . When output energies approached  $\sim 20\text{-}25\text{mJ}$  ( $E_f \sim 200\text{J}$ ), damage was observed on the dielectric coating of the *PBC*'s. This damage resulted from an inherent problem with the devices and forced the use of a different type of polarizing beamsplitter later in this work.

During the fabrication of the *PBC*'s, the dielectric polarizing coating was applied to one half of the cube while an optical cement, applied to the other half, was used to adhere the two halves together. It was believed that the cement was heated by the absorption of a small percentage of the incident radiation and that this temperature increase damaged the adjacent polarizing coating. Damage, then, undoubtedly occurred when the oscillator was cavity-dumped and the high-power pulse passed through the *PBC*'s. Care had to be taken in subsequent work using the *PBC*'s to keep output pulse energies below  $\sim 20\text{mJ}$ .

ORIGINAL PAGE IS  
OF POOR QUALITY

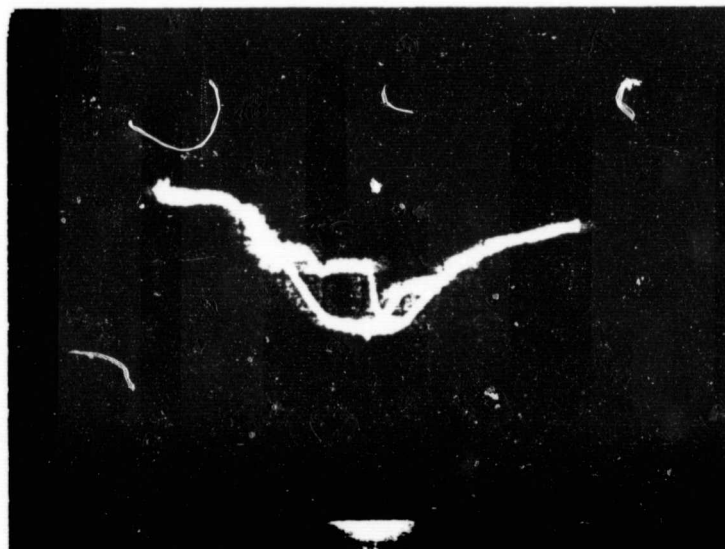


**Figure 3.10: Double Exposure of the Fluorescence Emitted from the Dye Cell With and Without Lasing.**

**Horiz: 200ns/cm;  $E_f$  : 140J.**



### 3.10 - Beam Waist Considerations

Only the basic resonator design, described in Section 3.5, had been used up to this point. With this basic design, however, the only influence that the resonator had on pulse energies, discounting the passive component losses, was in the beam shaping through the use of focusing optics. As described earlier, the only focusing optic in the cavity was a 20mRC spherical mirror. This choice was made so that the resonator would satisfy the Gaussian mode stability criteria while supporting as large a beam diameter as possible. It was thought that if a plane parallel resonator were used, the diffraction losses, especially for higher order modes, would offset the gains obtained through utilization of the entire dye volume. Although diffraction losses could have been minimized by the use of a shorter focal length mirror, astigmatic losses would then become a concern. The use of a shorter focal length mirror also would have decreased the beam diameter, thereby using less of the active dye volume.

To test these hypotheses, output energies,  $E_o$ , were recorded as a function of the Gaussian beam waist which was set by varying the curvature of the mirror used in place of  $M_2$  (Figure 3.6). The system was aligned and operated as discussed in the previous two sections with extraction times kept consistently late to insure temporally clean outputs. The results are displayed in the table below where

$$w_o = \left(\frac{\lambda}{\pi n}\right)^{0.5} \left(\frac{l}{2}\right)^{0.25} \left(R - \frac{l}{2}\right)^{0.25} \quad \text{[III.2]}$$

is the Gaussian beam waist found in a symmetric cavity of length  $l$ , containing a mirror with a radius of curvature  $R$ .

Beam Waist Effects			
RC(m)	$w_o$ (mm)	$E_f$ (J)	$F_o$ (mJ)
2	0.43	101	1.4
		113	3.9
		126	6.5
		140	8.5
20	0.93	101	1.5
		113	4.8
		126	7.5
		140	10.5
$\infty$	$\infty$	101	1.4
		113	3.6
		126	6.4
		140	9

The output pulse energies exhibited only a weak dependence on the Gaussian beam waist. A possible explanation for this is that, due to the large degree of gain saturation, the pulse developed in a highly multimodal fashion. If this was the case, the beam radius would grow as the gain spatially saturated until it filled the dye cell, regardless of the focusing element in the cavity. The marginal decrease in system performance in the plane resonator case was probably due to the increase in diffraction losses as expected. With the 2mRC mirror, output energies were also lower than those obtained with the 20mRC mirror, but not by the factor of  $\sim 2$  predicted by the Gaussian beam calculations. The lower output energies, in this case, were most likely attributable to increased astigmatic losses.

### 3.11 - Effects of the Organic Dye on System Performance

Time dependent losses within the organic dye itself also influenced the performance of the system. These losses occurred both on a per pulse basis, due to triplet state effects, and on a long term basis due to the photodegradation of the dye molecules. Triplet state absorption provided a likely explanation for the early cavity-dumping times required to optimize output pulse energies. Since  $k_{ST}$ , the intersystem crossing time, has been reported to be  $\sim 100$ - $300$ ns, an appreciable triplet state population could have developed by the time the peak of the flashlamp pulse occurred. The increased losses due to triplet state absorption could have forced the optimal extraction time to be at such an early point in the flashlamp pulse. It was thought that if these effects could be counteracted that the optimal extraction time could be pushed to a later point in the flashlamp pumping pulse. In this way, the trapped radiation could be regeneratively amplified for a longer period of time and output pulse energies could be further increased.

Attempts were made, by the addition of triplet state depopulation agents (quenchers) to reduce the triplet state lifetime,  $\tau_T$ . As mentioned in Chapter 2, these triplet quenchers reduce  $\tau_T$  by enhancing the intersystem-crossing rate,  $k_{TG}$ , through either collisional or spin transfer-ence mechanisms. One of the first triplet quenchers shown to be effective at this in R6G was  $O_2$  dissolved into the dye solution. Although it was since shown that  $O_2$  simultaneously increases  $k_{ST}$ , thereby counteracting its effectiveness to a large degree,  $O_2$  was bubbled through the dye reservoir in order to see if the optimal extraction time could be pushed to a later point in the flashlamp pumping pulse. To determine this, output

pulse energies were monitored as a function of the extraction time for various  $E_f$  and  $O_2$  flow rates. There was, however, no noticeable change in system performance as the optimal extraction time remained near the peak of the flashlamp pulse.

The above experiment was repeated using cyclooctatetraene (COT) as the triplet quencher instead of the  $O_2$ . COT uses a triplet-triplet energy transfer as the depopulation mechanism and although there are a number of other substances which use this mechanism, COT is the most often used and commonly regarded as being the most effective triplet depopulation agent for R6G. Being a liquid, it was added directly to the dye solution. A  $10^{-3}$ M/L concentration of COT in the dye solution was suggested by the manufacturer (Exciton) although various concentrations ranging from  $10^{-5}$ M/L to  $10^{-2}$ M/L were used as well. As with the  $O_2$ , the optimal extraction time remained near the peak of the flashlamp pulse. In this case, however, output pulse energies were generally smaller than those obtained previously and monotonically decreased with increasing COT concentration. This effect was previously noted by McManamon in his work on flashlamp pumped dye lasers [51]. In this work, he observed that COT had a negative influence on laser gain which resulted in a reduction in output pulse energies. He noted that the effect, however, was not as significant in systems with a high  $Q$  cavity, thus explaining the modest output energy reductions encountered here. Given that COT was considered to be the most effective triplet quencher, seemingly little was to be gained from further investigating techniques to reduce triplet state absorption losses. Throughout this work, the optimal extraction time remained near the peak of the flashlamp. This problem is discussed further in

### Section 6.3.

The photodegradation of the dye molecules also had a profound impact on the performance of the system although over a much longer term. When the dye molecules degrade they no longer contribute to the lasing process, thus the net effect is that of gradually lowering the effective dye concentration. The gains decrease with the effective concentration causing output pulse energies to decrease. This is an intrinsic property of laser dyes and although it is irreversible, there are ways of slowing the degradation rate. Use of smaller beam intensities and low energy visible pump sources are methods (although inconsistent with the objectives of this work) of extending the dye lifetime. The dye lifetime was an important parameter in this work, however, as it detailed the output pulse energies that could be expected as a function of dye exposure time. The "exposure time" actually measured was the total  $E_f$  seen per liter of dye solution. (The concentration was kept at a constant  $5 \cdot 10^{-5} \text{M/L}$  throughout this work). The dye lifetime, generally considered to be the "exposure time" at which output pulse energies have decreased by a factor of two, was found to be  $\sim 20,000 \text{J/L}$ . This figure is, of course, an average as the actual value depended greatly on the range of  $E_f$ 's used per batch.

### 3.12 - Time Dependent Wavelength Development

As mentioned in Section 3.9, the center wavelength of the cavity-dumped pulses was 590nm. This is identical with the peak lasing wavelength of Rhodamine 6G that was reported by the dye manufacturer (Exciton). What was not expected, however, was the presence of the yellowish-green radiation, centered at 575nm, after cavity-dumping. If

cavity-dumping occurred early enough in the flashlamp pumping pulse, the system had sufficient time and gain (especially at these wavelengths where triplet state losses were less; Figure 2.2) to begin to lase again. In this case, however, with the *EOM* "off", the system functioned as a two pass oscillator due to the polarization sensitive components in the resonator. In fact, whenever the system was operated without the *EOM* in the cavity, the center wavelength of the then  $\sim 1\mu\text{sec}$  output pulse was identically 575nm. There was naturally some confusion as to why the the same system would lase at two wavelengths 15nm apart depending on its mode of operation. One possible explanation was that the output pulse wavelength,  $\lambda_o$ , was a function of the photon cavity lifetime,  $t_c = l/cL$  where  $l$  is the cavity length (a ring cavity is assumed here), and  $L$  is the fractional loss per pass. In the cavity-dumped mode, where  $t_c$  was extremely large, the system lased at 590nm, where the single pass gains of the medium were the greatest. On the other hand, when the system was operated as an oscillator,  $t_c$  was extremely small ( $< 20\text{ns}$ ).

To see if, in fact,  $t_c$  was the critical parameter,  $\lambda_o$  was observed as it was varied. By varying the roundtrip cavity losses,  $t_c$  could be set to many different values. The losses could be continuously varied without changing the system design by "misadjusting" the  $\lambda/2$  plate. When properly adjusted, to yield a  $90^\circ$  rotation, the system functioned as a two pass oscillator with all of the radiation being *p*-polarized on its second transit through the system. When adjusted to yield a  $0^\circ$  or  $180^\circ$  rotation, the cavity-dumped mode of operation was emulated. By adjusting the rotation of the  $\lambda/2$  plate so that the linearly polarized light was changed into some elliptical polarization state, the *PBC*'s would act as variable output

couplers. In this way the cavity photon lifetime could be adjusted to any point between these two extremes. The results given below decidedly indicated that the lasing wavelength,  $\lambda$  was indeed a strong function of  $t_c$ .

Cavity Lifetime Effects	
$t_c$ (ns)	$\lambda$ (nm)
143	590
125	589
50	585
27	581
22	577
20	575

A number of studies were performed in the late 1960's investigating the factors which determined the natural lasing wavelength of various organic dyes. One of the factors that was investigated was that of cavity  $Q$  (i.e. cavity photon lifetime). These studies concluded that lasing is generally initiated at that wavelength where the fluorescence output of the dye is maximized. But, as the intensity of the intracavity radiation grows, absorption losses encountered at this wavelength begin to push the lasing wavelength further toward the red where these losses are smaller. Since, for a given pumping rate, the intracavity field intensity is a function of the cavity  $Q$ , the lasing wavelength,  $\lambda$ , naturally increases as the photon cavity lifetime increases. More details as to this dependency can be found in [23,34,54]. It is sufficient, for this work, merely to understand the origin of this "yellow-green" radiation and to understand that it is inherent when-

ever two-pass lasing is allowed to occur.



## CHAPTER 4 - INJECTION-LOCKING OF THE CAVITY-DUMPED CFP LASER

### 4.1 - Introduction

In Chapter 3, the development and performance of the cavity-dumped oscillator was discussed. Detailed descriptions of system components were given and a characterization of the properties of the dye was performed. Using a polarization-sensitive cavity-dumping technique, moderately high-energy, 10ns duration pulses were generated. Of primary importance during this preliminary work were efforts to maximize output energy while maintaining a temporally "clean", 10ns pulse shape. This required that the spectral, temporal and radiometric profiles of the outputs be monitored under a variety of operating conditions. There was, however, no attempt made to control the spectral characteristics of the outputs. Lasing invariably was centered at  $\lambda=590\text{nm}$  and the output pulses were very broadband ( $\Delta\lambda = 6\text{nm}$  FWHM). Spectral features were only considered if they impacted on the temporal profile. For example, the variation in  $\lambda$  when the system functioned as a cavity-dumped oscillator versus that of a "two-pass" oscillator became significant in optimizing cavity-dumping times to obtain the "cleanest" possible outputs.

This chapter, however, describes efforts aimed at suppressing the "two-pass" oscillation so that the extraction time may be made more optimal and at controlling the spectral properties of the output pulses. Specifically investigated was the use of injection-locking as a means of

spectral control. This technique, unlike more conventional means of controlling pulse wavelength and linewidth by the installation of lossy dispersive elements into the oscillator, did not compromise the capacity of the system to deliver high-energy, temporally "clean" outputs. Integral parts of the injection-locked system, including the Master Oscillator (*MO*), which generated the injected "seed" pulse, and the timing circuitry, which properly synchronized the operation of the system, are described in detail. Preliminary injection-locking investigations were then performed in order to determine, experimentally, the factors on which the system performance was dependent and the nature of the dependency. Of the factors investigated, most were explicitly mentioned in the general spectro-temporal evolution equation derived in the theoretical analysis performed in Chapter 2. The effects that various resonator designs had on system performance and operation were also discussed. Of particular importance, in this respect, were the effects that the installation of frequency selective devices into the amplifier had on the tunability and injection-locking performance of the system.

#### 4.2 - Master Oscillator

As discussed in Chapter 2, the basic principle in an injection-locked system is that when the output of a low-energy, but spectrally pure source, called the master oscillator (*MO*), is properly injected into an amplifier, the spectral characteristics of the amplifier can be controlled.

A  $N_2$ -laser pumped dye laser served as the pulsed master oscillator for this work. Both the  $N_2$ -pump laser and the dye laser were commercially manufactured by Molelectron Inc., (Models UV-24 and DL-300

respectively). A detailed schematic of the *MO* optical design as viewed from above is shown in Figure 4.1.

The DL-300 dye laser was transversely pumped by the 9mJ, rectangularly shaped (6 x 32 mm)  $N_2$ -laser beam. This UV pumping beam was focused to a 8mm long by 0.2 - 0.5mm high line in the quartz dye cell by an aspheric quartz lens,  $L_1$ . The dye cell contained ~ 3ml of a  $5 * 10^{-3}$ M/l concentration of R6G in ethanol. A magnetically coupled stirrer kept the dye solution from being bleached by the intense UV excitation.

The dye laser resonator, based on the Hansch design [55], was formed by a partially reflective output coupler and a grating used in Littrow configuration. The grating selected a particular wavelength within the emission band of the dye for return to the dye cell and subsequent amplification in the laser cavity. Single-pass gains in the dye were so high that a 96% transmission output coupler,  $M_1$ , was used. The glass grating, blazed at  $2.70\mu\text{m}$  with 600 grooves/mm, was mounted on a sine-drive assembly which converted the linear rotation of a remotely controlled DC motor to the sine function wavelength response of the grating. This resulted in a linear relationship between the motor rotation and the wavelength increment of the dye laser output. Using R6G, the output wavelengths were tunable from 575 - 602nm.

The dye laser cavity shown in Figure 4.1 also contained a 22.5x beam-expanding telescope which helped to increase output power and to reduce the optical linewidth of the beam. Use of this telescope together with the grating in the 5th order reflection mode yielded output pulse linewidths of 0.05nm. Further reduction in the optical linewidth and

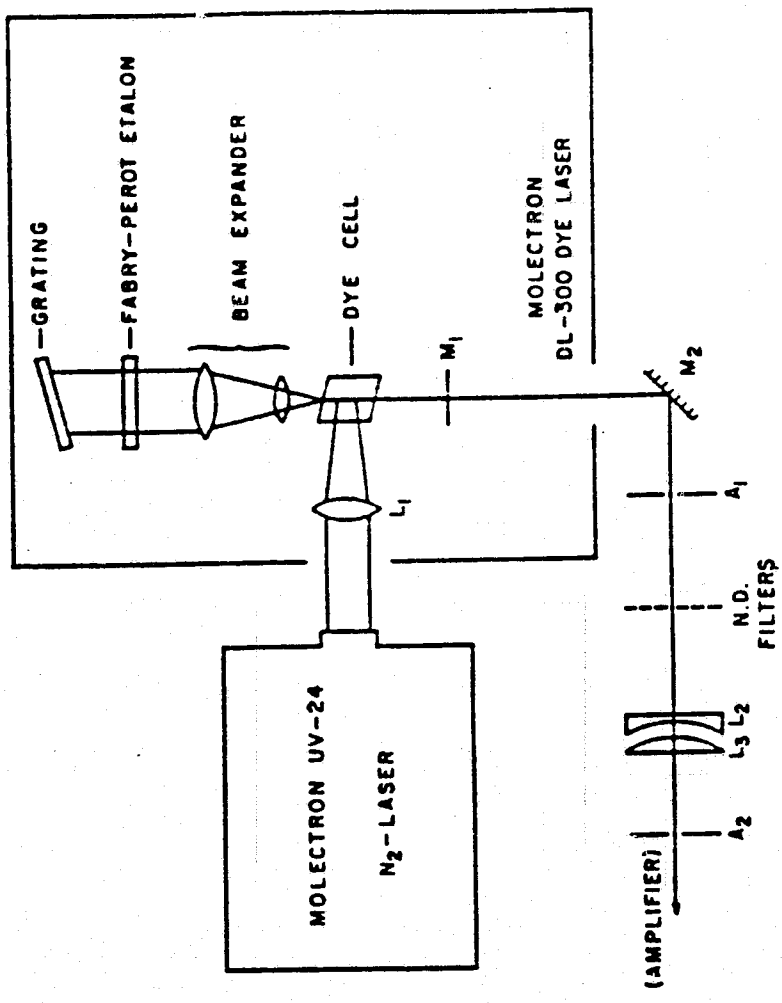


Figure 4.1: Schematic of the Master Oscillator (MO) and Coupling Optics

increased frequency stability, when required, were achieved by the installation of an etalon in the cavity.

Although the frequency stability of the output beam was generally very good, its amplitude stability and spatial characteristics were quite poor. The beam was decidedly nongaussian. It was ellipsoidal in shape and had a large divergence. Because of this poor beam quality, exact coupling of the *MO* beam into the amplifier was impossible. Instead, the *MO* beam was spatially filtered by  $A_1$ , and  $A_2$  and roughly mode coupled into the amplifier by the focusing system  $L_2$ , and  $L_3$ . The unpolarized *MO* beam was polarized by  $PBC_1$  as it entered the amplifier. Usable *MO* output pulse energies, before spatial filtering were  $\sim 120\mu\text{J}$  with shot-to-shot amplitude variations of  $\sim 10\%$ . After spatial filtering, focusing and polarizing, however, only  $\sim 40\mu\text{J}$  could be injected into the dye cell.

### 4.3 - Trigger and Timing Circuitry

The flashlamp pulse, the *MO* pulse, and the *EOM* all had to be carefully synchronized in order to insure that injection-locking would occur. The *MO* pulse had to arrive at the dye cell just as the amplifier achieved threshold. If it arrived much earlier, it would be attenuated as it passed through the amplifier by the losses associated with the optics and the dye solution. By the time threshold was then reached, insufficient *MO* pulse energy would remain to lock the amplifier. Typically, the injection time could precede threshold by as much as  $\sim 50\text{ns}$  and sufficient signal strength would remain to injection-lock the amplifier. The amount of "lead-time", of course, was a function of  $E_f$  and the injected pulse wavelength,  $\lambda_i$ . The tolerance was not so great for injection occurring

after the onset of lasing in the amplifier. Due to the rapid build-up of laser radiation after threshold, the injected pulse energy soon became insignificant in comparison with the already oscillating fields. Injection-locking then failed to occur. The consequence of this was discussed in more detail in Chapter 2.

The most critical timing consideration was the synchronization of the *EOM* turn-on time and the *MO* pulse injection time. The  $\lambda/2$  voltage had to be applied between the first and second transits of the *MO* pulse through the Pockels cell. Application of the  $\lambda/2$  voltage prior to its first pass through the Pockels cell caused the initially *p*-polarized *MO* pulse to undergo a net  $180^\circ$  polarization rotation and to exit the cavity, unamplified, through *PBC*<sub>2</sub>. If the *EOM* switching had not occurred by the second transit of the now *s*-polarized *MO* pulse through the Pockels cell, the *MO* pulse would be rotated another  $90^\circ$  by the  $\lambda/2$  plate and exit the cavity through *PBC*<sub>2</sub>. The cavity length thus had to be fixed to accommodate not only the 6ns *MO* pulse but the 1-2ns *EOM* rise time and any jitter in the *EOM* or *MO* switching circuitry as well.

Due to the thermal problems mentioned earlier, the amplifier was generally run at a repetition rate of 0.25pps. Control of the system at these low repetition rates with the accuracy required for the *EOM* switching was obtained with use of the timing/triggering circuitry shown in Figure 4.2.

The output of a stable function generator operating at  $\sim 16,400\text{Hz}$  was frequency divided by a factor of  $2^{16}$  by a cascaded series of 4-bit counters. This corresponded to the desired repetition rate of 0.25pps. The repetition rate could be altered by changing the frequency of the function

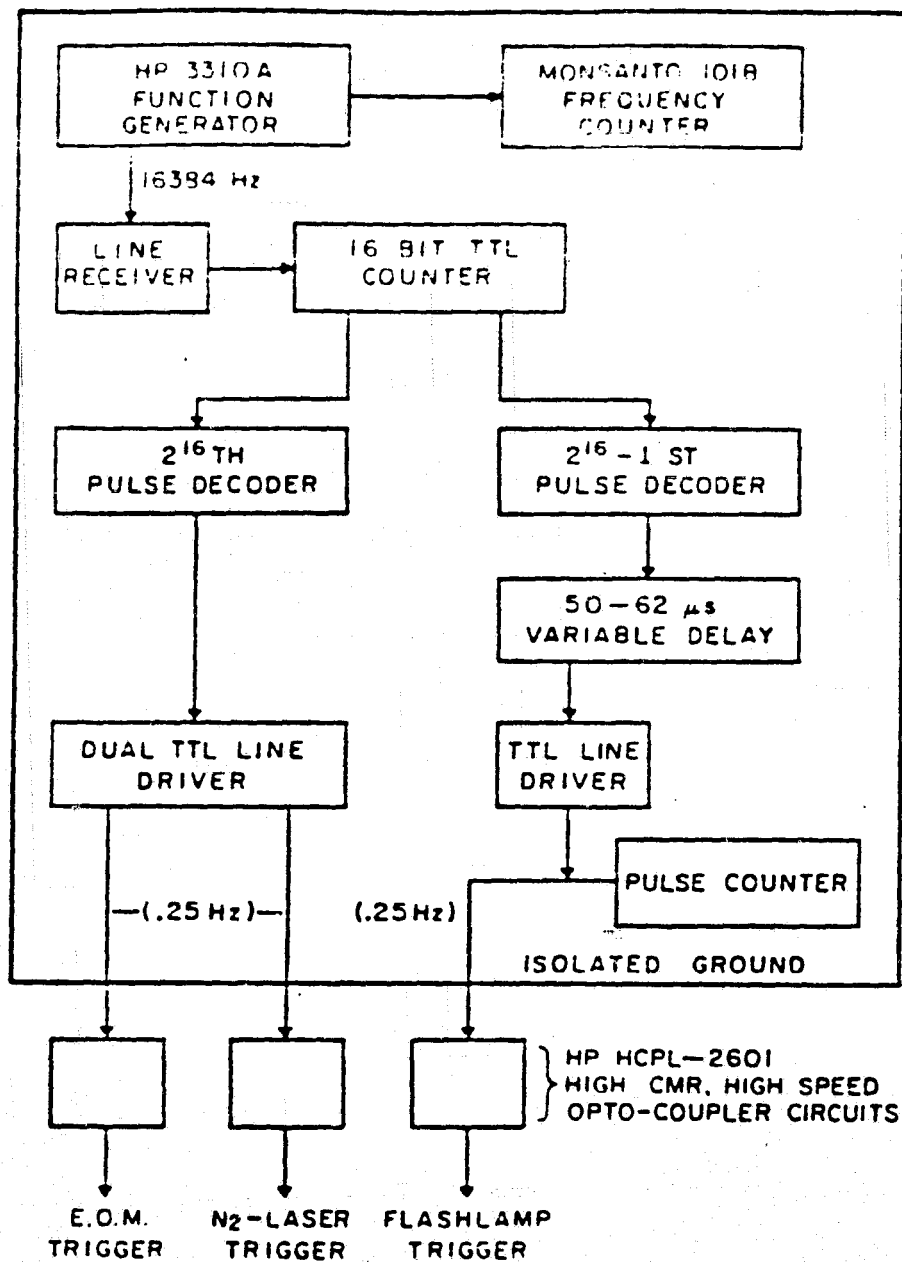


Figure 4.2: Block Diagram of the Timing Circuitry

generator. Decoding the outputs of the counters yielded two successive pulses, the  $(2^{16})$ th and the  $(2^{16}-1)$ st pulses. The  $(2^{16})$ th pulse was used to directly trigger the *MO* and the *EOM*. A 750ns delay existed between the arrival of this trigger pulse and the generation of the *MO* laser pulse. This delay was very stable due to the low-jitter ( $\sim 1$ ns) hydrogen thyratron used in triggering the  $N_2$ -laser. The delay corresponding to the propagation time between the *MO* and the amplifier ( $\sim 12$ ns) also had to be accounted for. A built-in, adjustable delay circuit in the *EOM* driver was used to compensate for the resulting  $\sim 762$ ns delay so that the Pockels cell was switched-on at the proper time with respect to the *MO* pulse.

The  $(2^{16}-1)$ st pulse was input to the flashlamp trigger circuitry shown in Figure 3.1. The flashlamp discharge, however, did not begin until  $\sim 2-5\mu\text{sec}$  after the arrival of the trigger pulse. This delay varied considerably depending on the energy stored on  $C_1$  and the  $SG_1$  operating conditions. As the  $(2^{16}-1)$ st pulse occurred  $\sim 60\mu\text{sec}$  earlier than the *MO/EOM* trigger, a fixed delay of  $50\mu\text{sec}$  together with a finely adjustable delay of  $0-12\mu\text{sec}$  were used to synchronize the flashlamp pulse with the arrival of the *MO* pulse and the switching time of the *EOM*.

The proper synchronization of these components depended on minimizing any jitter present in the triggering circuitry itself. Unfortunately, however, substantial jitter (up to 100ns) still existed in the flashlamp trigger circuitry. When severe enough, the uncertainty in the flashlamp firing time made injection-locking with the short duration *MO* pulses extremely difficult. With more than 100ns uncertainty, it became prohibitively difficult to inject the *MO* pulse close enough to the point at which the amplifier reached threshold to fully injection-lock the amplifier. As



will be discussed later, this condition could possibly be remedied through the use of CW *MO*'s.

In the flashlamp trigger circuitry, both the spark-gap switch and the flashlamp were suspected of contributing to the system jitter. The primary contributor, however, appeared to be the spark-gap switch as the jitter was a strong function of the gas pressure in the gap, and the condition of the electrodes and the spark-plug. The manufacturer (Tachisto) suggested pressurizing the spark-gap with either nitrogen or carbon-dioxide, but warned that use of nitrogen necessitated more frequent cleaning of the electrodes. Currently, spark-gap manufacturers are recommending pressurizing the gap with compressed air to minimize the jitter and cleaning intervals. As the required electrode cleaning interval was expected to be greater than  $10^6$  shots, nitrogen gas was used anyway. Unfortunately, with nitrogen, cleaning was required much more frequently than expected ( $\sim 10^4$  shots) and at each cleaning, the spark-plug had to be replaced due to excessive electrode wear. Although no other pressurizing gasses were tried, the use of nitrogen, undoubtedly, contributed significantly to the jitter problem. Nonetheless, by maintaining the pressure at just below the self-breakdown level and by periodically cleaning the electrodes and replacing the spark-plug, the jitter was kept to a tolerable level ( $< 50$ ns). Even though the jitter problem in triggered spark-gaps can be overcome, it is strongly recommended, for minimum service and jitter, that thyatron switches be used instead.

In addition to the "innate" electronic jitter problem, substantial jitter was induced by the high-voltage switching in the  $N_2$ -laser, the flashlamp, and the *EOM*. This jitter was induced in two ways. First, the high-

voltage switching resulted in the presence of a large amount of electromagnetic noise in the laboratory. The noise, when picked-up by the TTL timing/trigging circuitry, caused sporadic trigger pulses to be generated, ruining the required synchronization. Careful shielding of all electronics and cables, however, alleviated this problem. A more severe source of electrical instability resulted from the direct appearance of voltage-spikes on the electrical grounds of the high-voltage circuits. Although powered from an isolated, floating-ground supply, the voltage spikes were transmitted to the TTL circuitry by the shielding in the trigger cable. The effects were similar to those encountered above when radiated electromagnetic noise was picked-up. To eliminate this problem, the TTL circuitry was completely electrically isolated from the high-voltage circuitry by the installation of an opto-isolator in each trigger channel. The opto-isolators, located in a separate, shielded box, decoupled the TTL circuit ground from that of the high-voltage circuits. Only unidirectional transmission of signals was allowed, thereby eliminating any means of high-voltage feedback.

#### 4.4 - Amplifier Alignment

As discussed in Section 3.8, the cavity-dumped amplifier had to be aligned, at least initially, using an external laser. Since injection-locking is facilitated when the lasing axis of the amplifier is collinear with the path of the injected pulse, the *MO* output was used as the alignment beam in place of the CW dye laser beam used earlier. The alignment procedure, however, was essentially identical to that described in Section 3.8.

The *MO* beam, run at high pulse repetition rates ( $\sim 20$ pps) to ease visual alignment, was polarized by *PBC*<sub>1</sub> and directed to pass through the

center of the dye cell. With only pure ethanol circulating through the dye cell and the  $\lambda/2$  plate "misadjusted", as before, the amplifier cavity was aligned to the *MO* beam using the same "spatial overlapping" technique as described earlier. The extremely poor spatial properties of the *MO* beam, however, made it difficult to determine when the beams perfectly overlapped. This difficulty, coupled with the attenuation of the beam in the cavity and slight directional variations of successive *MO* pulses, made this alignment technique coarse at best.

A more sensitive alignment technique was also attempted. Again, with only pure ethanol flowing through the dye cell, the *MO* pulse was injected into the amplifier and centered in the dye cell. This time, low (0.25pps) *MO* repetition rates were used and the  $\lambda/2$  plate was properly adjusted to give a  $90^\circ$  polarization rotation. Using the timing/trigging circuitry discussed above, the Pockels cell was switched "on" just after the injected pulse had passed through the cell. With the  $\lambda/2$  voltage applied to the Pockels cell, the injected pulse was trapped inside the amplifier cavity. The amplitude of the injected pulse then decayed by an amount proportional to the optical cavity losses on each pass through the amplifier cavity. This decay was observed by placing a photodiode behind one of the turning mirrors. Although dielectric coated for maximum reflectivity, these mirrors ( $M_1$  and  $M_2$ ) transmitted a small percentage of the incident radiation which was detected by the photodiode. A typical decay, although for a slightly different cavity configuration, is shown in Figure 4.3. Successive passes of the *MO* pulse, while trapped inside the amplifier cavity, generated the pulse train.

ORIGINAL PAGE IS  
OF POOR QUALITY



Figure 4.3: Passive Decay of the Injected Pulse.

Horiz: 50ns/cm

The cavity was aligned by adjusting the optics to maximize the number of pulses observed. When the cavity was misaligned, the *MO* beam would no longer strike the mirrors at the same point on each pass. This would be indicated by a rapid decay in the intensity of the pulses striking the photodiode. It was believed that the cavity could be very accurately aligned using this technique and that an exact figure for the optical cavity losses obtained. The decay of the pulse train shown in Figure 4.3 was  $\sim 16\%$  per pass (a linear configuration was used here, hence two transits were required to generate one pulse) which was somewhat higher than the expected cavity losses. It was believed that some of the inaccuracy here was due to the divergence of the *MO* beam.

Developing an accurate alignment procedure for the amplifier, thus, remained a formidable problem because of the poor spatial properties of the *MO* pulse. The first of the two techniques presented above was the alignment technique generally used despite the fact that the amplified beam often developed along a different axis than that defined by the *MO* beam during the alignment procedure. As discussed in Section 3.9, this often resulted in the presence of a "shoulder" on the output pulse because the path of the amplified pulse was not parallel to the optic axis of the Pockels cell. The Pockels cell then had to be slightly readjusted during the operation of the system in order to eliminate the "shoulder".

The criterion that the lasing axis of the amplifier be made collinear with the path of the injected pulse is an especially critical one when the modal properties of the amplifier output are a concern. In this case, however, it was uncertain as to whether a high-power Gaussian or multimode pulse would emerge when the amplifier was operated in the highly gain-

saturated regime. In any case, the system must be first injection locked in the region where threshold first occurs (i.e. near the center of the dye cell). It was thought that as the intensity of the amplified pulse grew and approached the dye saturation intensity it would begin to injection-lock the radiation present in the extremities of the dye cell as they approached threshold. The entire dye volume would then eventually be injection-locked by the *MO* pulse.

#### 4.5 - Initial Injection-Locking Experiments

With the system identical to that shown in Figure 3.7, with the exception that the *MO* assembly, shown in Figure 4.1, was used in place of the CW dye laser, initial attempts to injection-lock the amplifier were made. Preliminary to these attempts, the amplifier was aligned using the procedure outlined above and operated as an oscillator in order to set the *EOM* switching times. The *MO* pulse wavelength,  $\lambda_i$ , was then set to the peak wavelength of the oscillator output,  $\lambda_o = 590\text{nm}$ , to enhance the probability that locking would occur.

In order to optimize the *MO* pulse injection time (with respect to the flashlamp pulse) the injection times were slowly varied until evidence of injection-locking was observed. At this point it was assumed that the *MO* pulse was being injected near the threshold point of the amplifier. The flashlamp discharge energies,  $E_f$ , were initially kept low. Once the system exhibited indications of being injection-locked, the injection times were optimized and  $E_f$  was gradually increased. Since the point in time that the amplifier crossed threshold was a function of  $E_f$ , the injection time had to be adjusted slightly for each value of  $E_f$ .

The *EOM* "turn-off" time was then adjusted to maximize amplified pulse energies,  $E_a$ . The factors involved in optimizing the cavity-dumping time were discussed in Section 3.9. The intensity of the cavity-dumped pulse (neglecting the trailing "shoulder" due to the two-pass oscillation) was generally maximized when cavity-dumping occurred near the peak of the flashlamp pulse. The optimal cavity-dumping time, however, was a slight function of  $E_f$ . For smaller values of  $E_f$ , the optimal extraction times occurred somewhat after the peak of the flashlamp pulse. As  $E_f$  increased, the optimal extraction time moved towards the peak of the flashlamp pulse. Presumably, this effect was due to the thermal and triplet state problems which become more pronounced with increasing  $E_f$ . It is, however, a very slight effect. The total variation in optimal extraction times as a function of  $E_f$  was  $\sim 100$ ns, and for a given  $E_f$ , there was only a slight variation in  $E_a$  within 100ns of the optimal extraction time.

With the system properly synchronized, the system could be almost completely (i.e.  $\rho=1$ ) injection-locked at  $\lambda_i = 590$ nm. In order to get an initial indication of how  $\rho$  and  $E_a$  would vary as a function of  $E_f$ , flashlamp pumping energies were then gradually increased. Pulse extraction times were set late enough in the flashlamp pulse in order to minimize the intensity of the "two-pass" oscillation. The injection-locking efficiency,  $\rho$ , remained equal to unity for all values of  $E_f$  recorded. The experiment was terminated when amplified pulse energies reached 25mJ for fear of again damaging the dielectric polarizing coating on  $PBC_2$ .

Temporally, the shape of the injection-locked amplifier output appeared similar to that of the oscillator output. The only difference, as

expected, was that the injection-locked output pulse had a larger amplitude. As a ring-oscillator, the pulse energy was stored equally in the two counter-propagating fields. Thus, when cavity-dumping occurred, only half of the total energy would exit the cavity through  $PBC_2$  and be detected by  $PD_1$ . The other half would exit the cavity through  $PBC_1$ . When completely injection-locked, however, the  $MO$  forced the radiation in the amplifier to circulate only in the direction of propagation of the  $MO$  pulse. All of the stored energy would then exit through  $PBC_2$ . Analyzing the output from both ends of the amplifier was useful in determining how complete the injection-locking was. This will be discussed later.

Using smaller flashlamp discharge energies, investigations were then performed to determine how tunable the injection-locked amplifier could be made without a reduction in the injection-locking efficiency,  $\rho$ . Since the amplifier was untuned, it was expected that the amplifier would be difficult to injection-lock once  $|\lambda_i - \lambda_o|$  became large with respect to the homogeneous linewidth of the dye. In fact, the results of previous investigations (detailed in Chapter 2) showed that, in untuned amplifiers, complete injection-locking occurred only for  $|\lambda_i - \lambda_o| = \sim 20\text{\AA}$ . The observations presented below confirmed these findings.

The amplified pulse spectrum was analyzed as the  $MO$  wavelength was tuned in 2nm steps from 581nm to 601nm. Both amplifier (with injection) and oscillator (w/o injection) output pulse energies were also recorded at each step. Due to the difficulty in obtaining information as to the relative energy in a given spectral band, precise determinations of  $\rho$  as a function of  $\lambda_i$  were not made at this time. This measurement was



performed later (Chapter 5) using an OMA. Only qualitative assessments as to the degree of injection locking were used at this time.

There existed a definite correlation between the observed output energies and the spectral content of the outputs. Injection-locking was observed from  $587\text{nm} \leq \lambda_i \leq 593\text{nm}$ . Throughout this range, amplified pulse energies were roughly twice that of the oscillator outputs, a further indication of the high degree of injection-locking. Incomplete locking was evidenced by the presence of varying amounts of broadband, off-color (i.e.  $\lambda \neq \lambda_i$ ) radiation which accompanied the amplified pulse. For  $583\text{nm} < \lambda_i < 587\text{nm}$  and  $593\text{nm} < \lambda_i < 597\text{nm}$  the amplifier was only partially injection-locked. Although most of the output energy appeared to be within  $\Delta\lambda_i$ , small amounts of off-color radiation were observed in the amplified pulse. The ratio of the injection-locked output pulse energies to the un-locked pulse energies dropped below 2 as expected for these values of  $\lambda_i$ . This fact was consistent with the observation of significant amounts of broadband radiation, centered at  $\lambda = 590\text{nm}$ , exiting the cavity through  $PBC_1$ . This radiation in the counter-clockwise propagating beam was allowed to build-up at those frequencies and areas in the dye cell that were not overridden by the presence of the  $MO$  pulse.

When  $\lambda_i$  was tuned even further from the peak of the R6G emission profile ( $\lambda = 590\text{nm}$ ), the percentage of output energy in the amplified  $MO$  pulse decreased even more. For  $\lambda_i \leq 583\text{nm}$  and  $\lambda_i \geq 599\text{nm}$  the spectrometer detected strong amounts of off-color radiation. It seemed that once  $|\lambda_i - 590\text{nm}|$  exceeded the homogeneously broadened linewidth of the dye, the molecules radiating at  $\lambda = 590\text{nm}$  could begin to lase independently of those contributing to the  $MO$  pulse amplification. In fact, even

with  $\lambda_i = 590\text{nm}$ , very small amounts of broadband green (centered at  $\lambda = 578\text{nm}$ ) and red (centered at  $\lambda = 602\text{nm}$ ) light were observed emanating from  $PBC_1$ . Thus, a bandpass filter, with a passband centered at  $\lambda_i$  must be installed to prevent the independent oscillation of light at other frequencies and to completely injection-lock the amplifier. The effectiveness of installing even a weakly dispersive filter (i.e. a prism), with a passband of  $\sim 1\text{nm}$ , will be discussed in Chapter 5.

#### 4.6 - *MO* Linewidth Considerations

Many of the applications which require tunable, high-energy laser pulses also require that these pulses be narrowband [1-4]. During the initial injection-locking experiments, presented in the last section, *MO* pulse linewidths of  $0.05\text{nm}$  were used. Considering the pulse energies obtained, their spectral brightness was extremely high for dye laser pulses of this duration. It was thus of interest to determine if the amplifier could be completely injection-locked to substantially narrower linewidths without sacrificing output energies so as to further increase the spectral brightness of the output pulses.

To conduct this experiment, a Fabry-Perot etalon was installed in the *MO* (as mentioned in Section 4.2) to reduce *MO* linewidths to  $0.0015\text{nm}$ . Installation of the etalon in the *MO* reduced usable *MO* pulse energies to a maximum of  $1\mu\text{J}$ . The experiment was performed in the same manner as the one performed in Section 4.5, where  $\rho$  and  $E_a$  were monitored as a function of wavelength, except that only three values of  $\lambda_i$  were used ( $585\text{nm}$ ,  $590\text{nm}$ ,  $595\text{nm}$ ). Measurement of the linewidth of the amplified pulses, with adequate precision, required the installation of the Fabry-

Perot etalon in the LS-1 spectrometer, as discussed earlier. With the spectrometer operated in this fashion, however, no quantitative information as to the intensity of any off-color radiation could be obtained. So, after completing the linewidth measurements for a given wavelength, the etalon had to be removed and the spectrometer operated in the standard mode, using the diffraction grating, in order to detect wideband emission.

With  $\lambda_i$  set to 590nm, output pulse linewidths remained identical to those of the narrowband *MO* pulse. Output pulse energies were also identical to those obtained with  $\Delta\lambda_i = 0.05\text{nm}$  and there was no evidence of any "off-color" radiation. For  $\lambda_i = 585\text{nm}$  and  $595\text{nm}$ , however, the results were somewhat different. In both these cases, the difference was attributable to the previously observed dependency of  $\rho$  on  $\lambda_i$ . Again, when  $\lambda_i \neq 590\text{nm}$ , broadband, "off-color" radiation emerged together with the amplified *MO* pulse. Output pulse energies for these wavelengths were also less than those obtained for  $\lambda_i = 590\text{nm}$ , where complete injection-locking occurred. In fact, the ratios of  $E_a$  to  $E_o$  for  $\lambda = 585\text{nm}$  and  $595\text{nm}$  were similar to those obtained using  $\Delta\lambda = 0.05\text{nm}$  which indicated that  $\rho(\lambda)$  was not a strong function of  $\Delta\lambda_i$ . A more significant indication of this, however, is that the linewidth of the injection-locked fraction of the output pulse remained identical to that of the injected *MO* pulse (i.e.  $0.0015\text{nm}$ ). No evidence of any spectral broadening during amplification was observed.

In general, it appeared that, given only the crude assessments of  $\rho$  obtainable from the spectrometer and the radiometer, that the injection-locking process was independent of  $\Delta\lambda_i$  for injected pulse linewidths  $> 0.0015\text{nm}$ . The spectral brightness of the output pulses at 590nm, using

these narrow linewidths increased to  $3 \times 10^9 \text{ W/nm}$ . Since no evidence of spectral broadening had yet occurred, it was naturally of interest to see if this figure could be improved on further. One fundamental restriction to the amount of possible improvement was imposed by the Fourier transform limit. For pulses of this duration, the transform bandwidth limit is  $\sim 150\text{MHz}$  which is roughly only a factor of 9 times smaller than the  $1.3\text{GHz}$  bandwidth of the *MO* pulses used above. However, due to the lack of available means for further reducing  $\Delta\lambda_i$ , it was uncertain as to how much closer to the transform limit the bandwidth of the amplified pulses would get while still retaining the spectral purity of the low-energy *MO* pulse.

#### 4.7 - Installation of High-Power Polarizing Beamplitters

The results presented in the last two sections indicated that the system could indeed be injection-locked to a narrowband *MO* pulse. While these results were promising, the injection-locked tuning range was smaller than desired and amplified pulse energies were still limited to  $\sim 25\text{mJ}$ . The limitation on the output pulse energy was imposed by the damage threshold of the *PBC*'s, as flashlamp discharge energies had to be moderated to keep from damaging these components. In order to safely use larger  $E_f$ 's, to extract more energy from the system, the broadband *PBC*'s had to be replaced with high damage threshold polarizing beam-splitters.

In addition to requiring that the beamsplitters possess a large damage threshold, the devices must have low insertion losses and a reasonably large extinction ratio, especially in the reflection mode. Two types of

polarizers were, thus, considered as replacements for the *PBC*'s, a Glan-type, air-spaced prism polarizer and an "open-faced", dielectric coated polarizer. The prism polarizers provided broadband polarization with extremely high isolation of the polarized components. When made of high-grade, Schlieren Free calcite, and AR coated, the transmission of these devices was 99%. Their damage threshold, however, was only slightly larger than that of the *PBC*'s. The dielectric polarizers, on the other hand, possessed substantially larger damage thresholds. For this reason, dielectric coated polarizers, although inferior in many respects, were used instead.

The high-power polarizing beamsplitters (*HPB*'s) used in this work were manufactured by CVI Laser Corporation (TFP2 Series). Their damage threshold was advertised as being  $5\text{GW}/\text{cm}^2$  for a nanosecond duration pulse. Like the *PBC*'s, they reflected greater than 99% of the incident *s*-polarized light while transmitting over 95% of the incident *p*-polarized light. However, unlike the *PBC*'s, they were not broadband polarizers. The quoted efficiencies were only for a given wavelength at a given angle of incidence,  $\theta_i$ .

The *HPB*'s were coated for 590nm light incident at  $57^\circ$ . Figure 4.4 shows the measured transmission and reflection characteristics as a function of  $\lambda$  and  $\theta_i$ . The most significant feature to note is that the reflectivity for *s*-polarized light remained near unity over the entire R6G emission spectrum. Had this not been the case, the polarizers would simply have acted as output couplers for wavelengths where  $\lambda \neq 590\text{nm}$ , thereby defeating the purpose of cavity-dumping the amplifier.

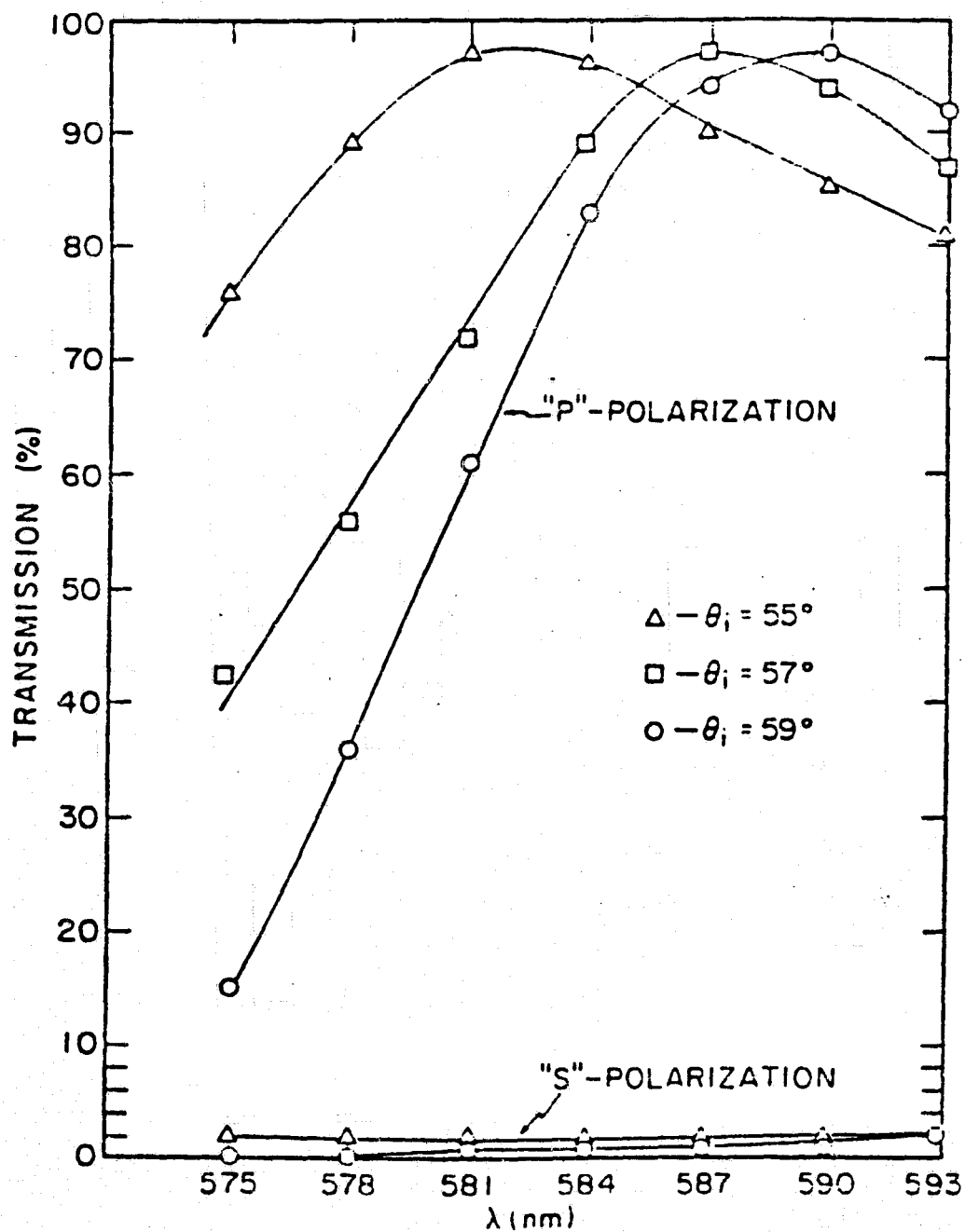


Figure 4.4: Transmission Profiles of the High Power Polarizing Beamsplitters

The transmission of the  $p$ -polarized light, however, was a strong function of both  $\lambda$  and  $\theta_i$ . As will be discussed later, the design of the amplifier had to be altered as result of this property. The net effect of the wavelength dependent  $p$ -transmission was that output pulse energies became proportional to the  $p$ -transmission at that wavelength. Since the performance of the *HPB*'s was also a function of the angle of incidence, the orientation of the *HPB*'s could be set to optimize performance at a given wavelength. To do this, however, a complete realignment of the amplifier would be required. The *HPB*'s were set to maximize the transmission of  $p$ -polarized light at  $\lambda = 590\text{nm}$ .

With  $\lambda_i = 590\text{nm}$  the system was aligned and operated as it had been with the *PBC*'s. The output pulse waveforms, however, were totally different than that of Figure 3.9. Large amounts of off-color radiation exited the cavity through both *HPB*<sub>1</sub> and *HPB*<sub>2</sub> prior to cavity-dumping. The off-color radiation, primarily green light centered at 578nm, continued to lase even after cavity-dumping. As no other changes in the system had been made, the problem was assumed to be caused by the *HPB*'s. This assumption was confirmed when the replacement of *HPB*<sub>1</sub> with a *PBC* alleviated the problem. The system injection-locked properly as before with little indication of off-color build-up.

As noted when the *PBC*'s were used, it was difficult to suppress the build-up of off-color radiation at a given  $\lambda$  when  $|\lambda - \lambda_i|$  greatly exceeded the homogeneous linewidth of the dye. Even for  $\lambda_i = 590\text{nm}$ , small amounts of off-color radiation were observed in the output pulse. The increased intensity of the off-color light with the use of the *HPB*'s was undoubtedly due to the reflectance of a significant percentage of the

incident  $p$ -polarized light. Thus, for the shorter wavelengths,  $p$ -polarized light, in addition to the  $s$ -polarized light, was fed back into the cavity. The amplifier then functioned as an oscillator for the  $p$ -polarized green light, allowing  $\sim 40\%$  of the incident light to exit through the  $HPB$ 's on each pass.

#### 4.8 - Effects of Cavity Dispersion on Injection-Locking Performance

The temporal profile of the output pulse could have been cleaned up by the installation of a linear polarizer in the amplifier to compensate for the poor extinction ratios of the  $HPB$ 's. Addition of a polarizer, however, would not have improved injection-locking efficiencies beyond those observed earlier with the  $PBC$ 's. It was thought that the installation of a birefringent (Lyot) filter would accomplish both objectives. In addition to providing the spectral dispersion, required to increase  $\rho$ , the 3-element filter, installed at Brewster's angle, would assist in removing the unwanted  $p$ -polarized light from the cavity. The passband of the filter, set by the thickness of the thickest element in the filter, was  $\sim 1\text{nm}$  FWHM. This increased dispersion (both polarization and spectral) was obtained with minimal additional optical loss, as the measured insertion loss of the filter was less than  $1\%$  for the transmitted  $s$ -polarized (with respect to the amplifier) light.

The filter was positioned in the cavity between the two turning mirrors,  $M_1$  and  $M_2$  (cf. Figure 4.5). Amplifier alignment was performed exactly as before except that  $\lambda_0$ , now determined by the birefringent filter, had to be adjusted so that  $\lambda_0 = \lambda_i$  for each  $\lambda_i$ . The filter was



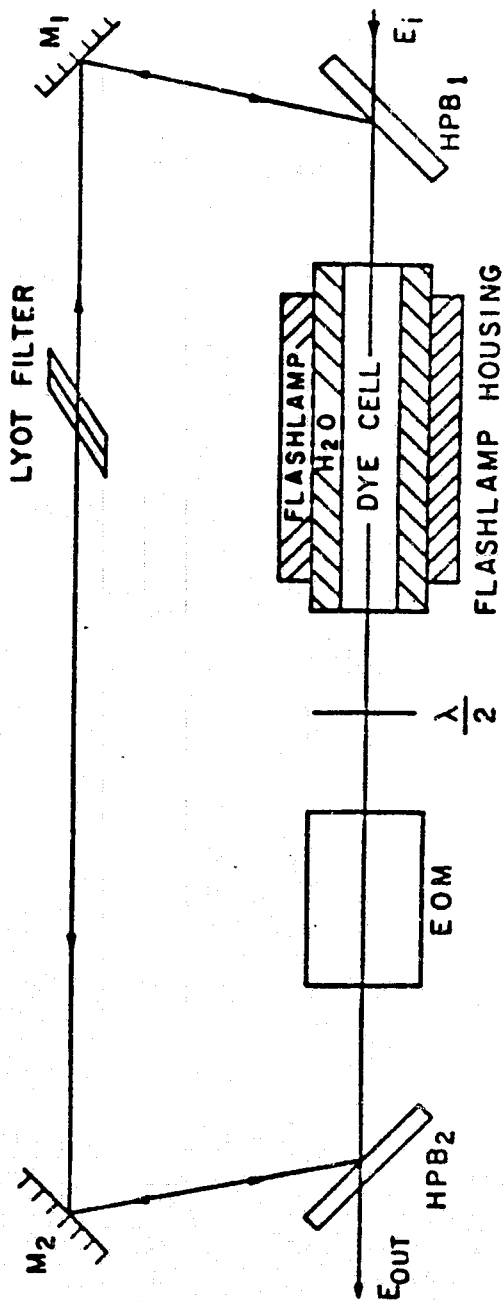


Figure 4.5: Schematic of the Cavity-Dumped CFP Dye Laser with a Birefringent Tuner

adjusted by rotating it until  $\lambda_i$  was transmitted with minimal loss and without any polarization rotation.

With the addition of the filter, the amplifier injection-locked as it had previously. The output pulses, however, were only "clean" when  $\lambda_i = 590\text{nm}$ . As  $\lambda_i$  and  $\lambda_o$  were tuned towards shorter wavelengths a "shoulder" appeared on the cavity-dumped pulse (Figures 4.6 - 4.8). By placing a monochromator, set to pass  $\lambda_i$ , in front of  $PD_1$ , the "shoulders" were found to be of the same wavelength as the cavity-dumped pulse. Clearly, this was another manifestation of the dispersive properties of the *HPB*'s. When cavity-dumped, the high-power, *p*-polarized pulse was to pass completely through *HPB*<sub>2</sub>. But for  $\lambda_i \neq 590\text{nm}$ , a percentage of the *p*-polarized amplified pulse was reflected back into the cavity. The exact percentage of the light reflected can be inferred from the *HPB* dispersion curves of Figure 4.4. The birefringent filter, although dispersive enough to eliminate the relatively low intensity off-color radiation which occurred prior to cavity-dumping, was not dispersive enough to stop a percentage of the high-intensity cavity-dumped pulse from continuing to oscillate in the amplifier cavity. The pulse waveforms shown in Figures 4.6 - 4.8 demonstrate this extremely well. As  $\lambda_i$  and  $\lambda_o$  were tuned towards shorter wavelengths, where the *p*-reflectivity of the *HFP*'s increased, the intensity and duration of the "shoulder" increased. The effect was not as pronounced for  $\lambda > 590\text{nm}$  because the *p*-transmission did not decrease as rapidly for the longer wavelengths.

Clearly, additional polarizing was required to remove the reflected *p*-polarized radiation from the cavity before it could be amplified again. It was obvious from the experiments with the birefringent filter that the

ORIGINAL PAGE IS  
OF POOR QUALITY

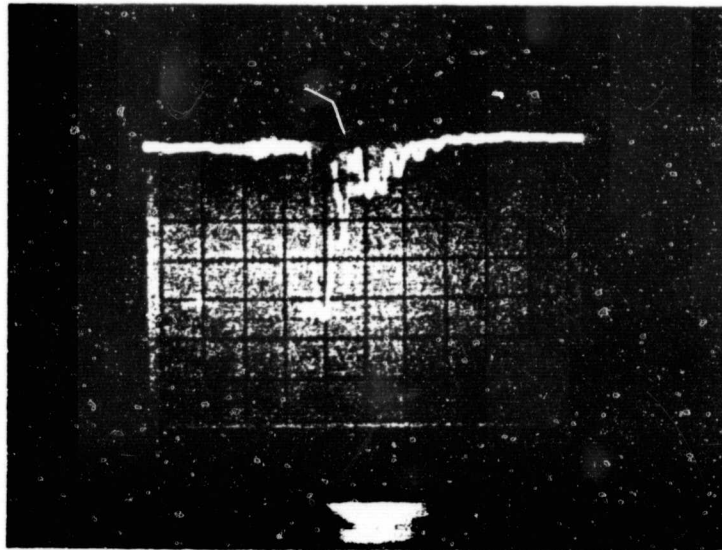


Figure 4.6: Injection-Locked Output for  $\lambda_i = 590\text{nm}$   
Horiz:  $20\text{ns/cm}$ ;  $E_a = 40\text{mJ}$ ;  $\Delta\lambda = 0.05\text{nm}$

ORIGINAL PAGE IS  
OF POOR QUALITY

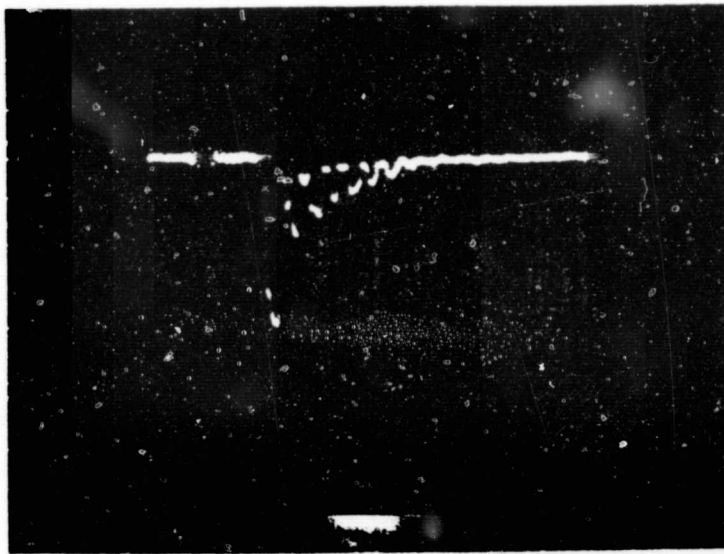


Figure 4.7: Injection-Locked Output for  $\lambda_i = 587\text{nm}$

Horiz: 20ns/cm;  $E_a = 45\text{mJ}$ ;  $\Delta\lambda = 0.05\text{nm}$

ORIGINAL PAGE IS  
OF POOR QUALITY

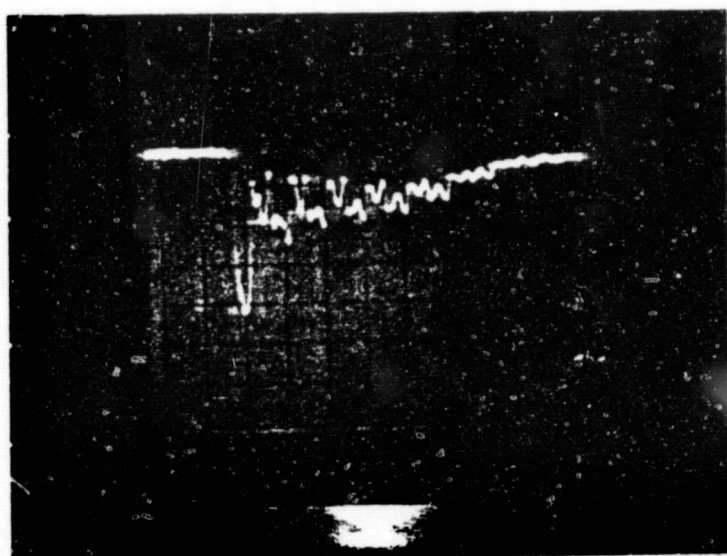


Figure 4.8: Injection-Locked Output for  $\lambda_i = 583\text{nm}$

Horiz:  $20\text{ns/cm}$ ;  $E_o = 52\text{mJ}$ ;  $\Delta\lambda = 0.05\text{nm}$

linear polarizer would have to have a large extinction ratio. It would also have to present minimal loss to the transmitted component and have to be capable of withstanding high peak powers.

The polarizer chosen was an air-spaced, Glan-type polarizing prism. Made of calcite, a birefringent crystal, the prism used the air-spacing as a dielectric interface at which one polarization component, due to the double refraction, was reflected while the other was transmitted essentially without loss. The prism was installed so that light, *s*-polarized with respect to the amplifier, was transmitted through the prism. Transmission loss was measured to be  $< 1\%$  while the extinction ratio of the device, for the transmitted *s*-polarized component, was 1000:1.

The amplifier cavity configuration was then as shown in Figure 4.9. The use of the birefringent filter, as a low-loss tuning element, together with the linear polarizer, allowed the extraction of both temporally and spectrally cleaner pulses than those shown in Figures 4.6-4.8. Although these pulses were much "cleaner" than before, throughout the entire R6G emission spectrum, some broadband, off-color green radiation still emerged after cavity-dumping.

It was thought that the birefringent filter, with a passband of  $\sim 1\text{nm}$ , should have been dispersive enough to suppress any oscillation at these frequencies. Birefringent (Lyot) filters, however, inherently have periodic passbands, each with a number of lesser sidebands. The sideband spacing and passband periodicity are both dependent on the ratio of the thicknesses of the plates which comprise the filter. Although the filter possessed only one passband in the R6G emission band, a set of weakly attenuating sidebands was found to exist at wavelengths approximately

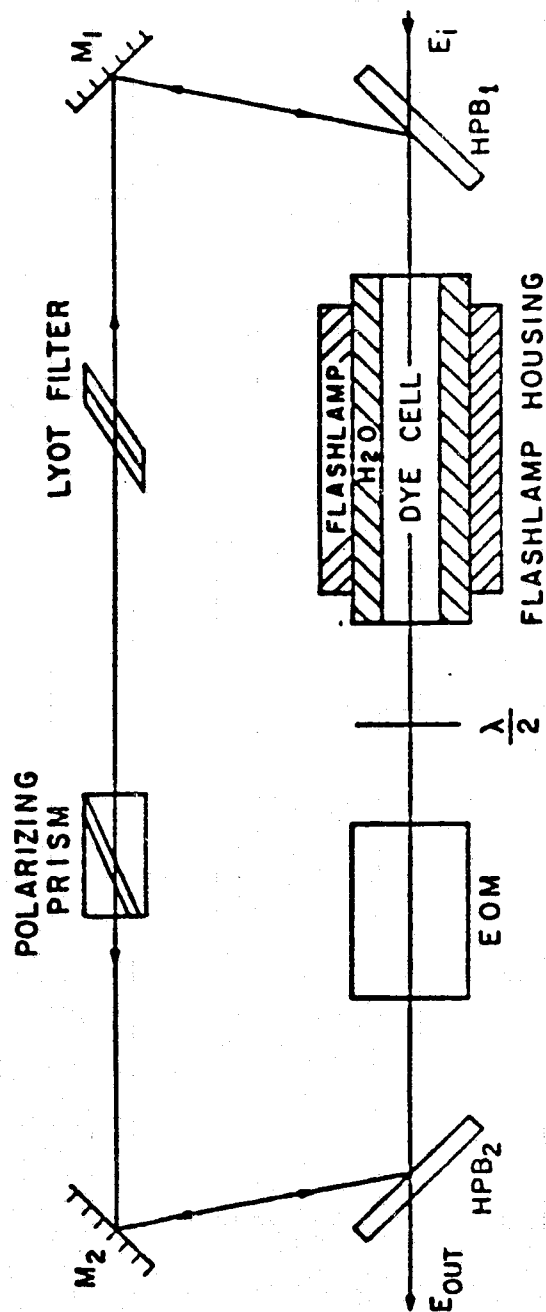


Figure 4.9: Schematic of the Cavity-Dumped CFP Dye Laser with a Birefringent Tuner and a Polarizing Prism

6nm from the central passband wavelength. Thus, green radiation centered at  $\lambda_i - 6\text{nm}$ , encountering little attenuation from the birefringent filter, would not be inhibited from lasing after cavity-dumping had occurred. And, as described in Chapter 3, after cavity-dumping, the amplifier became a two-pass oscillator with a propensity to lase in the green.

#### 4.9 - Use of a Prism as the Intra-Amplifier Tuner

From the experience with the birefringent filter, it was clear that the installation of an intracavity tuning element dramatically improved the injection-locking performance of the system. Output pulses were much "cleaner" over a broader range of wavelengths both temporally and spectrally than those obtained using a untuned amplifier. Imperfections in the output pulse profiles, discussed in the last section, were manifestations of the inherent periodicity of the birefringent filter used as the tuning element. Although by a proper combination of the plate thicknesses a suitable Lyot filter could have been designed to alleviate these problems, and further "clean-up" the outputs, a simpler solution was to use a dispersing prism as the tuning element. A Littrow or Brewster dispersing prism would function equally as well as a polarization sensitive, low insertion loss tuner but would not exhibit the periodicity problems inherent with the Lyot filter. The fact that these are only weakly dispersive elements was not expected to be a factor.

The Lyot filter was removed and a Littrow dispersing prism installed in the cavity as shown in Figure 4.10. A Littrow prism was chosen as the tuner so as to minimize the number of alterations that had to be made to



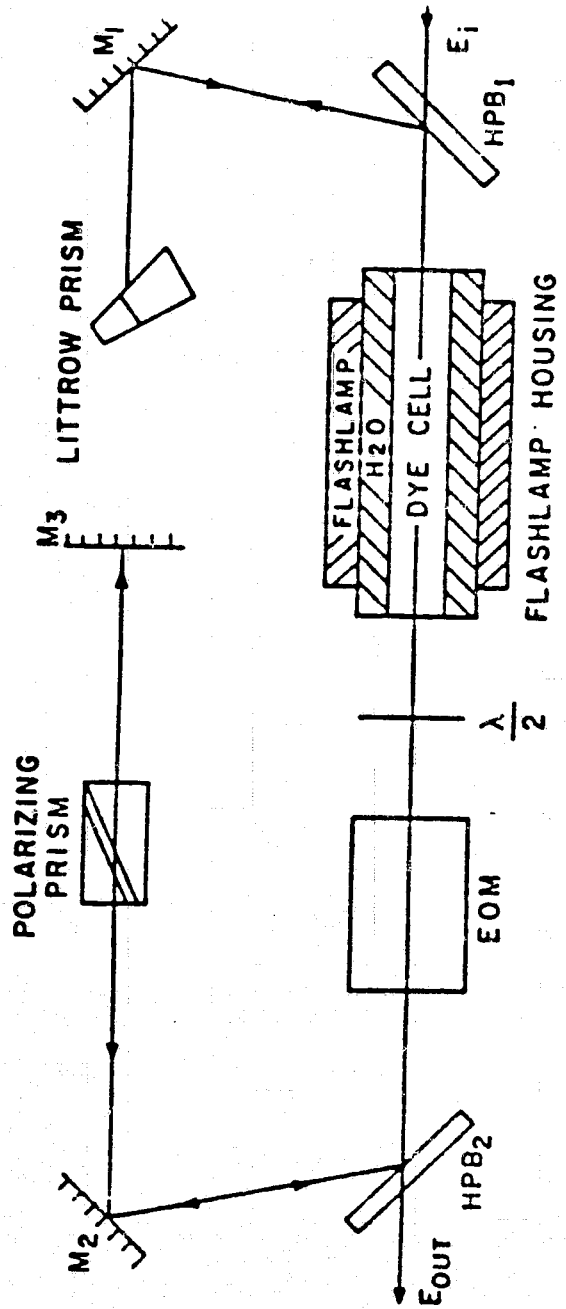


Figure 4.10: Schematic of the Linearly Configured CFP Dye Laser with a Littrow Prism Tuner. (The actual orientation of the littrow prism was orthogonal to that shown.)

the cavity. The only major change required was the reconfiguration of the amplifier into a linear cavity. This reconfiguration, however, introduced a number of new dimensional constraints into the design of the amplifier cavity. The most significant of these emerged from an inherent problem of cavity-dumping linearly configured oscillators. Unless an extremely accurate ( $\pm 1$  ns) account of the elapsed time between the initial arrival of the *MO* pulse at the *EOM* and the cavity-dumping time is maintained, it becomes probabilistic as to which *HPB* the amplified pulse will exit through. For only if the amplified pulse is between the *EOM* and the Littrow prism (cf. Figure 3.6) when the *EOM* is switched off will the amplified pulse exit through *HPB*<sub>2</sub>, as desired. Thus, the distance from the *EOM* to the Littrow prism had to be made large in comparison to the distance from the *EOM* to *M*<sub>3</sub>. There was, however, also a constraint on the distance from the *EOM* to *M*<sub>3</sub>. This distance had to be made long enough to store the 6 ns injected *MO* pulse while the *EOM* was switched from "off" to "on". Hence, including the  $\sim 1$ -2 ns rise time of the *EOM*, the round-trip distance from the *EOM* to *M*<sub>3</sub> and back had to be a minimum of  $c \cdot 8$  ns = 2.4 m. The distance from the *EOM* to *M*<sub>3</sub> used was 1.25 m. Initially the Littrow prism was placed a distance of 2.4 m from the *EOM*. With these cavity dimensions there was roughly a 2:1 probability that, when the amplifier was cavity-dumped, the *MO* pulse would exit through *HPB*<sub>2</sub>.

With the prism, the alignment of the amplifier became a much more significant concern for, unlike the Lyot filter, the prism is a directionally dispersive tuner. The Littrow prism had to be adjusted so that  $\lambda_i$  returned through the dye cell along the same axis that it had on its initial

pass. Due, in part, to the extremely poor spatial properties of the *MO* beam, however, this alignment technique proved to be extremely coarse. The amplified beam invariably emerged from the cavity on a slightly different axis than that of the *MO* beam which was used for alignment. In fact, it was not unusual to have  $\lambda_o$  differ from  $\lambda_i$ , for which the cavity and prism were supposedly aligned, by as much as 3nm. The system, thus, had to be operated first as an oscillator in order to determine the exact  $\lambda_o$  set by the prism. At this wavelength, the alignment of the Pockels cell was checked, as described earlier, to ensure that the lasing axis was still parallel to the optic axis of the crystal. A realignment of the Pockels cell often induced slight changes in  $\lambda_o$ . Then, when necessary,  $\lambda_i$  was tuned until  $\lambda_i = \lambda_o$ . Using the remotely controlled *MO* grating drive assembly, this adjustment was performed in a matter of seconds. Once aligned for a given  $\lambda_o$  there was little drift in  $\lambda_o$  throughout the course of an experiment.

The only change that had to be made in the operation of the system was that, now, the cavity-dumping time (*EOM* turn-off time) required adjustment as there was no guarantee as to which *HPB* the amplified pulse would exit through. This adjustment was performed by finely varying the  $\lambda/2$  pulse width control on the *EOM* driver until the *EOM* turn-off time occurred when the amplified pulse was between the *EOM* and the Littrow prism. Optimization of the *EOM* turn-off time was performed by noting the changes in output pulse energy (through *HPB*<sub>2</sub>) as a function of the *EOM* switching time. When these were maximized, it was assumed that the entire amplified pulse exited the cavity through *HPB*<sub>2</sub> as desired.

The injection-locking performance of the system was evaluated in the same manner as discussed in Section 4.5. The results obtained, however, using the Littrow prism as the tuning element, were much different than those presented earlier. Even functioning as an oscillator, the performance of the system improved dramatically. The temporal profiles of the outputs were extremely "clean" as there was no indication of any laser radiation exiting the cavity either prior to, or after, cavity-dumping (Figure 4.11). As expected, the prism prohibited the build-up of the green, "two-pass" oscillation that constituted the "shoulder" of the output pulse shown in Figure 4.8. The prism, of course, set  $\lambda_0$  and reduced  $\Delta\lambda_0$  to approximately 1nm FWHM. Output pulse energies were comparable to those obtained previously.

The most significant impact that the installation of the prism had was on the injection-locking performance of the system. As observed while using the Lyot filter, the ability to set  $\lambda_i = \lambda_0$  allowed the amplification of the *MO* pulse to occur over a broad range of  $\lambda'$ s with near unity injection-locking efficiencies. Using the prism complete injection-locking was observed for  $582\text{nm} \leq \lambda \leq 602\text{nm}$ . Amplified pulse energies were again comparable to those previously obtained, but, this time the temporal profile of the pulse was exceedingly clean.

With this configuration, it appeared that the generation of widely tunable, narrowband, cavity-dumped pulses was indeed possible. And that by injection-locking a weakly-tuned amplifier, which still had only minimal optical cavity losses, that these characteristics could be obtained without sacrificing output pulse energies. What needed to be investigated, at this point, was the dependency of  $E_a$  on  $E_f$  and experiments which would

detail the dependency of the injection-locking process on such parameters as  $E_i$ ,  $\Delta\lambda_i$ , etc..

#### 4.10 - Additional Resonator Design Considerations

The reconfiguration of the amplifier into a linear cavity imposed many constraints on the resonator design. Some of these were discussed in detail in the last section although many were not mentioned. During the course of these investigations a variety of different resonator designs were used. Although it is not feasible to detail the description and performance of each of these designs, certain general features which influenced system performance became apparent and are worthy of mention.

The placement of the prism with respect to the dye cell, in the linearly configured resonator, was an important consideration. For, when the positions of  $M_3$  and the Littrow prism (c.f. Figure 4.10) were interchanged there was a dramatic change in the output as the green, "two-pass" oscillation that was observed earlier, after cavity-dumping, again reappeared. Although unexpected, the reason for its reappearance was obvious. After cavity-dumping, the green radiation propagating counterclockwise through the dye cell could be reflected back through the dye cell by  $M_3$ , for a second pass, and exit the cavity without ever having "seen" the dispersing prism that was to remove this radiation. The green radiation propagating through the dye cell in a clockwise manner, however, was dispersed by the prism so it never developed into laser radiation. It was thus concluded that the tuning element must be placed so that the dye cell is between it and  $HPB_2$ , the output coupler.

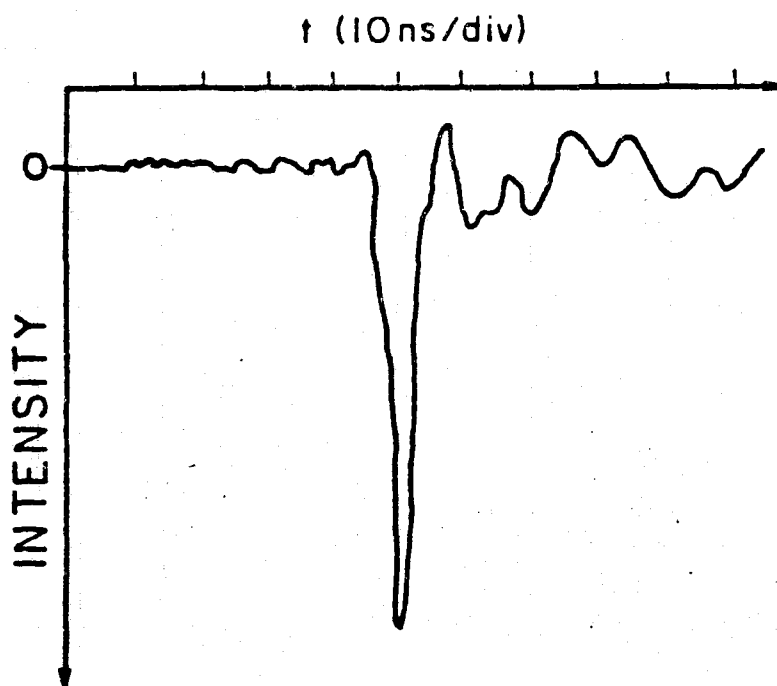


**Figure 4.11: Temporal Profile of the Injection-Locked CFP Dye Laser Output Pulse.**

As mentioned in the last section, it was desired that the distance between the prism and the *EOM* be made as large as possible in order to relax the constraints on the *EOM* "turn-off" time. Increasing this distance also had the desired effect of reducing  $\Delta\lambda_0$ , which, in turn, reduced the amount of fluorescence noise with which the injected *MO* pulse had to compete. However, when the distance between the dye cell and either of the end reflectors became much larger than half of the spatial displacement of the 6ns pulse (i.e. 0.9m), the performance of the system began to degrade. Although output pulse energies remained constant, injection-locking efficiencies dropped below unity, regardless of  $\lambda$ , and the temporal profiles of the output pulses broadened. Apparently, during the period of time that the amplified pulse was spread-out, spatially, between the dye cell and one of the end reflectors, the depleted laser medium recovered and laser radiation developed independently at  $\lambda_0$ . But, since, for this fraction of the stored energy,  $\Delta\lambda = \Delta\lambda_0$  (not  $\Delta\lambda_i$ ), the net injection-locking efficiency of the pulse was less than unity. The presence of this "independent" oscillation also accounted for the observed temporal "broadening" of the outputs. There, consequently, existed a range of cavity lengths where optimal performance was obtained. The value of these lengths was directly proportional to the duration of the *MO* pulse. For the 6ns duration *MO* pulse used in this work, cavity lengths of between 2.5m and 4m worked extremely well.

In order to examine the effects that an increase in cavity dispersion, and the corresponding reduction in  $\Delta\lambda_0$ , would have, without significantly increasing cavity losses, a variety of configurations, which incorporated two or more of the low-loss tuning elements were tried. For example, in

one configuration,  $M_3$  was replaced with a second highly-reflective Littrow prism. In this case, as with most of the multiple tuner configurations, output energies were significantly lower than those obtained using only one tuning element. Considering the alignment problems faced with the use of only a single Littrow prism, it seemed likely that the reduction in the output energies was due to the fact that multiple tuners could not be identically aligned (i.e. to the same wavelength). This was another problem introduced by the poor spatial quality of the  $MO$  beam used for alignment. Although the use of multiple tuners would have reduced  $\Delta\lambda_0$ , it is highly doubtful that the reduction would have been substantial enough so as to impact the already good injection-locking performance of the system.

#### 4.11 - Installation of Low Loss Pockels Cell

One other alteration made to the cavity was the replacement of the original Pockels cell with a 99% deuterated, low insertion loss  $KD^*P$  Pockels cell. Despite the broadband AR coatings on the cell windows and the refractive index matching fluid used in the original  $KD^*P$  Pockels cell to minimize losses, the insertion loss for the device was still 8%. This loss was considered excessive as it accounted for approximately half of the total cavity round-trip losses. The replacement cell, manufactured by Cleveland Crystals (Model No. QX1630), with AR coated windows, had a single pass insertion loss of 1.5% at 632.8nm. Its 10-90% risetime was  $\sim 1$ ns when driven by the same Lasermetrics Model 5016 High Speed Electro Optic Gating System as used before. With the new cell installed, total round-trip losses were reduced to 7%.



The effect that the reduction in cavity losses had on output pulse energies was profound. Using the linear cavity configuration, shown in Figure 4.10, output pulse energies at 590nm were an average of 23% higher after the installation of the new Pockels cell than those recorded with the previous crystal. In highly gain-saturated systems, such as this, this strong dependency of  $E_a$  on cavity losses is expected. For this reason, minimization of cavity losses was a fundamental consideration in the system design.

## CHAPTER 5 - PARAMETRIC ANALYSIS OF LASER PERFORMANCE

### 5.1 - Introduction

The past two chapters dealt primarily with the developmental stages of the amplifier. Chapter 3 concentrated on various factors that influenced the performance of the system as a cavity-dumped oscillator. Specifically, efforts there were devoted to optimizing pulse energies while maintaining a temporally "clean", though broadband, output pulse.

In Chapter 4 it was discovered that under the proper circumstances the cavity-dumped oscillator could be injection-locked to a spectrally pure master oscillator. Operated in this manner, the system was then capable of generating narrowband, high-power output pulses although over only a limited tuning range. Even larger amplified pulse energies were obtained after the *PBC*'s were replaced with the high-power, thin-film polarizing beamsplitters. Once the dispersive properties of the *HPB*'s were compensated for and a tuning element was installed in the cavity, extremely temporally and spectrally clean output pulses were generated. By adjusting the tuning element so that  $\lambda_o = \lambda_i$ , these outputs were found to be obtainable over a wide tuning range.

In this chapter the final developmental stage of the system is presented and a detailed characterization of the outputs is given. Included in this characterization are results indicating under what conditions the

system can be injection-locked and the effects of the installation of an intracavity tuning element.

To aid in the analysis, a Tracor Northern TN-1710 optical multichannel analyzer (OMA) was used in place of the spectrometer shown in Figure 3.7. The OMA functioned as a spectrometer with a  $\sim 0.1\text{nm}$  resolution, and had an integrating feature that enabled the relative energies of the various spectral bands emitted by the amplifier to be compared. Using this feature, an exact determination of  $\rho$ , the injection-locking efficiency, as a function of a variety of parameters was performed.

The final amplifier cavity configuration used was actually only a slight modification of that shown in Figure 4.10. By installing the Littrow prism so that the incident beam struck its highly-reflective back surface at an angle of incidence,  $\theta_i$ , of  $\sim 2^\circ$ , the amplifier, once again, became a ring laser. The primary advantage of this configuration, shown in Figure 5.1, was that it removed the constraint on the  $\lambda/2$  voltage pulse width which was required in the linear cavities to insure that the amplified pulse exited the amplifier through  $HPB_2$  (Section 4.9). The use of a ring configuration also removed a number of dimensional constraints that the use of a linear cavity imposed on the resonator design. Many of these were discussed in detail in Section 4.10.

It should be noted that the degree to which the prism could be tilted was limited by the reflectivity of the dielectric coating applied to the back surface of the prism. Transmission loss, through the coating, was a strong function of  $\theta_i$ . For  $\theta_i$  less than  $5^\circ$  this loss remained negligible ( $< 1\%$ ). However, when  $\theta_i$  exceeded  $10^\circ$ , a significant fraction of the incident light was transmitted through the coating. Again, although a Brewster or other



type of dispersing prism could have been used, the Littrow prism, for small  $\theta_i$ , was easier to install and made the cavity relatively easy to align. The alignment, following the procedure discussed in Sections 3.9 and 4.9, however, still remained extremely coarse.

## 5.2 - Measurement of $\rho$ Using the OMA

When properly aligned, the amplifier again generated pulses with extremely clean temporal profiles for wavelengths throughout the range from 583nm - 602nm. These profiles were identical to that shown in Figure 4.11. However, as discovered during the development of the cavity-dumped oscillator in Chapter 3, the temporal cleanliness of the output pulses revealed little information as to their spectral content.

The *MO* pulse linewidth (without the intracavity etalon),  $\Delta\lambda_i$ , was measured by the LS-1 spectrometer to be 0.05nm. Although these linewidths were slightly beyond the resolution of the OMA, its 0.1nm resolution was thought to be adequate enough to indicate any significant spectral broadening of the amplified *MO* pulse or the presence of any off-color radiation. An OMA display of the *MO* pulse with  $\Delta\lambda_i = 0.05\text{nm}$  is shown in Figure 5.2. When the linewidth of the amplified pulse,  $\Delta\lambda_a$ , appeared identical to the display shown in Figure 5.2, and there was no indication of any off-color radiation, complete injection-locking was assumed to have occurred.

Using an untuned amplifier, complete injection-locking had been observed only for wavelengths close to 590nm ( $\lambda_o$ ). When  $|\lambda_o - \lambda_i|$  exceeded  $\sim 2\text{nm}$ , broadband radiation centered at  $\lambda = 590\text{nm}$  was emitted together with the amplified pulse at  $\lambda_i$ . The intensity of this broadband

ORIGINAL PAGE IS  
OF POOR QUALITY

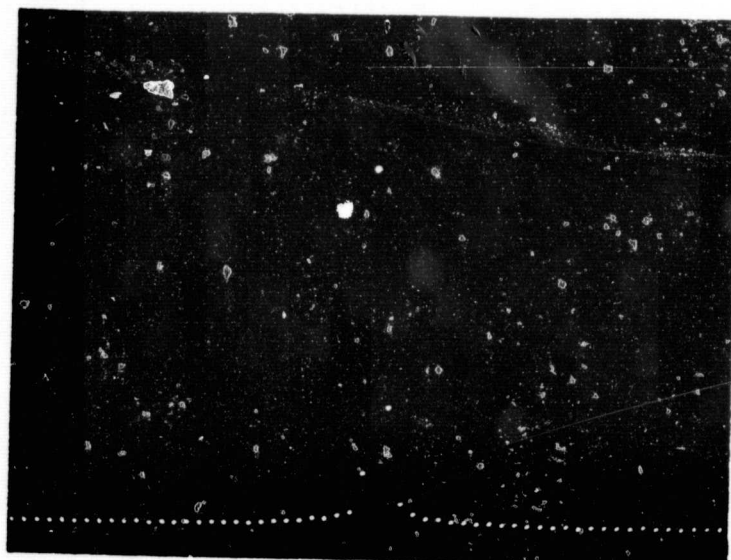


**Figure 5.2: OMA Display of the Spectral Profile of the MO Output.**

**Horiz: 0.12nm/pixel**

radiation increased as  $|\lambda_o - \lambda_i|$  increased. Use of the OMA allowed a quantification of the corresponding reduction in  $\rho$  as a function of  $\lambda$ .

In the OMA, the intensity of the radiation incident on a given pixel was digitized by a 12 bit A-D converter and displayed linearly on the CRT screen. An integrating feature of the OMA automatically integrated the digitized intensity information within a user specified range of pixels. As the linewidth of the output pulse most certainly did not exceed the  $\sim 50\text{nm}$  display range of the OMA, an integration of the total display yielded a number which was proportional to the total output pulse energy. (Counts induced by uniform background radiation were automatically subtracted.) By observing the total number of counts within a specified spectral band, the percentage of the total pulse energy contained within that band could be inferred. In this manner, a direct quantitative assessment of  $\rho$  was obtained for each output pulse.

### 5.3 - Dependence of $\rho$ on Cavity Dispersion

The use of the OMA enabled a quantitative determination of the dependence of  $\rho$  on a variety of parameters. for a given  $\lambda_i$ . Since a broadly tunable system was desired, the dependence of  $\rho$  on  $\lambda$  was of fundamental concern. The investigations performed in Chapter 4 made clear the effects that the installation of an intracavity dispersive element had on the tunability of the system (i.e. the range of wavelengths where  $\rho \sim 1$ ). At that time, however, due to the limitations imposed by the spectrometer, only qualitative assessments of the dependence of  $\rho$  on  $\lambda_i$  were possible. In order to more precisely evaluate this dependence, the following measurements, using the OMA, were performed.

With the amplifier configured as shown in Figure 5.1,  $\rho$  was recorded for various  $\lambda_i$  in the R6G emission band. For each value of  $\lambda_i$ , the prism was adjusted so that  $\lambda_o = \lambda_i$ . MO pulse energies varied from 1-5  $\mu$ J, depending on  $\lambda$ , while  $E_f$  was kept constant at 140J. In each case, from  $578\text{nm} \leq \lambda_i \leq 602\text{nm}$ , the amplifier was capable of being completely injection-locked. The spectral profiles of typical oscillator and amplifier outputs are shown in Figures 5.3a and 5.3b. The linewidth of the oscillator output, determined by the dispersiveness of the prism and the dimensions of the amplifier, was about 1.0nm FWHM. No significant changes in either of these profiles was observed as a function of  $\lambda$ . The temporal profiles were again identical to that displayed in Figure 4.11 and were also independent of  $\lambda$ .

The completeness of the injection-locking was manifest in several ways. First, as displayed by the OMA, there was a visually obvious reduction in the linewidth of the output pulse with no evidence of any significant "off-color" radiation. These observations were both quantified using the integrating feature of the OMA as discussed in Section 5.2. The OMA also quantified the dramatic increase in the spectral brightness of the amplified pulse as compared to the oscillator output. This was seen by noting the CNT readouts (indicating the relative intensity of the highlighted pixel) present on the OMA displays in Figures 5.3a and 5.3b. An independent verification of the data extracted from the OMA was provided by noting the relative energies of the oscillator and amplifier outputs. The output pulse energies when the system was injection-locked were double those of the unlocked system. When completely injection-locked, all of the radiation was coupled into the direction of the MO pulse and no radiation exited the cavity through  $HPB_1$ . It should be noted that



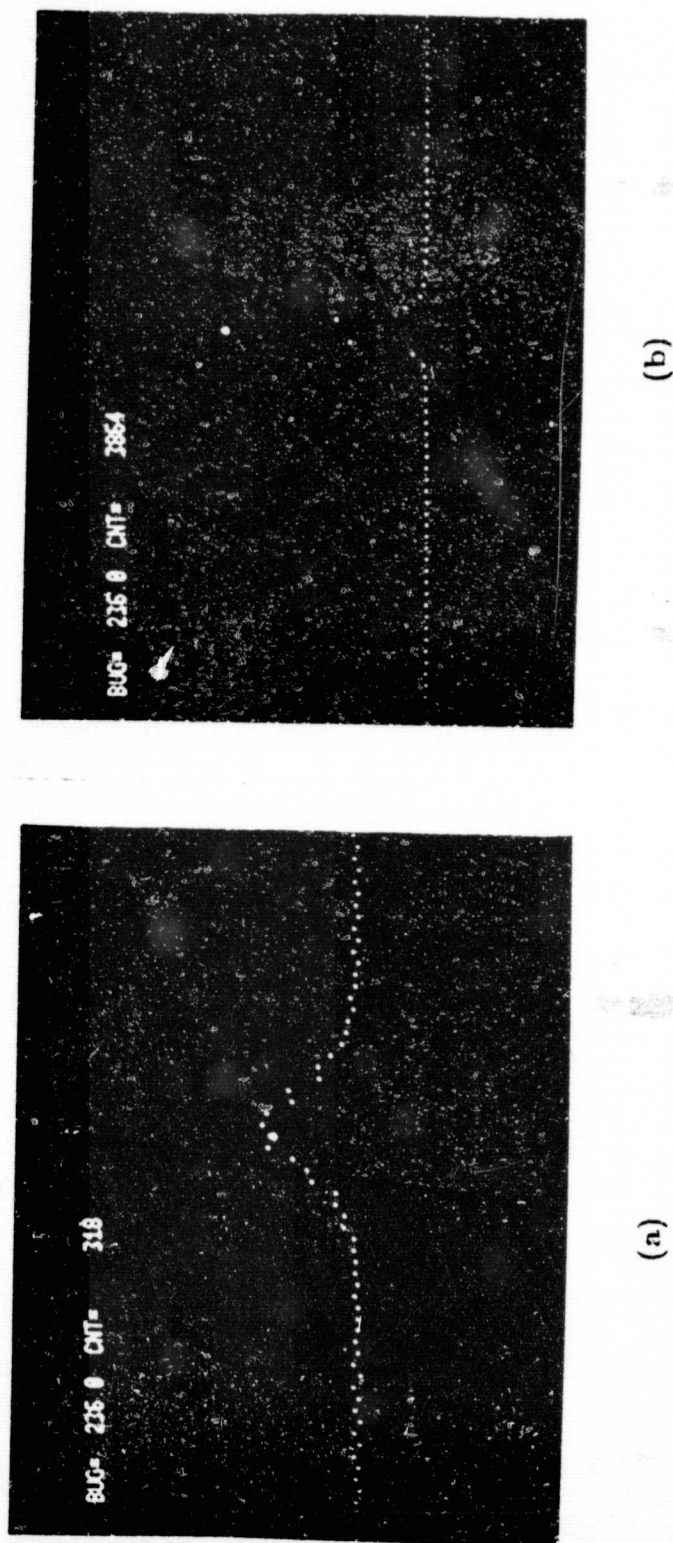
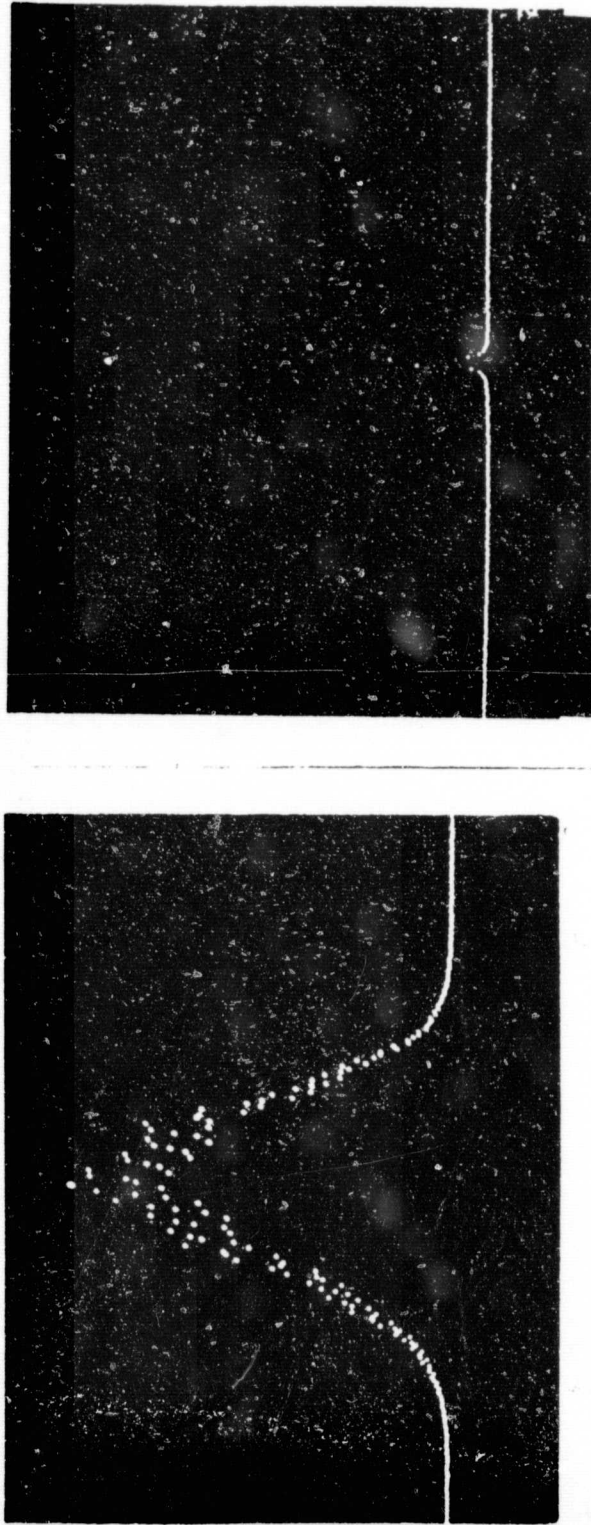


Figure 5.3: OMA Display of the Tuned Laser Output, (a) without injection-locking and (b) injection-locked with a  $3\mu\text{J}$  MO pulse for  $578\text{nm} \leq \lambda_i \leq 602\text{nm}$ .

OMA Resolution:  $0.12\text{nm}/\text{pixel}$



(a)

(b)

Figure 5.4: OMA Display of the Untuned Laser Output, (a) without injection-locking and (b) injection-locked with a 3.6J MO pulse at  $\lambda_i = 590\text{nm}$ . (The sensitivities of the vertical scales are not identical.)

OMA Resolution: 0.12nm/pixel

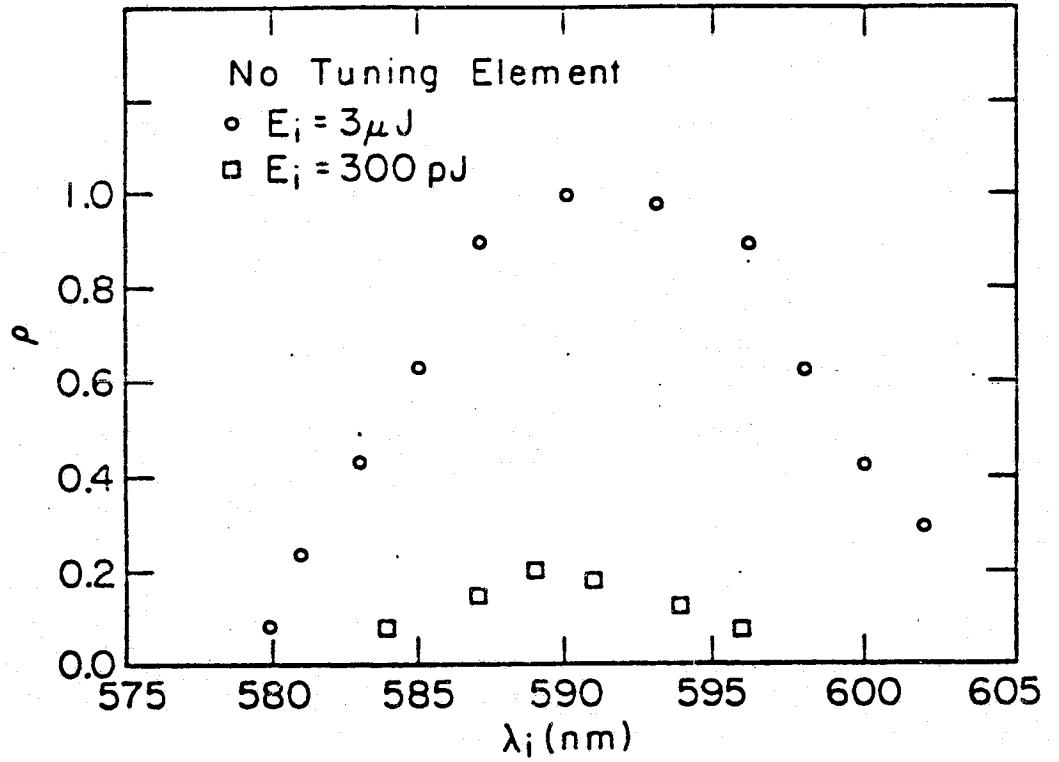


Figure 5.5: Variation of  $\rho$  with  $\lambda$  in an Untuned Cavity.

due to the jitter in the flashlamp discharge circuitry,  $\rho$  varied occasionally from shot-to-shot for a given  $\lambda_i$ . For this reason, only average values of  $\rho$  were recorded.

By replacing the prism with a plane mirror, the variation of  $\rho$  as a function of  $\lambda_i$  was then investigated for an untuned cavity. The spectral composition of both the injection-locked and "unlocked" outputs are shown in Figure 5.4. The procedure for this experiment was identical to that used with the Littrow except that, of course,  $\lambda_o$  remained fixed at 590nm. A similar, but more qualitative, investigation was performed in Section 4.5 prior to the installation of the OMA. The results, plotted in Figure 5.5, although more precise, are essentially identical to those obtained earlier as complete injection-locking occurred only for  $\lambda_i$  within  $\sim 20\text{\AA}$  of 590nm.

#### 5.4 - Variation of $\rho$ With $E_i$

For many of the applications discussed in Chapter 1, compactness was one of the key advantages of using a flashlamp as the dye laser pump. Indeed, when used as an oscillator, the system was capable of being made extremely compact. However, with the current injection-locking scheme, the rather large size of the *MO* compromised the compactness of the system. It was thus of interest to determine if the relatively large pulse energies output by the current *MO* were required, or whether a smaller, less powerful *MO* would suffice. Consequently, measurements were made to determine the minimum *MO* pulse intensity necessary to force complete injection-locking of the amplifier stage.

For this investigation, the exact synchronization of the two laser sys-

tems was imperative. Any jitter in the timing circuitry would significantly alter the amount of fluorescence noise the *MO* pulse would have to compete with in the amplifier as it attempted to induce a preferential buildup of radiation at  $\lambda_i$ . This was especially critical when the *MO* pulse intensity was the same order of magnitude as the spontaneous emission noise present in the amplifier at threshold. However, as discussed previously, the electronic jitter could not be completely eliminated. Timing jitter of  $\sim 50$ ns, attributable primarily to the flashlamp discharge circuitry, was typical. Thus, for smaller *MO* pulse intensities, it became difficult to discern whether the failure of even partial locking was due to a fundamental deficiency in the energy of the injected pulse or because the injected pulse failed to arrive at the amplifier precisely at threshold due to the electronic jitter.

By attenuating the *MO* pulse a known amount, through the use of neutral density filters, the variation of  $\rho$  with the injected pulse energy,  $E_i$ , was directly observed. The data was taken with  $\lambda_i = 590$ nm ( $\Delta\lambda = 0.05$ nm) so that the injected *MO* pulse would not have to compete with fluorescence noise at frequencies which exhibited intrinsically higher gains. This condition was only required for the dispersionless amplifier and could have been simulated for other  $\lambda_i$ 's by the inclusion of a tuning element in the amplifier. The tuning element would then have simply removed noise present at those frequencies with intrinsically higher gains than that at the desired  $\lambda_i$ . Since a characterization of  $\rho$  as a function of  $\lambda_i$  for the dispersionless case had been previously performed it was considered unnecessary to conduct this investigation as a function of  $\lambda$ .

The experimental results are plotted in Figure 5.6. Injection-locking,

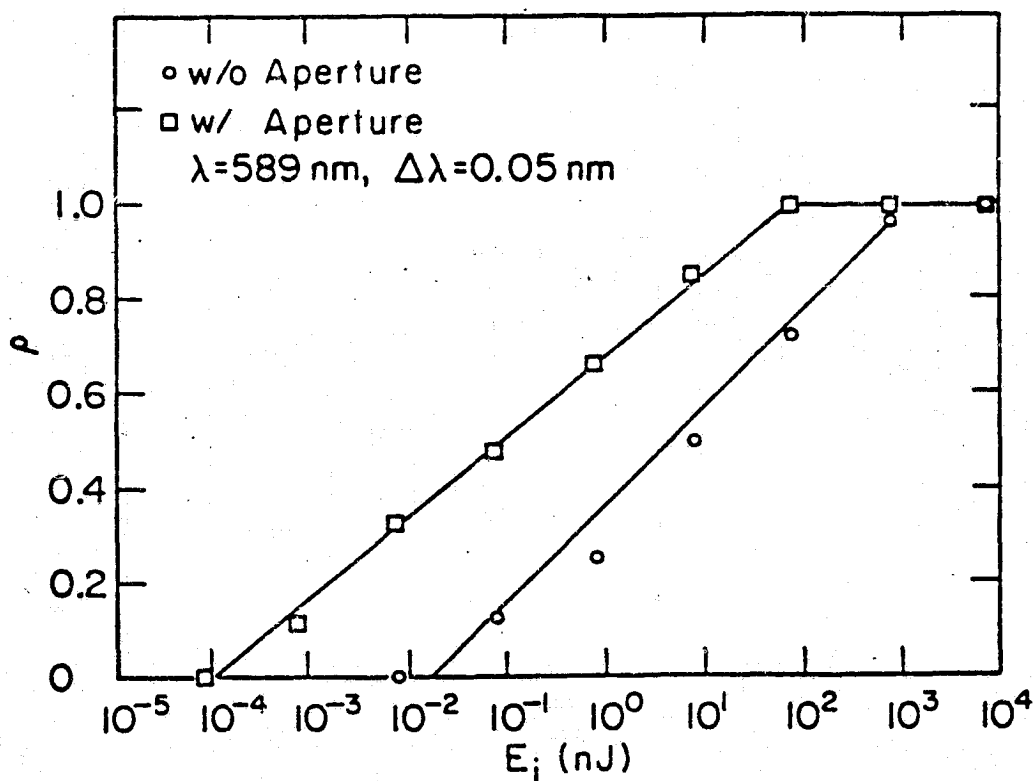


Figure 5.6: Variation of  $\rho$  with Injected Pulse Energy,  $E_i$

although incomplete ( $\rho = 0.15$ ), was first observed using injected pulse energies as small as 10pJ. Complete injection-locking of the laser required 100nJ. Between these extremes, the injection-locking efficiency,  $\rho$ , exhibited a logarithmic dependence on  $E_i$ . The observed logarithmic dependence of  $\rho$  on  $E_i$  was consistent with both the analysis presented in Chapter 2 and the findings of previous injection-locking studies [17]. The amplified pulse energies were also monitored as a function of  $E_i$ . They exhibited a dependency on  $E_i$  which was similar to the variation of  $E_a$  with  $\rho$  that was discussed in Section 4.5 and was attributable to similar causes.

As detailed in Chapter 2, the amount of fluorescence noise present in the amplifier prior to threshold should be proportional to the square of the Fresnel number of the cavity. It was thus thought that, by decreasing the amount of noise that the injected pulse had to compete with during the buildup of laser radiation, the injection-locking threshold (i.e. the lowest value of  $E_i$  such that  $\rho = 1$ ) could be decreased. In an effort to demonstrate this, apertures were installed near both ends of the dye cell. Restricting the aperture diameter decreased the effective Fresnel number of the cavity by decreasing the exposed cross sectional area of the dye solution. This not only decreased the radiating area, and hence the radiated noise, but it also reduced the solid angle that the noise would have to be emitted into in order to be fed back to the dye cell. Together, these factors contributed to the square law dependence of  $\rho$  on the Fresnel number of the cavity. With the use of the apertures, the value of  $E_i$  required to obtain a given value of  $\rho$  should thus be reduced.

The diameter of the apertures, centered on the cylindrical axis of the

dye cell, were set to 3.0mm and resulted in a 9-fold reduction in the area of the exposed dye solution. The *MO* pulse still passed completely through the apertures leaving the unattenuated value of  $E_i$  unchanged. As before,  $\rho$  was monitored as a function of  $E_i$ . A comparison of this data, plotted in Figure 5.6, along with the data taken without the apertures, revealed that the amount of injected pulse energy now required to achieve a given value of  $\rho$  was reduced by about two orders of magnitude. Under these conditions, evidence of injection-locking was observed with  $E_i$ 's as small as 1pJ while the injection-locking threshold was reduced to about 1nJ (as compared to the previous 100nJ figure). Although the injection-locking threshold was significantly reduced by this technique, output pulse energies were severely diminished. Pulse energies were  $\sim 8$  times smaller than those obtained when the entire dye volume was exposed. As will be shown later, there was a nearly linear relation between the active (exposed) dye volume and the output pulse energy which is characteristic of highly gain-saturated systems.

### 5.5 - *MO* Beam Diameter Considerations

Throughout these experiments, the *MO* beam diameter was set to  $\sim 3$ mm so as to maximize the injected pulse energy present at the center of the dye cell. Since the dye concentration was set to maximize gains in this region, it was here that threshold should first have been achieved. It was thought that if the presence of the *MO* pulse could induce a preferential build-up of radiation at  $\lambda_i$  in this region, then, as the amplified pulse grew and spatially broadened due to saturation effects, that its presence would injection-lock the outer regions of the dye cell as they, in turn, reached threshold. If, however, the outlying dye volume achieved



threshold before the amplified *MO* pulse had spatially broadened enough to influence the development of laser oscillation in the region, broadband laser radiation would develop independently at  $\lambda_0$ . Complete injection-locking would then fail to occur.

This hypothesis is consistent with the observation, made during these experiments, that for  $E_i$ 's where  $\rho < 1$ , the spectral content of the amplified pulse was spatially dependent. Evidence of this was obtained by monitoring the "unlocked" radiation exiting the amplifier through *HPB*<sub>1</sub>. Since the injection-locked fraction of the radiation propagated in the same direction as the *MO* pulse, only unlocked radiation, which developed independently of the *MO* pulse, propagated in the direction so as to exit the amplifier through *HPB*<sub>1</sub>. The annular shape of this pulse then directly indicated that the unlocked fraction of the total pulse emanated from dye molecules which were in the outer regions of the dye cell. It was thus conceivable that by enlarging the *MO* beam diameter that less energy would be required to injection-lock the entire dye volume. If the energy density of the *MO* pulse "near" the center of the dye cell was greater than that required to injection-lock that particular region, then by enlarging the *MO* beam diameter a greater percentage of the dye volume could be injection-locked for a given  $E_i$ . Since the spatial broadening of the amplified pulse would occur at a more rapid rate the entire system would be capable of being injection-locked using smaller *MO* pulse energies.

A proper investigation of this hypothesis would have required a *MO* beam with very good spatial quality. That is, the beam would have had to possess a known energy profile (e.g. Gaussian) and have been capable of being smoothly enlarged and coupled into the amplifier. The output of

the  $N_2$ -pumped dye laser, serving as the *MO* for this work, certainly did not meet these requirements. It had a decidedly nongaussian profile and was incapable of being nicely collimated and expanded. For the experiments described herein, the beam had to be gradually focused so that its spot size on the initial pass through the dye cell was 3mm. The primary consideration was that the *MO* pulse not converge or diverge too rapidly during the first few transits through the dye cell. After a few passes, however, the spatial profile of the amplified pulse became independent of that of the injected pulse. The poor spatial quality of the *MO* beam made precise studies of these effects impossible.

### 5.6 - Evaluation of Spontaneous Emission Noise Level

As revealed in the last section, injection-locking was observed using injected pulse energies as low as 1pJ ( $\rho = 0.15$ ). At this point, where injection-locking was first observed, it can be assumed that  $E_i$  was comparable in magnitude to the inherent radiation "noise" level within the oscillator. Thus, as an independent test of this data, the fluorescence "noise" level, which competed with the *MO* pulse during the onset of laser oscillation, was measured. An accurate evaluation of the noise level would yield information as to the lower limit on  $E_i$  required to injection-lock this system. Also, if the measured noise level was on the order of magnitude of  $\sim 1$ pJ, the lowest  $E_i$  for which injection-locking occurred, it would independently support the validity of the data presented above.

The spontaneous emission (fluorescence) noise level was monitored by placing the UDT radiometer along the lasing axis  $\sim 25$ cm from one end of the dye cell. A pair of apertures, centered on the lasing axis, were placed

between the dye cell and the entrance to the detector. The diameters of these apertures were set to produce the solid angle that the radiation emitted from one end of the dye cell would have to be coupled into in order to return to the other side of the dye cell and hence have a chance at developing into laser radiation. The temporal profile of the fluorescence was monitored, as before, with  $PD_2$ . Flashlamp discharge energies were identical (140J) to those used in the previous experiment.

The radiometer detected 25nJ of fluorescence energy that was coupled into a solid angle capable of sustaining oscillation. This energy, however, was emitted during the entire duration of the flashlamp discharge hence only a small percentage of it actually contributed to the initiation of laser oscillation. To determine this percentage, a Gaussian distribution was used to model the temporal distribution of the radiated noise energy. A Gaussian distribution was chosen because it closely approximated the 600ns FWHM temporal profile of the spontaneous emission displayed by  $PD_2$ . Using the Gaussian model, it was determined that only about 0.7% of the total noise energy was emitted within a  $\sim 10$ ns interval around the threshold point.

The fluorescence was also distributed spectrally over a broad range. Since  $\lambda_i$  was set to 590nm, for this experiment, much of the radiation noise is at frequencies where the gain was significantly less than that at  $\lambda_i$ . Hence, even much of the noise emitted near threshold did not directly compete with the  $MO$  pulse during the onset of laser oscillation. In fact, only the noise whose frequencies were close to 590nm needed to be considered.

The spectral distribution of the fluorescence was governed by the

singlet state absorption and emission cross sections of the dye. The percentage of the noise within a range of frequencies  $\Delta\lambda$  is given by:

$$\frac{\int_{\delta\lambda} (\sigma_e(\lambda) - \sigma_a(\lambda)) d(\lambda)}{\int_{\lambda | \sigma_e = \sigma_a} (\sigma_e(\lambda) - \sigma_a(\lambda)) d(\lambda)} \quad [V.1]$$

Specifically, using the stimulated emission and absorption cross sections given in Figure 2.2, the ratio of the fluorescence within 2nm of  $\lambda_i = 590\text{nm}$  to the total noise level was  $\sim .036$ .

The net amount of "noise" in direct competition with the *MO* pulse at threshold is then given by:  $(25\text{nJ} \times .007 \times .036 \times .43) = 2.7\text{pJ}$  where the factor of .43 accounted for the optical cavity and polarization losses. Although this value is subject to a good deal of error, due to the estimation technique, it should be representative within an order of magnitude of the competitive fluorescence "noise" energy. As such, it is a value which is consistent with the data presented in Section 5.4.

### 5.7 - Power Curve

Most of the data characterizing the injection-locking process, presented in the preceding sections, was taken using moderate flashlamp discharge energies (i.e.  $E_f \sim 150\text{J}$ ). It was assumed that the characterization was independent of  $E_f$ , although this had not been formally verified. To verify this and to determine the output power capability of the system, both  $\rho$  and  $E_a$  were measured as a function of  $E_f$ .

The amplifier cavity was, again, configured as shown in Figure 5.1. Since  $\rho$  was previously shown to be independent of  $\lambda_i$  and  $\Delta\lambda_i$ , values of

590nm and 0.05nm, respectively, were used, although other arbitrary choices could have been made. Injected pulse energies,  $E_i$ , were set to  $\sim 3\mu\text{J}$ . It was assumed that the  $E_i$  required for complete injection-locking would not be a function of  $E_f$ . If, however,  $\rho$  did appear to be a function of  $E_f$ , this assumption would have to be checked.

Amplified pulse energies, plotted as a function of  $E_f$ , are shown in Figure 5.7. The variation of  $E_a$  with  $E_f$  was nearly linear from the point at which threshold occurred, at  $E_f = 59\text{J}$ , to  $E_f = 220\text{J}$  where  $E_a$  reached 62mJ. The slope efficiency of the system was thus  $\sim 0.04\%$ . Although the flashlamp was capable of discharging up to 350J,  $E_f$  was limited to 220J because minor damage to the HPB's was observed at this point. As the damage occurred only sporadically, it was highly doubtful that the amplified pulse intensity exceeded the quoted HPB damage threshold of  $\sim 5\text{GW}/\text{cm}^2$ . Rather, it was suspected the the damage resulted from either the existence of "hot spots" in the beam or local defects in the dielectric coatings of the HPB's. If the slope efficiency remained constant at 0.04% the system would be capable of producing  $\sim 115\text{mJ}$ , 20MW (peak-power) pulses.

The data presented in Figure 5.7 is, however, only valid for  $\lambda=590\text{nm}$ . Although  $\rho$  is independent of  $\lambda$ , the extracted pulse energy,  $E_a$ , is not. This is due to the dispersive properties of the HPB's. Figure 5.8 shows the output of the system as a function of  $\lambda$ . As expected, this curve closely resembles the "p" transmission profiles of the HPB's.

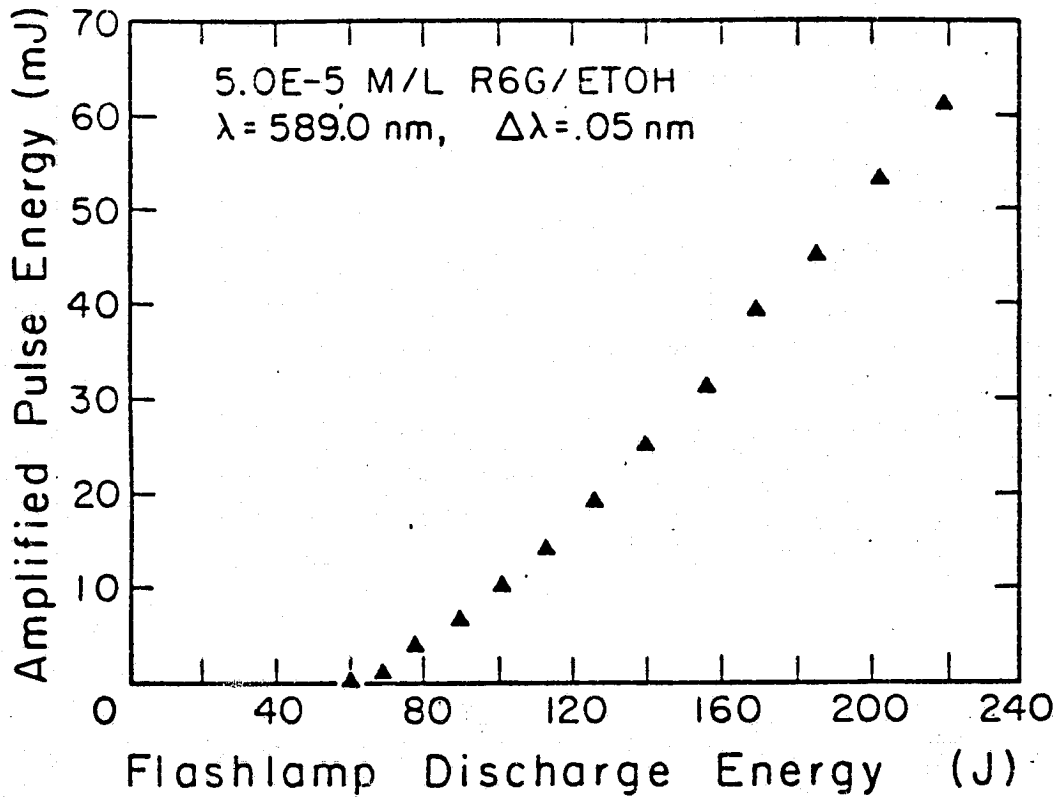


Figure 5.7: Injection-Locked Output Pulse Energy,  $E_o$ , as a Function of the Flashlamp Discharge Energy,  $E_f$ .

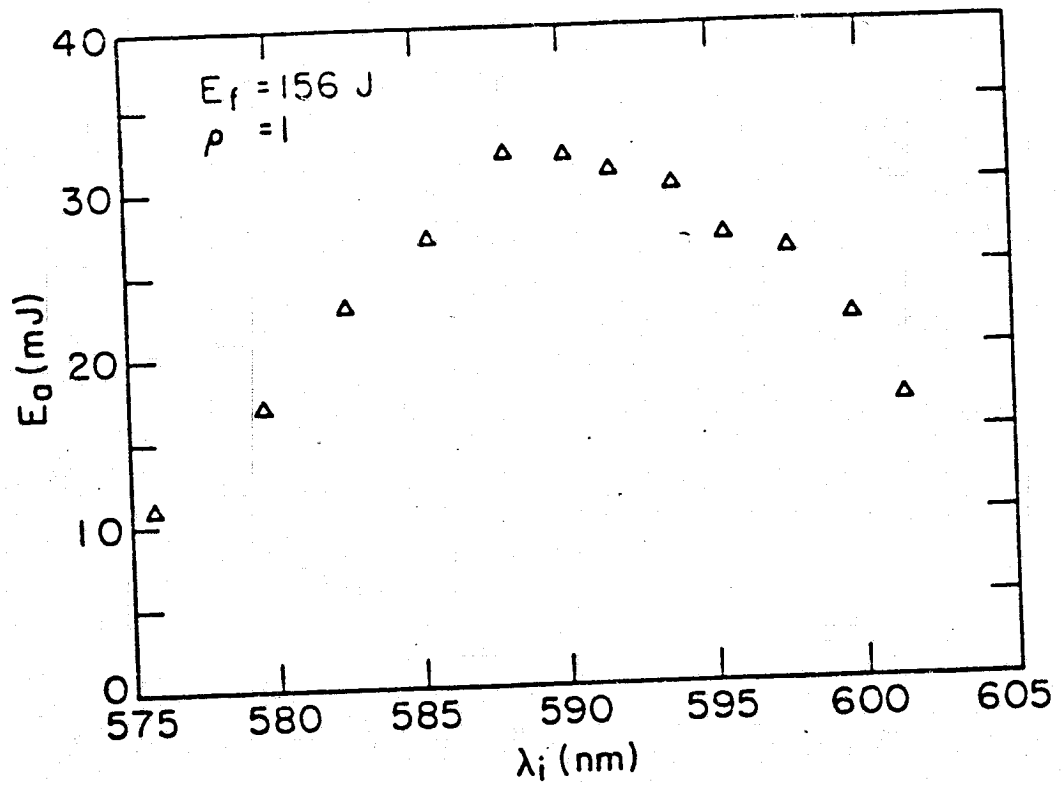


Figure 5.8: Injection-Locked Output Pulse Energy,  $E_o$ , as a Function of Wavelength.

## 5.8 - Spatial Profile of the Output Pulse

Although there were definite indications that the system had been driven well into the saturation regime, there was no information as to whether or not the system had been fully saturated (i.e. that as much energy as possible had been extracted from the system). In order to determine the level of saturation the spatial profile of the amplified pulse was examined.

If the amplified pulse had developed strictly as a  $TEM_{00}$  Gaussian pulse, its beam waist, while inside the dye cell, would have been  $\sim 1.0$ mm. In this case  $\sim 86\%$  ( $1/e^2$ ) of the amplified pulse energy would have been extracted from only the central 5% of the total dye volume. In such a highly gain saturated system, however, this type of pulse development was considered unlikely. The rapid gain saturation experienced by the  $TEM_{00}$  pulse together with the high gains that existed throughout the remainder of the dye cell made higher-order modal development highly probable. The higher-order modes, by increasing the size of the beam, allowed the contribution of dye molecules which had little effect on the  $TEM_{00}$  mode. Through this multimodal development the circulating radiation would eventually fill, and saturate the gain of, the entire dye volume. Eventually for a completely saturated system the energy output per unit of dye volume would be identical throughout the cross-section of the dye cell. In this manner the maximal amount of energy could be extracted from the system.

To determine the spatial profile of the amplified pulse an aperture was placed near the entrance of the dye cell. Output pulse energies were then recorded as a function of the aperture diameter, which was directly



related to the cross sectional area of the active dye molecules. The data is plotted in Figure 5.9. Also depicted in Figure 5.9 are a pair of theoretical spatial profiles. In one instance the pulse obeys a  $TEM_{00}$  Gaussian profile, while, in the other, the gain-medium has been fully saturated. Both profiles shown have been normalized to assume identical output pulse energies of 13mJ.

In a fundamental Gaussian mode, as mentioned above, most of the pulse energy emanates from a small fraction of the total dye volume. In the other limiting case, in which complete gain-saturation occurs, a perfectly linear relationship exists between the output pulse energy,  $E_a$ , and the percentage of the total active dye volume. The actual recorded spatial profile came close to that of the latter case, indicating that the system was approaching complete gain saturation and that little additional energy was capable of being extracted. The data did indicate, however, that a slightly greater percentage of the pulse energy was concentrated near the center of the dye cell. It was difficult to attribute this observation to a particular cause as many explanations, including poor alignment or the presence of thermally induced turbulents in the dye solution, were plausible.

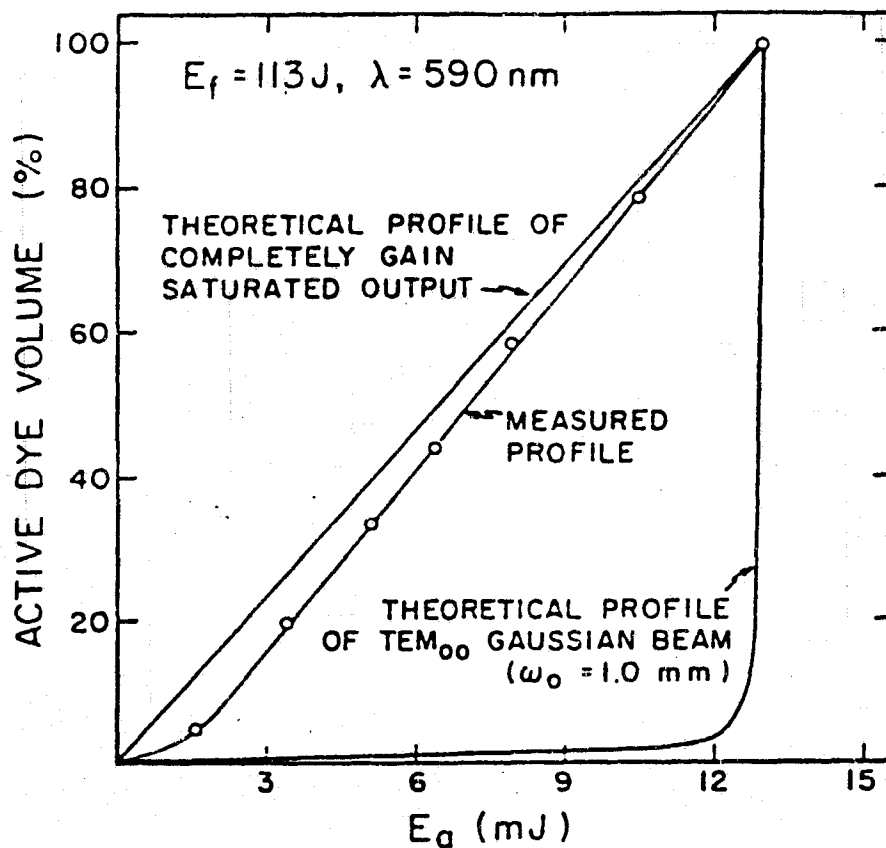


Figure 5.9: Comparison of the Spatial Profile of the Output Pulses with the Theoretically Predicted Profiles of a Completely Gain Saturated Pulse and an Unsaturated  $TEM_{00}$  Gaussian Pulse.

## CHAPTER 6 - CONCLUSIONS & SUGGESTIONS FOR FUTURE INVESTIGATIONS

### 6.1 - Conclusions

These investigations have demonstrated the feasibility of simultaneously generating high energy as well as narrow-linewidth nanosecond duration pulses by injection-locking a cavity-dumped laser. Using this technique, a standard CFP dye laser generated 6ns duration output pulses which had energies in excess of 60mJ and linewidths as narrow as 0.0015nm. The investigations also indicated the effectiveness of using low insertion loss tuners in the injection-locked laser. The low loss tuners, although only weakly dispersive, allowed the free oscillation wavelength of the cavity-dumped laser to be coarsely tuned to the wavelength of the injected pulse. In this way, the narrow-linewidth injection-locked outputs were obtained over a tuning range of 24nm without the appearance of significant broadband background radiation. The added dispersion also minimized the injected pulse energies required to obtain these outputs. Injected pulse energies of only  $\sim 100$ nJ were found to be sufficient in obtaining near unity injection-locking efficiencies over the entire emission profile of the dye. It is suspected that even lower injected pulse energies would be sufficient if the arrival time of the injected pulse could be better synchronized to the flashlamp discharge.

The overall performance of the system was gauged by the energy, linewidth, temporal "cleanliness", and tunability of the output pulses.

Optimizing this performance required investigating the effects of varying a number of parameters. Specifically, experimental investigations were conducted to determine performance dependencies on such parameters as injection time and cavity dispersion as well as on such injected pulse parameters as wavelength, energy, and linewidth. This parametric study enables an analysis of the differences between the injection-locking of "long-pulse" systems, which has been reported on, and the injection-locking of cavity-dumped systems. The primary theoretical distinctions between the two cases were exposed during the development of the spectro-temporal evolution equation in Chapter 2. This equation suggested that both triplet state and saturation effects, which are insignificant in the performance of "long-pulse" injection-locked systems, "aid" the injection-locking of the cavity-dumped system by increasing the spectral evolution time. With the experimental characterizations performed here, a more direct and quantitative comparison of the two cases is now possible.

Although the development and characterization of the system has been carefully detailed in this work, there were a number of additional considerations and investigations that there was neither time, equipment or funding to pursue at this time. Included in this chapter are some specific suggestions of areas where further study could prove useful as well as some possible means of increasing system performance. It should be noted that, while these investigations were performed using a CFP dye laser system, the techniques used in this work should be adaptable to other types of laser systems as well. In particular, it is anticipated that these techniques could be directly applied to the tuning and linewidth control of tunable solid-state lasers such as emerald and alexandrite. Due to

the longer excited state lifetimes and higher saturation intensities of such lasers, pulses with much larger peak-powers and greater spectral brightness should be attainable.

## 6.2 - Use of CW Master Oscillators

Throughout the course of this work, numerous problems were encountered with the use of the  $N_2$ -pumped dye laser as the master oscillator. Most of these resulted from the poor spatial properties of the *MO* beam. For example, amplifier alignment, performed using the *MO* beam, could be made, at best, extremely coarse. This alone, undoubtedly, adversely affected system performance in a number of ways. The poor spatial characteristics of the *MO* beam also restricted the analysis of the injection-locking performance of the system that was described in Chapters 4 and 5. Clearly, the use of a CW *MO* would provide many advantages over the current pulsed system. The *MO* beam would be temporally, spatially, spectrally and radiometrically more stable than that produced by a pulsed source. It would also be more "flexible" in that the spatial properties of the beam could be varied as desired. Detailed below are some of the advantages, disadvantages and considerations of using CW master oscillators.

The first and foremost consideration of the use of CW *MO*'s is the injected energy requirement. As discovered in Section 5.5, *MO* pulse energies of roughly 100nJ were required from the  $N_2$ -pumped dye laser system to force complete locking ( $\rho=1$ ) of the amplifier. In order to insure that at least this much energy would be present in the  $\sim 3$ m resonator, at any given time, a 10W CW source would be required. While there are no such

sources of continuously tunable CW radiation, monochromatic injection-locking studies could be performed on this system using commercially available CW sources as the master oscillator. For example, the 5145A line of an Argon-ion laser could be used to injection-lock the amplifier where a dye such as Coumarin 504 is used. Operationally, the loss of tunability is a concern, but for the purpose of system characterization it is not since, as evidenced in this work, the characteristics of a tuned, injection-locked system are essentially wavelength independent.

To minimize the  $E_i$ 's required for injection-locking, the path of the injected beam must be collinear with the natural lasing axis of amplifier. In an attempt to insure collinearity, in this work, the *MO* beam, itself, was used to align the amplifier cavity. However, due to the difficulty in collimating the pulsed dye laser beam, its divergence and shot-to-shot spatial instability made accurate alignment impossible. As mentioned above, this problem undoubtedly had an adverse effect on system performance and on some of the characterization studies performed in Chapter 5. In particular, if the *MO* and amplifier assembly were properly axially coupled, smaller  $E_i$ 's would probably have been sufficient to lock the system. Using a more spatially stable CW *MO* beam, where a proper axial and mode coupling of the two lasers can be assured, the alignment would, undoubtedly, have been more accurate.

Use of a CW *MO* would also have relaxed some of the stringent timing considerations discussed in Section 4.3. With a pulsed *MO*, the arrival time of the pulse must be carefully synchronized to the switching of the EOM, and the firing of the flashlamp so that the pulse is present and trapped inside the amplifier as it achieves threshold. A CW injected signal

would be constantly circulating through the dye cell so that the only timing consideration would be that of synchronizing the switching of the EOM with the proper point in the flashlamp discharge. There is one minor complication introduced by this arrangement, however. Once the EOM is switched, the fraction of the CW beam that is not trapped inside the amplifier would continuously pass through the dye cell, and exit the cavity after only a single pass. Assuming single-pass gains of  $\sim 50$ , a small, but nonnegligible, CW background signal ( $< 0.05\%$  of the power of the cavity-dumped pulse) would be present. This "noise" could be eliminated completely by the installation of a second EOM switch, between the *MO* and the amplifier, which, when activated, would isolate the amplifier from the *MO*. Nonetheless, since the second EOM could be switched synchronously with the one inside the amplifier, the timing problem is still much simpler, in this case, than that encountered with a pulsed *MO* signal.

A better characterization of the dependency of the injection-locking efficiency on various *MO* beam parameters could be obtained using a CW *MO*. One such study, the dependence of  $\rho$  on  $\Delta\lambda_i$ , was considered in Section 4.6. This investigation, however, had to be halted although no evidence of spectral line broadening had yet been observed as there was no available means of reducing  $\Delta\lambda_i$  to below 9 times the transform limit. Use of a CW *MO*, where  $\Delta\lambda_i$  would be significantly below the transform limit of the cavity-dumped pulses, would have given a quick indication as to the attainability of transform limited pulses.

Since the CW beam diameter could be easily enlarged, studies detailing the dependency of the injection-locking threshold on the injected beam

diameter could also be performed. It is conceivable, as explained in Section 5.5, that for a larger *MO* beam the injection-locking threshold would be smaller. If true, *MO* energy requirements could be reduced significantly. Use of a CW *MO*, where the TE mode the *MO* beam can be controlled, also allows  $\rho$  and possibly the modal development of the amplified pulse to be characterized as a function of the TE mode of the *MO* beam.

### 6.3 - Use of Shorter Rise-Time Flashlamps

In typical cavity-dumped systems, energy from the pump source is continuously added to the recirculating field throughout the duration of the pumping pulse. With the radiation totally trapped inside the resonator, the cavity photon flux should increase monotonically as long as the net gains exceed unity. The output pulse energies obtained at a given extraction time are directly related to the photon flux at that point the growth which is limited only by cavity losses and the pump-laser photon conversion efficiency. It was thus unexpected and undesirable that the optimal extraction time for our system occurred near the peak of the flashlamp pulse. This indicated that the intracavity photon flux was maximized at the mid-point of the pumping pulse. The pumping energy dissipated in the later half of the flashlamp pulse, thus, made no contribution to the output laser pulse which resulted in extremely low slope efficiencies ( $\sim 0.04\%$  - see Figure 5.7).

By solving a simplified set of rate equations, Morton et al. [6] arrived at an analytical expression for the resonator photon density in a cavity-dumped oscillator. Based on this expression, they concluded that if cavity



losses could be kept to extremely low levels (i.e.  $< 5\%$ ) that the cavity photon flux would follow the integral of the flashlamp pulse. The peak photon flux would then occur well after the peak of the flashlamp pulse as desired. In this way more of the the pumping energy would be coupled into the recirculating field resulting in larger output energies. They stated that such a situation might be expected if the cavity decay time,  $t_c = l/cL$  (ring lasers) was comparable to the flashlamp pulse duration. Here,  $l$  is the cavity length and  $L$  is the fractional loss per round trip. However, if cavity losses were higher ( $\gamma_T > 0.05$ ) the cavity photon flux tended to follow the profile of the flashlamp pulse, rather than its integral, resulting in early extraction times and lower system efficiency. They concluded, however, that, even for cavities with small intrinsic cavity losses, the actual loss is dominated by the self-absorption and triplet losses in the dye and thus, regardless of the intrinsic loss level, the cavity photon density followed the profile of the pumping pulse.

If this analysis is correct, as their theoretical and experimental investigations indicate, significantly larger pulse energies and higher slope efficiencies should be obtainable by using shorter rise time flashlamps. Assuming equal discharge energies, the short rise time flashlamp peak would not only occur earlier, it would be more intense. The advantage of having the peak occur earlier is obvious. Extraction times could be pushed to a later point in the pumping pulse before triplet state and other time dependent losses terminated the net gains. This would allow both the slope efficiency and output energies to be increased. However, even if the time dependent loss mechanisms were still significant, and the photon flux followed the profile of the pumping pulse, output pulse energies would still

be larger due to higher peak intensity of the flashlamp pulse. In the work quoted above, Morton et al. demonstrated this experimentally. Using a  $\sim 300$ nsFWHM coaxial flashlamp and a basic polarization sensitive cavity-dumping scheme, they were able to generate  $\sim 400$ mJ, 20ns pulses using flashlamp discharge energies of only  $\sim 100$ J. Their reported slope efficiency was as high as 0.85% which was  $\sim 20$  times larger than that obtained in our work.

With shorter pumping pulse durations, however, the recirculating radiation makes fewer passes through the gain medium before cavity-dumping is required. Thus, if the pumping pulse is made too short, extraction occurs before the gain has been fully saturated resulting in lower output pulse energies. Pulse time compressions of the order of 10-20 have been shown to be obtainable without a loss in the efficiency of the system [6].

As mentioned in Chapter 3, the coaxial flashlamp system used in this work was chosen simply because it was indicative of a standard high-energy flashlamp system. Any results obtained with it then could be extended to most other flashlamp pumped systems as well. Nonetheless, based on our results, where "premature" extraction times were required, and those of Morton et al. presented above, one criteria that should be considered in the choice of the flashlamp is its rise time. To obtain both maximal system efficiency and output pulse energies, the flashlamp pump source should be as intense as possible (with the proviso, as noted above, that the pumping pulse not be made too short).

## REFERENCES

- [1] F.P. Schaefer (Ed.), *Dye Lasers*, Springer-Verlag, Berlin, Germany, 1977.
- [2] H. Walther, "Application of tunable dye lasers to atomic spectroscopy," *Physica Scripta*, vol. 9, pp. 297-305, 1974.
- [3] J. Pinard and S. Liberman, "A frequency locked, single mode pulsed dye laser. Application to single frequency tunable UV generation," *Opt. Commun.*, vol. 20, pp. 344-346, Mar. 1976.
- [4] E.D. Hinkley, (Ed.), *Laser Monitoring of the Atmosphere*, Springer-Verlag, Berlin, Germany, 1976.
- [5] P. Ewart, "Frequency tunable, nanosecond duration pulses from flash-lamp pumped dye lasers by pulsed Q-modulation," *Opt. Commun.*, vol. 28, pp. 379-382, Mar. 1979.
- [6] R.G. Morton, M.E. Mack, and I. Itzkan, "Efficient cavity dumped dye laser," *Appl. Opt.*, vol. 17, pp. 3268-3274, 15 Oct. 1978.
- [7] R. Wallenstein and T.W. Hansch, "Powerful dye laser oscillator-amplifier system for high resolution spectroscopy," *Opt. Commun.*, vol. 14, pp. 353-357, July 1975.
- [8] U. Ganiel, A. Hardy, G. Neumann, and D. Treves, "Amplified spontaneous emission and signal amplification in dye laser systems," *IEEE J. Quantum Electron.*, vol. QE-11, pp. 881-892, Nov. 1975.
- [9] L.E. Erickson and A. Szabo, "Spectral narrowing of dye laser output by injection of monochromatic radiation into the laser cavity," *Appl.*

*Phys. Lett.*, vol. 18, pp. 433-435, May 1971.

- [10] G. Magyar and H.J. Schneider-Muntau, "Dye laser forced oscillator," *Appl. Phys. Lett.*, vol. 20, pp. 406-408, May 1972.
- [11] J.J. Turner, E.I. Moses, and C.L. Tang, "Spectral narrowing and electrooptical tuning of a pulsed dye laser by injection locking to a CW dye laser," *Appl. Phys. Lett.*, vol. 27, pp. 441-443, Oct. 1975.
- [12] S. Blit, U. Ganiel, and D. Treves, "A tunable, single mode, injection-locked flashlamp pumped dye laser," *Appl. Phys.*, vol. 12, pp. 69-74, Jan. 1977.
- [13] P. Burlamacchi and R. Salimbeni, "Spectral narrowing of a flashlamp-pumped, waveguide dye laser by amplification of tunable narrow-band CW radiation," *Opt. Commun.*, vol. 17, pp. 6-10, Apr. 1976.
- [14] T. Okada, M. Maeda, and Y. Miyazoe, "Spectral narrowing of a flashlamp-pumped high-energy dye laser by two-stage injection locking," *IEEE J. Quantum Electron.*, vol. QE-15, pp. 616-623, July 1979.
- [15] P. Flamant and G. Megie, "Frequency locking by injection in dye lasers: analysis of the CW and delta pulse regimes," *IEEE J. Quantum Electron.*, vol. QE-16, pp. 653-660, June 1980.
- [16] Y.H. Meyer and P. Flamant "A basic property of dye lasers: spectral evolution," *Opt. Commun.*, vol. 19, pp. 20-24, Oct. 1976.

- [17] U. Ganiel, A. Hardy, and D. Treves, "Analysis of injection locking in pulsed dye laser systems," *IEEE J. Quantum Electron.*, vol. QE-12, pp. 704-716, Nov. 1976.
- [18] A. Yariv, *Quantum Electronics*, John Wiley and Sons, Inc., New York, 1975.
- [19] B.B. Snavely and F.P. Schaefer, "Feasibility of CW operation of dye lasers," *Phys. Lett.*, vol. 28A, pp. 728-729, Mar. 1969.
- [20] J.P. Webb, W.C. McColgin, O.G. Peterson, D.L. Stockman, and J.H. Everly, "Intersystem crossing rate and triplet state lifetimes for a lasing dye," *J. Chem Phys.*, vol. 53, pp. 4227-4229, Dec. 1970.
- [21] M.E. Mack, "Measurement of nanosecond fluorescence decay times," *J. Appl. Phys.*, vol. 39, pp. 2483-2485, 1968.
- [22] P.P. Sorokin and J.R. Lankard, "Stimulated emission observed from an organic dye, chloro-aluminum phthalocyanine," *IBM J. Research and Develop.*, vol. 10, p. 162, Mar. 1966.
- [23] F.P. Schaefer, W. Schmidt, and J. Volze, "Organic dye solution laser," *Appl. Phys. Lett.*, vol. 9, pp. 306-309, Oct. 1966.
- [24] M.L. Spaeth and D.P. Bortfeld, "Stimulated emission from polymethine dyes," *Appl. Phys. Lett.*, vol. 9, p. 179, Sept. 1966.
- [25] B.B. McFarland, "Laser second-harmonic-induced stimulated emission of organic dyes," *Appl. Phys. Lett.*, vol. 10, p. 208, May 1967.

- [26] P.P. Sorokin and J.R. Lankard, "Flashlamp excitation of organic dye lasers," *IBM J. Research and Develop.*, vol. 11, p. 148, March 1967.
- [27] P.P. Sorokin, J.R. Lankard, V.L. Moruzzi, and E.C. Hammond, "Flashlamp-pumped organic-dye lasers," *J. Chem. Phys.*, vol. 48, pp. 4726-4741, May 1968.
- [28] B.B. Snavely and F.P. Schaefer, "Feasibility of CW operation of dye-lasers," *Phys. Lett.*, vol. 28A, pp. 728-730, 1969.
- [29] J.B. Marling, D.W. Gregg and S.J. Thomas, "Effect of oxygen on flashlamp-pumped organic dye lasers," *IEEE J. Quantum Electron.*, vol. QE-6, pp. 570-572, Sept. 1970.
- [30] R. Pappalardo, H. Samelson, and A. Lempicki, "Long pulse laser emission from Rhodamine 6G using cyclooctatetraene," *Appl. Phys. Lett.*, vol. 16, pp. 267-269, Apr. 1970.
- [31] O.G. Peterson, S.A. Tuccio, and B.B. Snavely, "CW operation of an organic dye solution laser," *Appl. Phys. Lett.*, vol. 17, pp. 245-247, 1970.
- [32] P.P. Sorokin, J.R. Lankard, E.C. Hammond, and V.L. Moruzzi, "Laser pumped stimulated emission from organic dyes," *IBM J. Research Develop.*, vol. 11, p. 130, 1967.
- [33] G.T. Schappert, K.W. Billman, and D.C. Burnham, "Temperature tuning of an organic dye laser," *Appl. Phys. Lett.*, vol. 13, pp. 124-127, 1968.

- [34] M.J. Weber and M. Bass, "Frequency and time dependent gain characteristics of dye lasers," *IEEE J. Quantum Electron.*, vol. QE-5, pp. 175-188, Apr. 1969.
- [35] B.H. Soffer and B.B. McFarland, "Continuously tunable narrow-band organic-dye lasers," *Appl. Phys. Lett.*, vol. 10, p. 266, May 1967.
- [36] M. Hercher and H.A. Pike, "Single mode operation of a continuous tunable dye laser," *Opt. Commun.*, vol. 3, p. 65, 1971.
- [37] R. Adler, "A study of locking phenomenon in oscillators," *Proc. IRE*, vol. 34, pp. 351-357, June 1946.
- [38] H.L. Stover and W.H. Steier, "Locking of laser oscillators by light injection," *Appl. Phys. Lett.*, vol. 8, pp. 91-93, Feb. 1966.
- [39] C.J. Buczek and R.J. Freiberg, "Hybrid injection locking of high power  $CO_2$  lasers," *IEEE J. Quantum Electron.*, vol. QE-8, pp. 641-650, July 1972.
- [40] J.E. Bjorkholm and H.G. Danielmeyer, "Frequency control of a pulsed optical parametric oscillator by radiation injection," *Appl. Phys. Lett.*, vol. 15, pp. 171-173, Sept. 1969.
- [41] Q.H.F. Vreken and A.J. Breimer, "Spectral properties of a pulsed dye laser with monochromatic injection," *Opt. Commun.*, vol. 4, pp. 416-420, Mar. 1972.
- [42] I.J. Bigio and M. Slatkine, "Injection-locking unstable resonator excimer lasers," *IEEE J. Quantum Electron.*, vol. QE-19, pp. 1426-1436, Sept. 1983.

- [43] W.W. Chow, "Theory of line narrowing and frequency selection in an injection locked laser," *IEEE J. Quantum Electron.*, vol. QE-19, pp. 704-716, Nov. 1976.
- [44] B. Couillaud, A. Ducasse, and E. Freysz, "Injection locking of CW ring dye lasers," *IEEE J. Quantum Electron.*, vol. QE-20, pp. 310-318, Mar. 1984.
- [45] ILC Technology Inc., Sunnyvale, California 94086
- [46] H.W. Furomoto and H.L. Cecon, "Optical pumps for organic dye lasers," *Appl. Opt.*, vol. 8, pp. 1613-1623, Aug. 1969.
- [47] B.B. Snavely, "Flashlamp-excited organic dye lasers," *Proc. IEEE* vol. 57, pp. 1374-1390, Aug. 1969.
- [48] P. Burlamacchi and D. Cutter, "Energy transfer in flashlamp pumped organic dye lasers," *Opt. Commun.*, vol. 22, pp. 283-287, Sept. 1977.
- [49] T.G. Pavlopoulos, "Laser dye mixtures," *Opt. Commun.*, vol. 24, pp. 170-174, Feb. 1978.
- [50] S. Blit and U. Ganiel, "Distribution of absorbed pump power in flashlamp-pumped dye lasers," *Optical and Quantum Electronics*, vol. 7, pp. 87-93, 1975.
- [51] P.F. McManamon, "An investigation of flashlamp pumped dye lasers," thesis available through University Microfilms Int., 1977.
- [52] Exciton Chemical Co, Inc., P.O. Box 31126, Overlook Station, Dayton, Ohio 45431.



- [53] Phase R Corporation, Box G-2, New Durham, NH 03855.
- [54] M. Bass and J.I. Steinfeld, "Wavelength dependent time development of the intensity of dye solution lasers," *IEEE J. Quantum Electron.*, vol. QE-4, pp. 53-58, Feb. 1968.
- [55] T.W. Hansch, "Repetitively pulsed tunable dye laser for high resolution spectroscopy," *Appl. Opt.*, vol. 11, p. 895, 1972.

**VITA**

The author was born in [REDACTED] on [REDACTED]. He attended Alexis I. duPont High School in Greenville, Delaware until graduating in June of 1976. He received a B.S. in Physics and Mathematics from Haverford College, Haverford, Pennsylvania in May 1980. In September of that year he began graduate study in electrical engineering at the Johns Hopkins University. He received a M.S.E. in Electrical Engineering from that institution in June of 1982. He is currently employed as a member of the technical staff in the Engineering Physics Laboratory of E.I. duPont de Nemours & Co. in Wilmington, Delaware.